SMALL-ANGLE X-RAY SCATTERING FROM PROTEIN SOLUTIONS

by

WILLIAM STANLEY ROTHWELL

A Thesis Submitted in Partial Fulfillment of
the Requirements for the Degree of

DOCTOR OF PHILOSOPHY

at the

UNIVERSITY OF WISCONSIN

1954

SMALL-ANGLE X-RAY SCATTERING FROM

PROTEIN SOLUTIONS

Approved:

W. W. Beeman

W. W. Beeman
Professor of Physics

Date Jan 14, 1954

Table of Contents

Introduction

In recent years the development of the theory of x-ray scattering from macromolecules and of the associated experimental techniques has provided a useful method for studying properties of protein molecules. X-ray diffraction by sub-microscopic particles is somewhat analogous to light diffraction by opaque objects with dimensions one or two orders of magnitude greater than the wave length. The angular width of the x-ray diffraction pattern is similarly proportional to the ratio of the radiation wave length to the particle dimensions. Since proteins are large compared to the monochromatic x-ray wave lengths which are practicable to use, most of the diffracted or scattered x-rays from such particles are confined to a small angular range of five degrees or less, thus the expression, "small-angle x-ray scattering." Interpretation of the scattered radiation intensity distribution yields information about the size and shape of the particle.

The usual procedure for determining the small-angle x-ray scattering from a particle is to present to a beam of x-rays a large number of such particles in as near random arrangement as possible in order to keep interparticle interference to a minimum. A dilute solution of the particles is usually used as an approximation to random arrangement. The intensity of the x-rays scattered at a

given angle from the central beam by any irradiated point of the sample will be constant around the circular intersection of these x-rays with any plane perpendicular to the central beam. The ideal system would involve a perfectly collimated incoming beam, thus giving a well defined scattering geometry. However, most previous workers have been obliged, because of intensity requirements, to use slit geometry. The resulting pattern is then the sum of those from every element of the slit and must be corrected using appropriate calculations. In this thesis a collimating system will be described which has been successfully designed to use pinhole geometry. It approaches the ideal much more closely than do slit systems.

The theory of the scattering of x-rays from solutions of three-dimensional particles is necessarily more complicated than that for a simple optical case for visible light and a single opaque object. A discussion of this theory including the derivation of formulae to be used will be presented.

The properties of proteins are of particular interest because proteins play an essential role in the processes of all living organisms. The experiments to be described here include an extensive investigation of the protein, bovine serum albumin, and the study of some size and shape characteristics of rat and bovine hemoglobin and bovine fibrinogen.

I. The Pinhole Collimating System

A. Geometry

Figure 1 is a schematic drawing of the pinhole collimating system. X-rays from the focal spot at f enter the system through the first pinhole, P1, of diameter, d. The beam is further defined by pinhole P_2, also of diameter, d, and then strikes the sample which is directly in front of the guard ring, G. Scattered radiation from the sample then passes through an annular slit, A, of width, t, and diameter, D.. A detector is mounted directly behind A. For infinitely small t and d the paths of all scattered radiation detected for a given D and L will describe the surface of a right circular cone with its axis along the path of the central beam. Thus, all the radiation scattered at any given angle can be detected by properly choosing D and L. In practice, D is kept constant and L is varied.

The term, resolution, will be used here to describe the angular range of the x-ray scattering which is detected for a given angular setting. Its quantitative definition will be taken as $\Delta\theta$ for the absolute angular resolution and $\Delta\theta/\theta$ for the relative angular resolution, where θ is the nominal angle of detection and $\theta - \Delta\theta$ to $\theta + \Delta\theta$ is the range of angle actually detected. A resolution of 0 is perfect and would exactly reproduce the scattering pattern. Using these definitions a comparison of resolution will be made for slit and pinhole collimating systems. The conventional rectangular slit system employs a detector slit, at a fixed distance

Figure 1

A schematic drawing of the pinhole collimating system. X-rays from the focus at f pass through pinholes P_1 and P_2 and guard ring, G, and are scattered by the sample, immediately before G, toward the annular slit, A. The diameter of the pinholes is d, of the guard ring, 3d, and of the annular slit, D. The width of the annular slit is t.

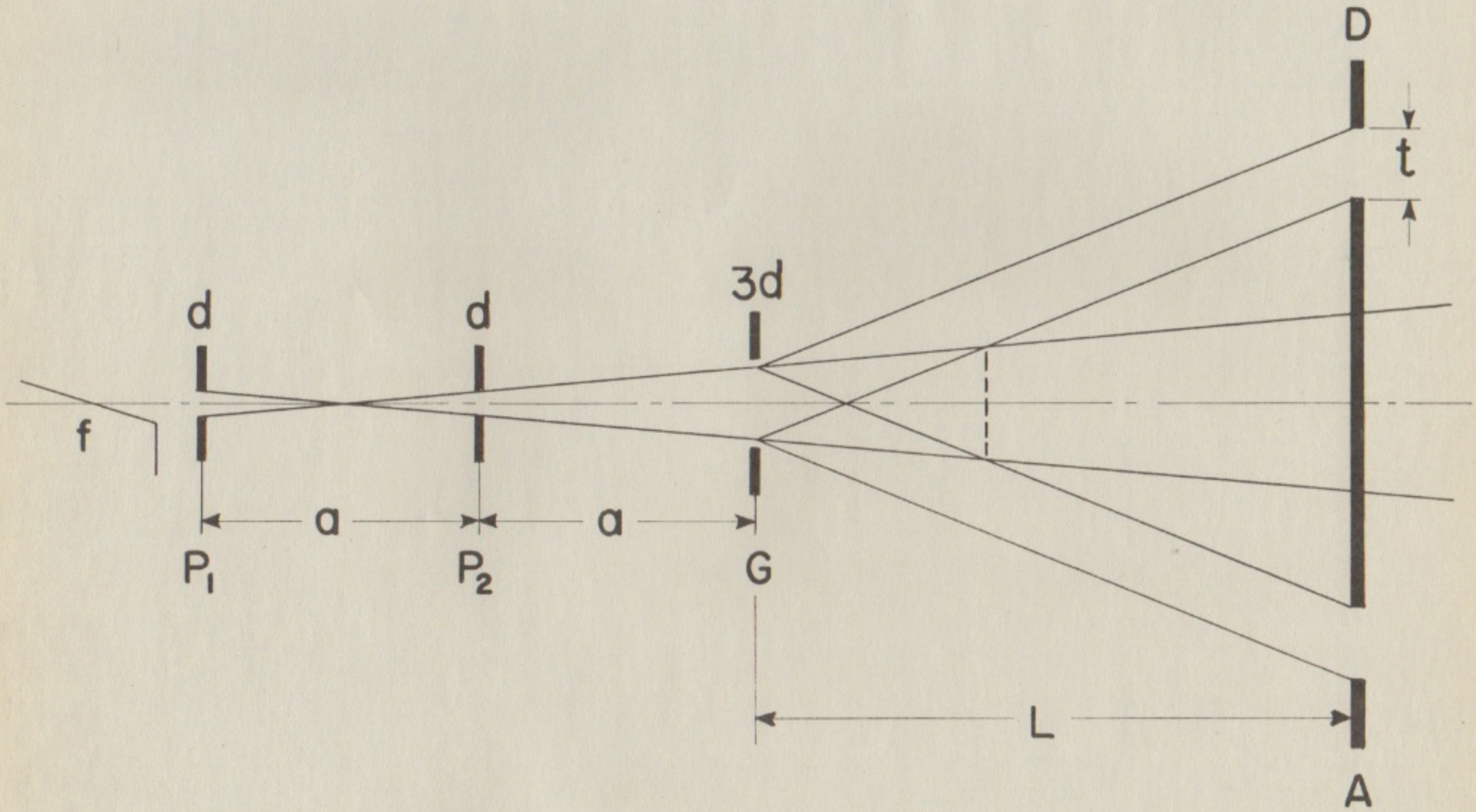
D
t
d
d
3d
f
a
a
P_1
P_2
G
L
A

from the sample, which is swung along an arc about the sample position as center to measure the scattered radiation intensity distribution. For such an arrangement the solid angle intercepted by the slit, and the absolute resolution, $\Delta\theta$, remain constant. Thus the relative resolution, $\frac{\Delta\theta}{\theta}$, varies inversely with scattering angle, θ. The measured intensity drops at the same rate as the diffration pattern intensity. The intensity in the diffraction pattern drops off rapidly with increasing angle and may be quite small at larger angles where, however, it is still important to get good data. This has proved to be a serious disadvantage when working with low scattering power dilute solutions. The sliding annular slit detector intercepts a solid angle which increases as $1/L^2$ and thus as θ^2. As the angle of detection increases, the gain in solid angle tends to compensate for the decrease in scattered intensity. This advantage is gained by a sacrifice of relative resolution at large angles. As will be shown in the next section, the relative resolution is nearly constant for all θ. However, theoretical and experimental evidence to be discussed in later sections shows that this is not a serious disadvantage and is certainly outweighed by the gain in statistical accuracy.

Since d is finite, the central beam is not perfectly collimated. Its limiting rays are drawn in Figure 1, but its actual effective extent may be determined by the size

of the focal spot as well as by d, if the focal spot is too small. If the focal spot does not fill the target area cut out by the extension and rotation of these lines, only scattered radiation from the first pinhole edges will occupy the limiting angle in Figure 1. Such radiation is too weak compared to the direct x-rays to make an effective contribution to the sample illumination.

The results of an experimental study of the angular intensity distribution for the central beam of a slit collimating system are shown in Figure 2. This curve was obtained by scanning the slit collimated central beam with an angular sweep of the two slit analyzer of the slit system. The measurement was made about the sample position in the conventional plane, which is perpendicular to the slits. No scattering sample was used. The curve is analogous to the angular intensity distribution obtainable in any plane containing the axis of the central beam of a pinhole system. The line focus for this slit system did not fill the area viewed by the slits. Analysis of the geometry used places the edge of the beam due to direct radiation from the focus at A, to scattered radiation from the first slit edges at B, and to scattered radiation from the second slit edges at C. B and C correspond to angles d/a and 2d/a in the pinhole system.

It is often desirable to measure sample scattering as low as 2 or 3 counts per second. In order to keep the

Figure 2

The angular intensity distribution for the central beam of a slit collimating system. Analysis of the geometry used places the edge of the beam due to direct radiation from the focus at A, to scattered radiation from the first slit edges at B, and to scattered radiation from the second slit edges at C. θ is measured in radians.

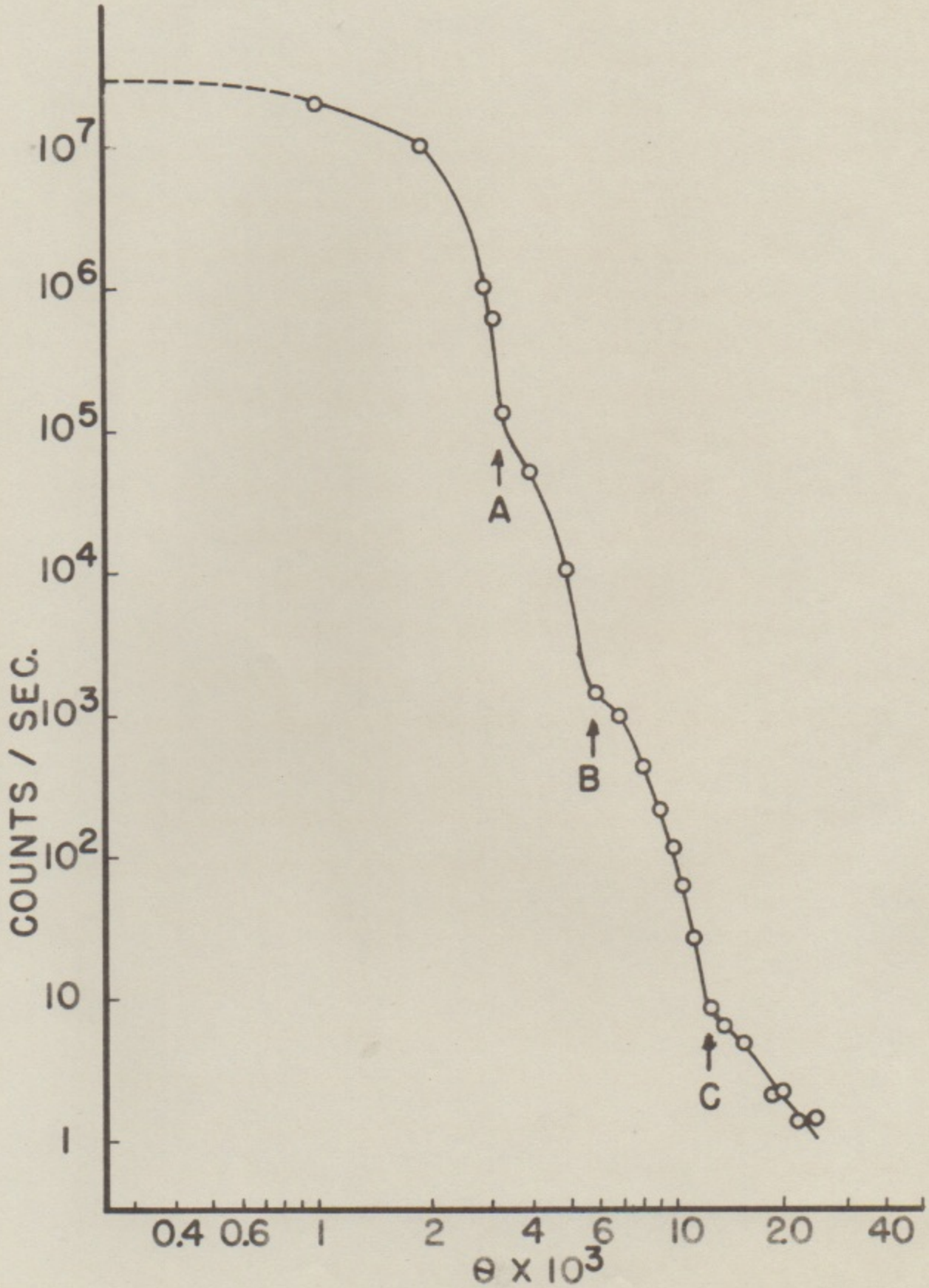
COUNTS / SEC.
10^7
10^6
10^5
10^4
10^3
10^2
10
1
A
B
C
0.4 0.6 1 2 4 6 10 20 40
$\theta \times 10^3$

background scattering low it is essential that once-scattered radiation from pinhole edges be kept to a minimum. For this reason the guard ring, G, in Figure 1 is employed at the sample position to block from the detector once-scattered x-rays from the second pinhole edges. It is actually made slightly greater than 3d, the size of the central beam at this point, so it is not itself illuminated by the central beam. It will be illuminated by the once-scattered radiation from the second pinhole edges, but this would have to be scattered once more to reach the detector, and twice scattered radiation can be neglected. The smallest angle at which measurements can be taken will be determined by the maximum angle at which radiation is scattered from the second pinhole. From Figures 1 and 3, it is seen that this is equal to 19d/8a when measured from the sample position.

The vertical dotted line in Figure 1 indicates the optimum position of a central beam stop to be discussed in paragraph C 5.

B. Resolution

Since d and t are finite and the central beam is not parallel, radiation scattered at more than one angle will reach the detector for any single setting of L. It is seen from Figure 2 that the intensity of the scattered radiation reaching the sample is 10^{-2} or less of the direct radiation. Thus, it can be ignored in calculating the resolution. The

Figure 3

A ray diagram indicating the limits of resolution of the collimating system. Pinhole, P_2, guard ring, G, and the annular slit, A, of width, t, are shown. The angle, d/a, includes the part of the central beam defined by pinholes, P_1 (not shown) and P_2. Angle 2d/a indicates the limiting angles of scattering reaching the sample from the edges of P_2. The measured scattering angle is θ and the limiting angles of the radiation received from the scattering sample are θ_1 and θ_2.

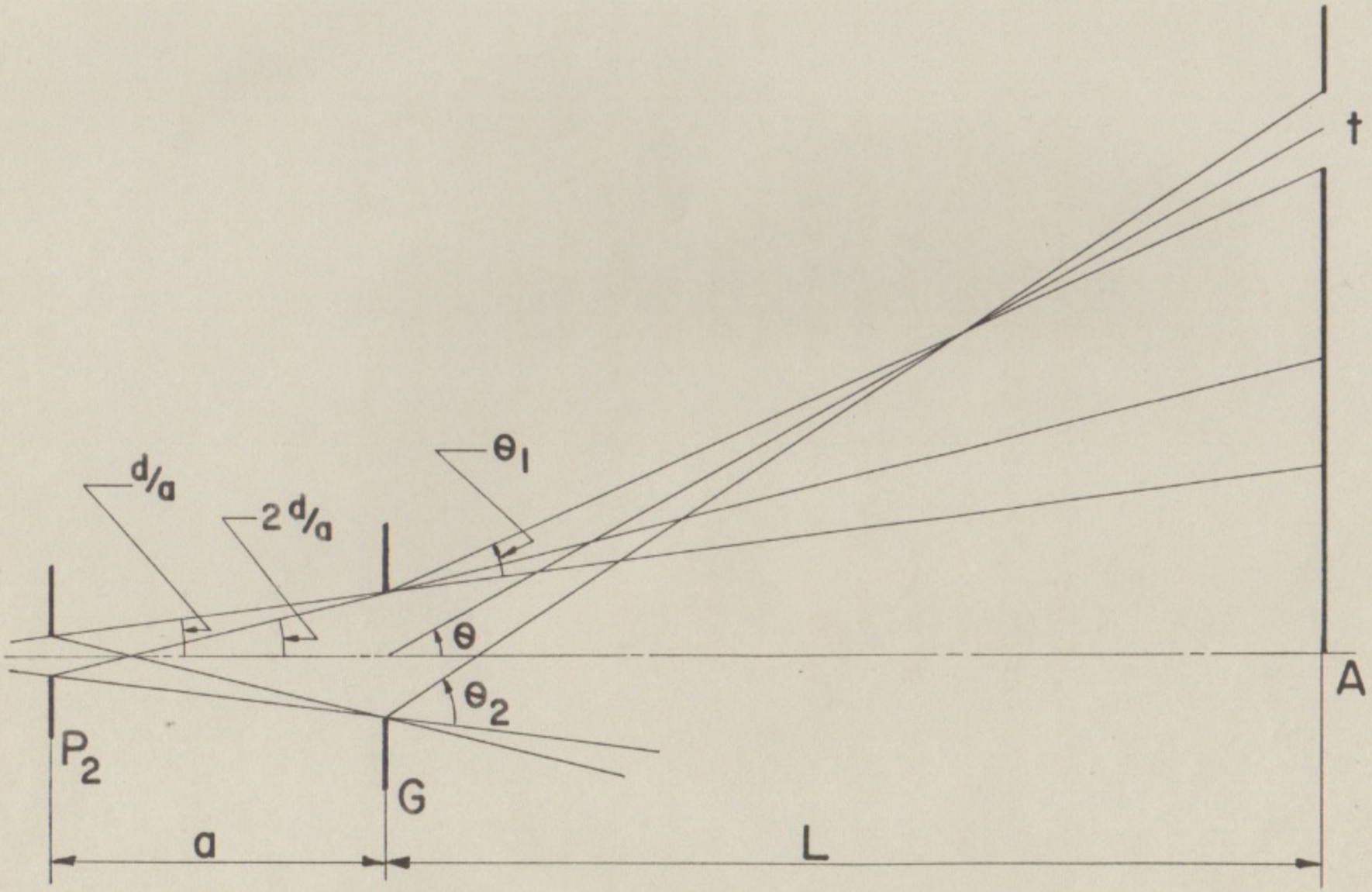
t
d/a
2 d/a
θ1
θ
θ2
A
P2
G
a
L

limiting angles actually received by the detector for a given L are indicated as θ_1 and θ_2 in Figure 3. For the small angles involved we can take $\theta = D/2L$. Then $\theta_1 = \theta - \Delta\theta$, $\theta_2 = \theta + \Delta\theta$. It can easily be shown that

$$\frac{\Delta\theta}{\theta} = \frac{t}{D} + \frac{3d}{D} + \frac{2dL}{aD}$$

where the first term is due to the finite width of the annular slit, the second to the width of the scattering portion of the sample, and the third to the angular spread of the central beam. The values of a, d, D and t are chosen in a compromise between intensity and resolution. The size of the particles to be examined must be taken into account in determining the limiting resolution necessary. As stated previously, the spread of the diffraction pattern is proportional to λ/d, where d is the effective diameter of the particle. Thus it is seen that the absolute resolution, $\Delta\theta$, necessary to detect similar detail in the scattering from particles differing only in linear dimensions is inversely proportional to d.

The resolution of the system used in these experiments and its effect on the data will be discussed in Section II.

C. Description of the Apparatus

A perspective drawing of the collimating system and x-ray tube is shown in Figure 4. The essential elements for obtaining pinhole geometry are contained in the first and second pinhole diaphragms, E, the guard ring support, H, and the annular slit diaphragm, N. The guard ring support

Figure 4

A perspective drawing of the collimating system and x-ray tube. The parts are labeled as follows:

A - Vertical Cathode Assembly

B - Electron Gun

C - Rotating Anode

D - X-ray window

E - Adjustable Pinhole Diaphragms

F - Connecting Tube

G - Vacuum Extension

H - Sample Holder and Guard Ring Support

J - Adjustable Vacuum Chamber

K - Helium Bellows

L - Beam Stop

M - Pre-Amplifier

N - Annular Slit Diaphragm

O - Proportional Counter Detector

P - Slide

Q - Steel Way

R - I-beam

S - Outlet to Diffusion Pump

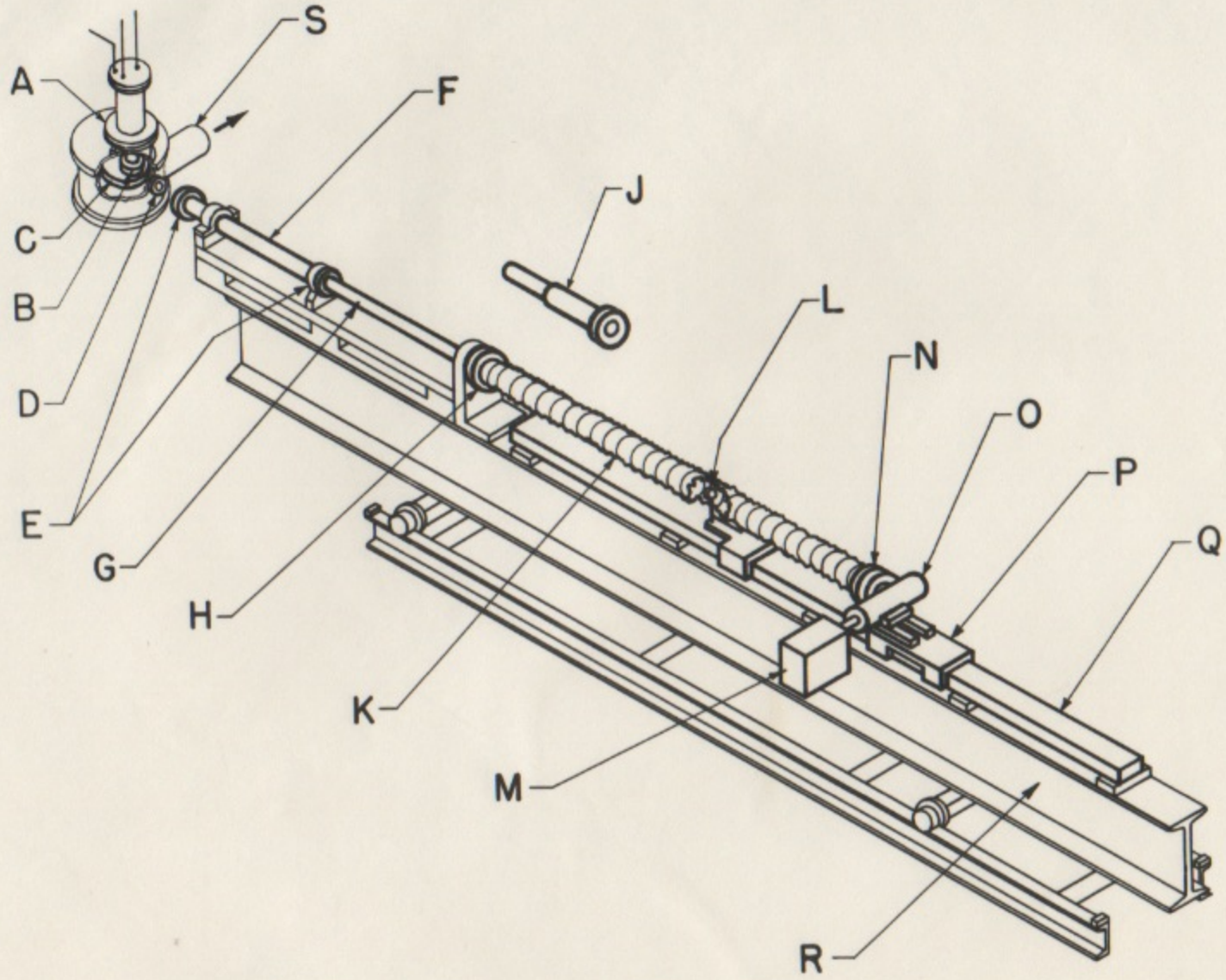
A
S
F
J
C
B
L
N
O
P
D
Q
E
G
H
K
M
R

is bolted to the I-beam and contains the only fixed aperture. Its center is used as reference point for alignment. The whole apparatus is supported by two concrete piers, not shown. A detailed description of each component follows.

1. X-ray Tube and Cathode Assembly

A drawing of the x-ray tube is shown in Figure 5. Except for the vertical cathode assembly, B, which has been added for use with the pinhole system, the design and construction of the tube has been discussed in detail elsewhere.[1] Its essential feature is the 4" diameter, rotating, water-cooled, copper anode, A. The horizontal cathode provides a vertical line focus on the periphery of the anode for a slit collimating system. The top surface of the anode is inclined from the center at an angle of 4 degrees so that a line focus formed on a radius of its surface by the vertical cathode will appear as a square in geometric perspective when viewed end-on by the pinhole collimating system. The x-rays leave the evacuated tube through a beryllium window shown at D in Figure 4.

In the vertical cathode assembly an electron gun, F_2, is suspended at the end of a 1" diameter steel tube which is silver soldered to the brass flange that fits over the top of the 6" ceramic insulator, B. The bottom of the insulator fits into the top flange of the brass sylphon. The bottom flange is bolted to the top of the x-ray tube over a hole with center located above a point $\frac{1}{8}$" from the edge of

Figure 5

A section drawing of the x-ray tube. The essential parts discussed in this thesis are the rotating anode, A, the vertical cathode assembly, B, and the electron gun, F_2.

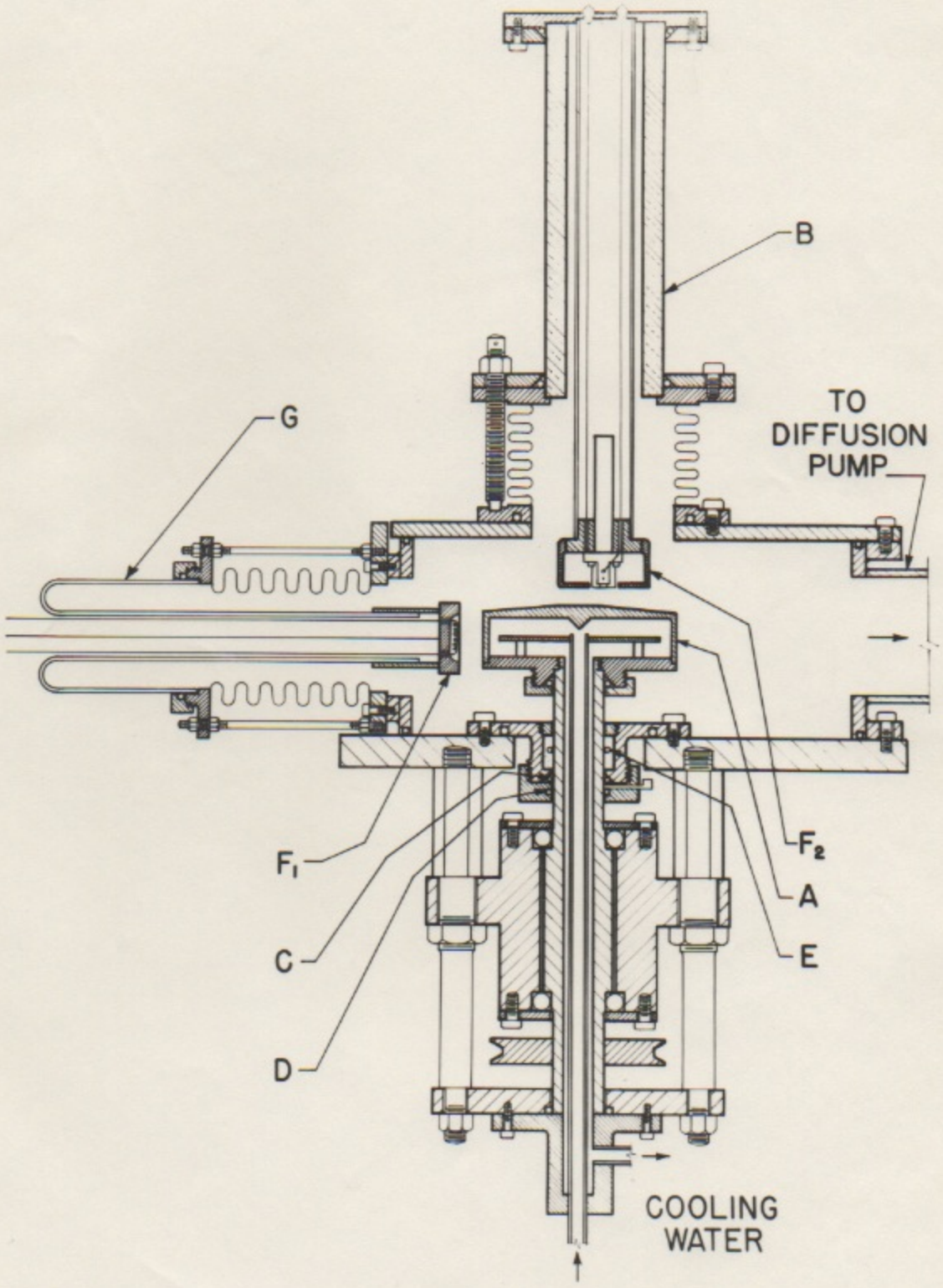
B
TO
DIFFUSION
PUMP
G
F1
C
D
F2
A
E
COOLING
WATER

the anode. The sylphon permits adjustment of the filament to anode distance.

The details of construction of the electron gun are shown in Figure 6. All parts are steel. The filaments are made of 12 mil tungsten wire wound in a tight 30 turn spiral on a 20 mil mandril and then pulled to a length of 3/4". Single strand tungsten of various diameters, thoriated tungsten, and smaller diameter spiral tungsten filaments were tested before the above choice was made as the most satisfactory. After installation, all filaments are flashed in helium to remove strains and facilitate outgassing. The adjustable focussing element, E, is made by welding a block of steel to the end of a tube and then milling out the required slot width. The present slot is 5mm wide. The electron gun is operated with the end of the focussing element flush with the surface of the shielding cap, C. This places the filament at a depth of 4mm in the slot and 1cm above the anode. The focussing element is in electrical contact with the top plate of the cathode through the vertical support tube. Bias is therefore applied directly to this plate. A bias of -400 volts gives a line focus on the anode approximately .5mm wide when the tube is operated at 30 kv and 80 ma. The filament current required under these conditions is 7.6 amperes in an operating vacuum of 3×10^{-6} mm of Hg. Eighty per cent of the radiation from the focal spot at 30 kv is Cu K-alpha of wave length 1.539 Å. This

Figure 6

A section drawing of the electron gun. The detail section shows how the filament support posts are insulated from the base. The parts are labeled as follows:

A - Insulating Ceramic Tubing over Filament Leads

B - Base

C - Cap

D - Support Posts for Filament

E - Focussing Element

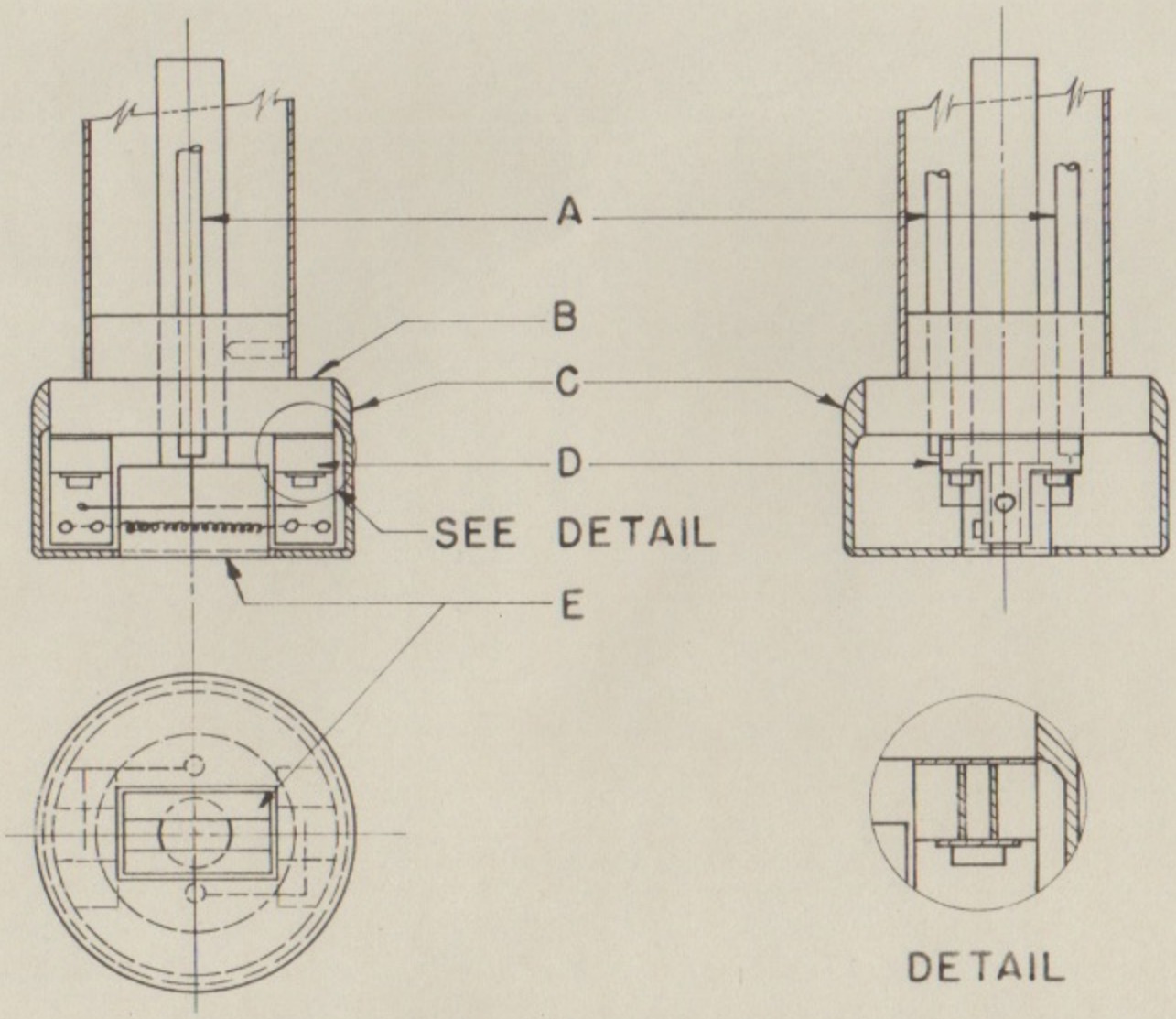

ELECTRON GUN

makes the monochromatization problem less critical.

It was convenient to use the same power supply for both the horizontal and vertical cathodes. Since it has been found that keeping a filament heated increases its lifetime, a separate transformer was provided for the vertical cathode filament and a switching arrangement permits changing high voltage leads without disturbing the filament current. The bias voltage is taken from the low side of a resistor in series with the high voltage line.

2. Support Member (See Figure 4)

The system of supports includes the concrete piers, the channel iron framework, the I-beam, R, the steel way, Q, and the angle-block precision support for the pinhole sections. Since structural rigidity is obviously of paramount importance, consideration was given to the elastic problems involved. Mathematical solutions of these problems were used to determine the size, shape, and materials of the various members and in locating the positions of optimum support. For example, with the I-beam supported 2 feet from each end, the maximum deviation from linearity is calculated as .06 mils. If the beam were supported at each end the calculated sag at the center would be 2 mils. The maximum sag of the channel iron framework as presently supported is 1.5 mils.

a. Channel Iron Framework

This frame consists of two 3" channel iron beams $6\frac{1}{2}$' long held 10" apart by 4 accurate lengths of 2-3/8" pipe.

Five-eighth inch bolts pass through the pipes to hold the frame together. Rectangular steel bars are bolted laterally across the bottom of the frame at the two support positions. Bolts, ½" x 20, screw vertically through the ends of these bars. At the rear support these bolts bear on a steel plate which rests directly on the concrete pier. The steel support bar is clamped to this plate at its center. At the front support the end bolts set into indentations in the steel plate which slides on a second steel plate that rests on the concrete pier. This provision for vertical and horizontal adjustment of the framework is made for aiming the aligned pinhole system at the x-ray tube focus.

b. I-beam

This is a steel 4" x 8" x 9' I-beam with opposite surfaces planed parallel. Steel axles are attached to the under side of the beam at the support positions. Tapered steel wheels with guide lips and bronze bushings are accurately machined and fitted to the ends of the axles to provide smooth and parallel motion of the I-beam over a 2' longitudinal range. This permits the use of alternate length pinhole sections and the access of other equipment to the x-ray tube window.

c. Steel Way

The steel way, obtained from the Gisholt Machine Co., is a 3" x 1½" x 80" lathe bed way accurately ground over its length to ±1 mil. It is bolted to five steel blocks which are bolted to the I-beam in the positions shown in Figure 4.

The alignment of the way will be discussed in a later section.

d. Precision Pinhole Section Support

This support, shown mounted on the front end of the I-beam in Figure 4, consists of a 4" x 1" x 19½" machined and ground steel base on which are mounted 3 pair of precision 45° angle blocks to form a cradle support. The bases of the two interchangeable pinhole sections are accordingly bevelled and ground to fit precisely into the blocks, which were accurately positioned with a pinhole section base in place. The support is bolted securely to the I-beam and shimmed to be the correct height relative to the reference point on the guard ring support.

3. Pinhole Sections

The pinhole tube consists of two adjustable diaphragms, E, 3" in diameter, connected by a 2" diameter brass tube,F, and with a 1" diameter vacuum extension, G, as shown in Figure 4. The extension is capped on the end except for a ¼" center hole. The pinhole tube is bolted to a support at the second diaphragm and clamped to a support at a point on the large brass tube. These supports are bolted to the section base of 2" x 4" aluminum which is bevelled on its lower edges as described in 2 d. The pinhole section in use at the present time is of the necessary longitudinal dimensions to provide a distance, "a" (Figure 1) of 30 cm. A longer base is available for attaching a tube with "a" equal to

60 cm. A detail drawing of the second pinhole diaphragm is shown in Figure 7. The first diaphragm is the same except that the pinhole is on the opposite end of the central cone and the vacuum extension is replaced by a 1/8" center hole. The pinhole aperture, corresponding to d in Figure 1, is drilled in a 20 mil tantalum disc. This disc is secured with cement in an inset on the end of a brass cone section with 10° included angle. This forms a replaceable unit so that pinhole diameters may be changed. It is secured by friction in a steel ring with an identical conical inside bevel. Three set screws with steel balls cemented to their tips bear against an annular V-groove on the periphery of the steel ring to hold the ring in place and provide adjustment. The set screw holes are sealed with vacuum clay after adjustment is completed. Each conical pinhole insert contains threaded holes on its base to receive a special tool for inserting and removing the inserts. Inserts have been prepared with precisely centered pinholes of diameters, 2mm, 1mm, .5mm and .25mm. All inserts were machined under identical conditions to make them interchangeable once alignment is obtained. To prevent absorption of the relatively soft x-rays used, the entire pinhole tube is evacuated through an outlet on the large brass tube by a continuously operating mechanical fore-pump. The 1/8" front hole is sealed with scotch tape and the $\frac{1}{4}$" rear hole is sealed with a .6 mil low scattering mica window. The combined transmission of these windows is .81 for Cu K-alpha radiation.

Figure 7

A detail drawing of the second pinhole diaphragm.

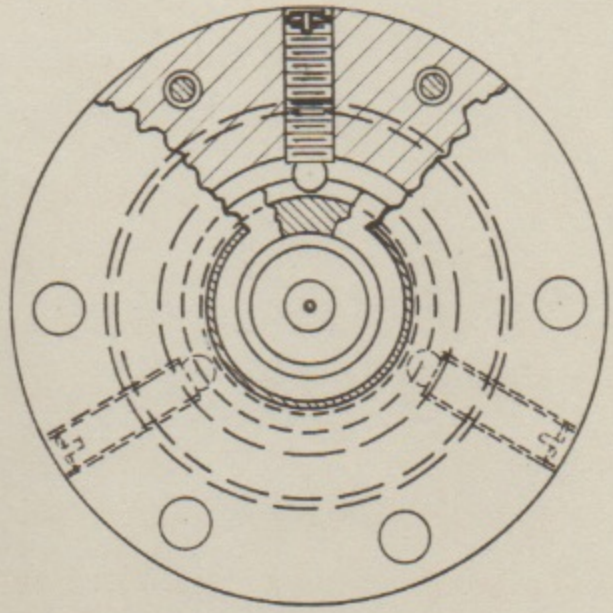

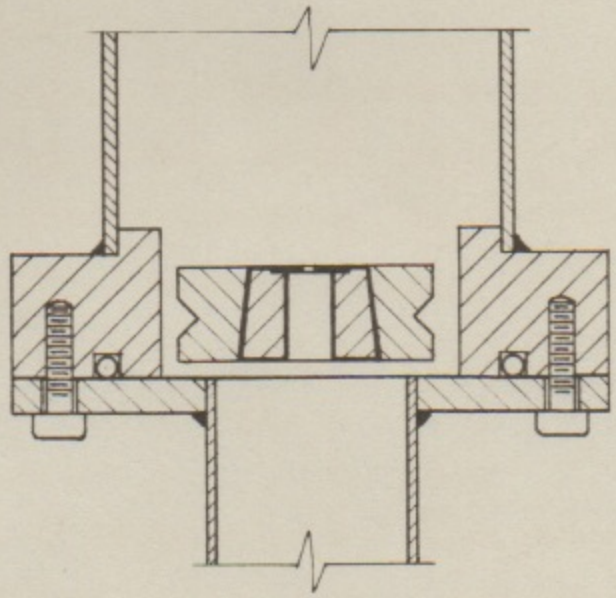

ADJUSTABLE PINHOLE DIAPHRAGM

4. Sample Holder and Guard Ring Support

The sample holder and the guard ring are supported by the heavy L-shaped steel piece shown at H in Figure 4. A conically bevelled hole through it determines the center line of the system at about 5" above the I-beam. Brass plug inserts for this hole contain the guard ring apertures of diameter slightly more than 3d. A flat L-shaped piece of brass with clips is attached to the front face of the support and just below the opening to provide a means of accurately and reproducibly positioning the sample holders in front of the guard ring aperture.

5. Detector Assembly

Referring to Figure 4, the detector assembly can be divided into the helium bellows, K, the beam stop and support, L, the annular slit diaphragm, N, the proportional counter detector, O, with attendant circuitry, and the slide, P. The helium bellows and beam stop are replaced by the vacuum chamber, J, at large angles.

a. Helium Bellows

A major problem in constructing the detector assembly lay in obtaining a low absorption and low scattering path between the sample and the proportional counter. An ideal system would employ a vacuum path in this region, but the problems associated with providing a vacuum path of variable length were postponed for the present by using a bellows filled with helium. The bellows was formed by heat-sealing

2 mil polyethylene over a "Slinky Toy" which is soldered to brass end plates. The front end plate seals to the rear face of the guard ring support and the rear end plate is attached to the front face of the annular slit diaphragm. O-rings set into grooves in the guard ring support and diaphragm provide an air-tight seal. The bellows has an expansion range from 15 cm to 200 cm. Helium is blown into the bellows through a channel drilled in the guard ring support. An outlet valve is provided on the annular slit diaphragm. The bellows is supported by two parallel telescoping rods which fit into supports in the end plates.

b. Beam Stop

Though the helium absorbs a negligible fraction of the sample-scattered intensity, the scattering of the central beam by the entire helium path is serious. Referring to the diagram below, an analysis of this scattering can be made as follows:

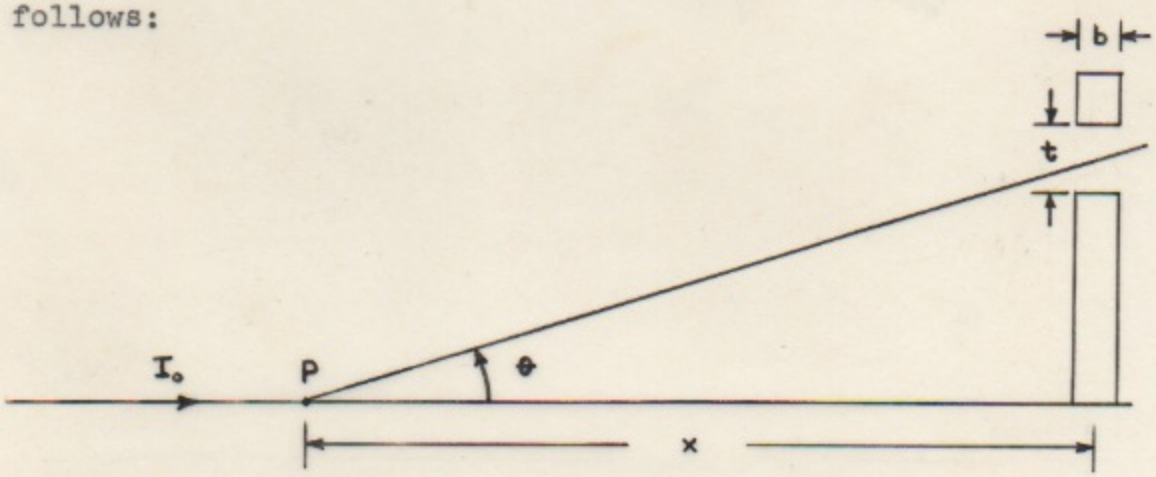

Assume that the central beam produces scattered intensity in the forward direction of I_o per unit length. The

amount of this which reaches the detector from an elementof the beam at point, P, a distance, x, from the annular slit depends upon the following factors:

1. The scattering angle of the radiation which enters the slit from point P. From the atomic structure factor for helium this dependence can be approximated by

$$I \sim I_o \left(1 - \frac{\sin \theta}{2} \right)$$

2. The solid angle subtended by the annular slit:

$$I \sim I_o \sin^2 \theta$$

3. The effective slit width. This decreases for increasing angle because of the finite slit depth. Calling the depth of the annular slit b, and its width t, the dependence on effective slit width is

$$I \sim I_o \left(1 - \frac{b}{t} \tan \theta \right) \cos \theta$$

Combining all these,

$$I \sim I_o \left(1 - \frac{b}{t}\tan \theta\right) \left(1 - \frac{\sin \theta}{2}\right) \cos \theta \sin^2 \theta$$

To find the total intensity contributed between some arbitrary point, x, and the limiting point where $\tan \theta_o = t/b$, this expression must be integrated over the range. Letting $x = r_o \cot \theta$, $r_o = D/2$

$$I_T \sim I_o r_o \int_{\theta}^{\theta_o} \left(1 - \frac{b}{t} \tan \theta\right) \left(\cos \theta - \tfrac{1}{2} \sin \theta \cos \theta\right) d\theta$$

This integration is easily made. Then, since θ is small,

the following approximations hold: $\sin\theta = \tan\theta = \theta$, $\cos\theta = 1$. Then

$$I_T \sim \left(\frac{\theta^2}{4} - \theta + K\right) \quad , \quad K = \frac{b}{t}\left(\frac{\theta_0}{4} - 1\right) + \sqrt{1 + \left(\frac{b}{t}\right)^2} - \frac{1}{4}$$

Neglecting $\theta^2/4$ compared to θ;

$$I_T \sim (K - \theta)$$

For the reasonable range of b/t, $0 \leq b/t \leq 1$, it is found that $.75 \geq K \geq .4$. Since 90 per cent of the total intensity is received from points where $\theta \geq .1K \simeq 50 \times 10^{-3}$ radians, most of the scattered intensity detected comes from the helium closest to the annular slit, where θ is large. This fact suggests that a stop placed somewhere in the path to cut off the central beam but not the scattered x-rays would be practical. The optimum position and diameter of the stop would be determined by the intersection of the central beam and the limiting edge of the scattered radiation as indicated by the dotted line in Figure 1. In practice the position has been chosen slightly closer to the annular slit in order to make the diameter of the stop and its alignment less critical. In any case, it is impractical to use different sized stops for each position of the detector, so the fit is made for the minimum angle at which the detector will be placed, and then the same ratio of stop to annular slit distance is maintained over the whole range of angles. This keeps the stop at the same relative cut-off position with respect to the scattered radiation. It has been found convenient to keep the stop half way between the sample and the detector.

Thus it must be moved each time the angle of detection is changed. Using the previously derived formula, it can be shown that this results in an average reduction of the helium scattering background of about 96 per cent.

A drawing of the actual stop and its adjustable support is shown in Figure 8. The stop is made of lead, molded and tamped into a steel form of the correct diameter and 1/16" thick. It is mounted on a steel needle which is soldered into a 1/8" rod to make a replaceable unit that is attached to the support as shown. The support adjusting screws permit vertical and horizontal adjustment of the stop position. The support clamps to the way under the bellows and is kept accurately positioned by the various ball contacts shown. The stop extends vertically into the bellows through a sleeve which is sealed around the cylinder that holds the replaceable stop unit. The stop is aligned in the beam to the position of minimum scattering with helium in the bellows. Its position is set using the wire pointer shown in the diagram. A 2 meter stick is clamped along one edge of the way as a reference scale.

c. Adjustable Vacuum Chamber

When the detector is less than 25 cm from the sample the beam stop method of eliminating helium scattering background is inadequate. Therefore, an adjustable vacuum chamber has been constructed to replace the helium bellows in this range. A drawing of the chamber is shown in Figure 9.

Figure 8

The adjustable beam stop support. This support is clamped on the steel way..

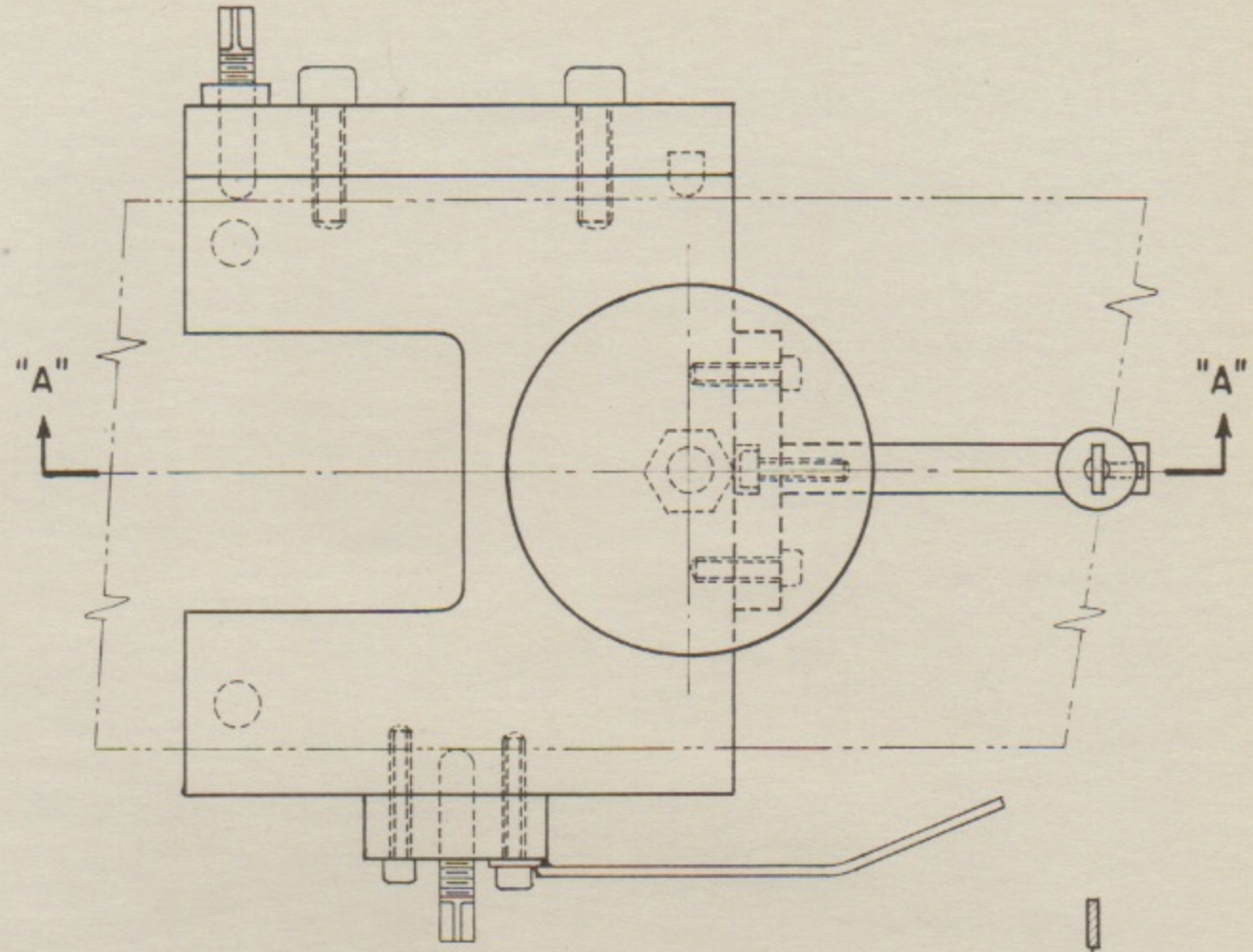

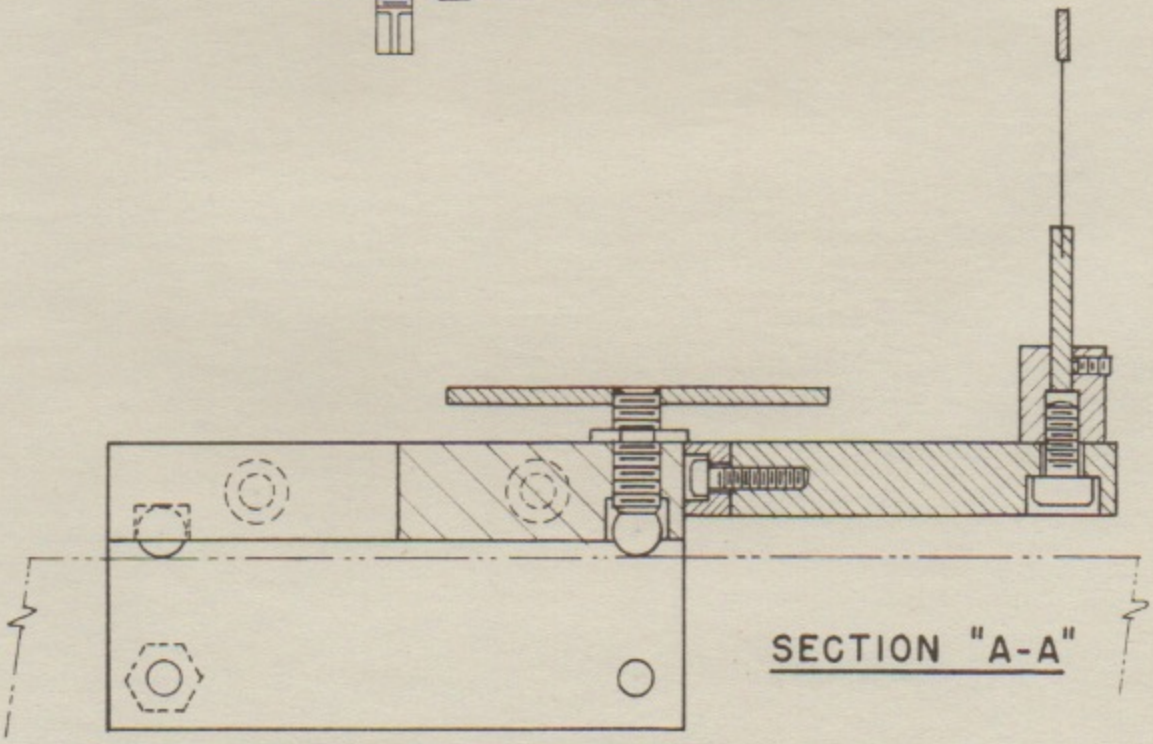

SECTION "A-A"

BEAM STOP SUPPORT

Figure 9

The adjustable vacuum chamber. This chamber replaces the helium bellows when large angles are measured. It attaches to the front of the annular slit diaphragm.

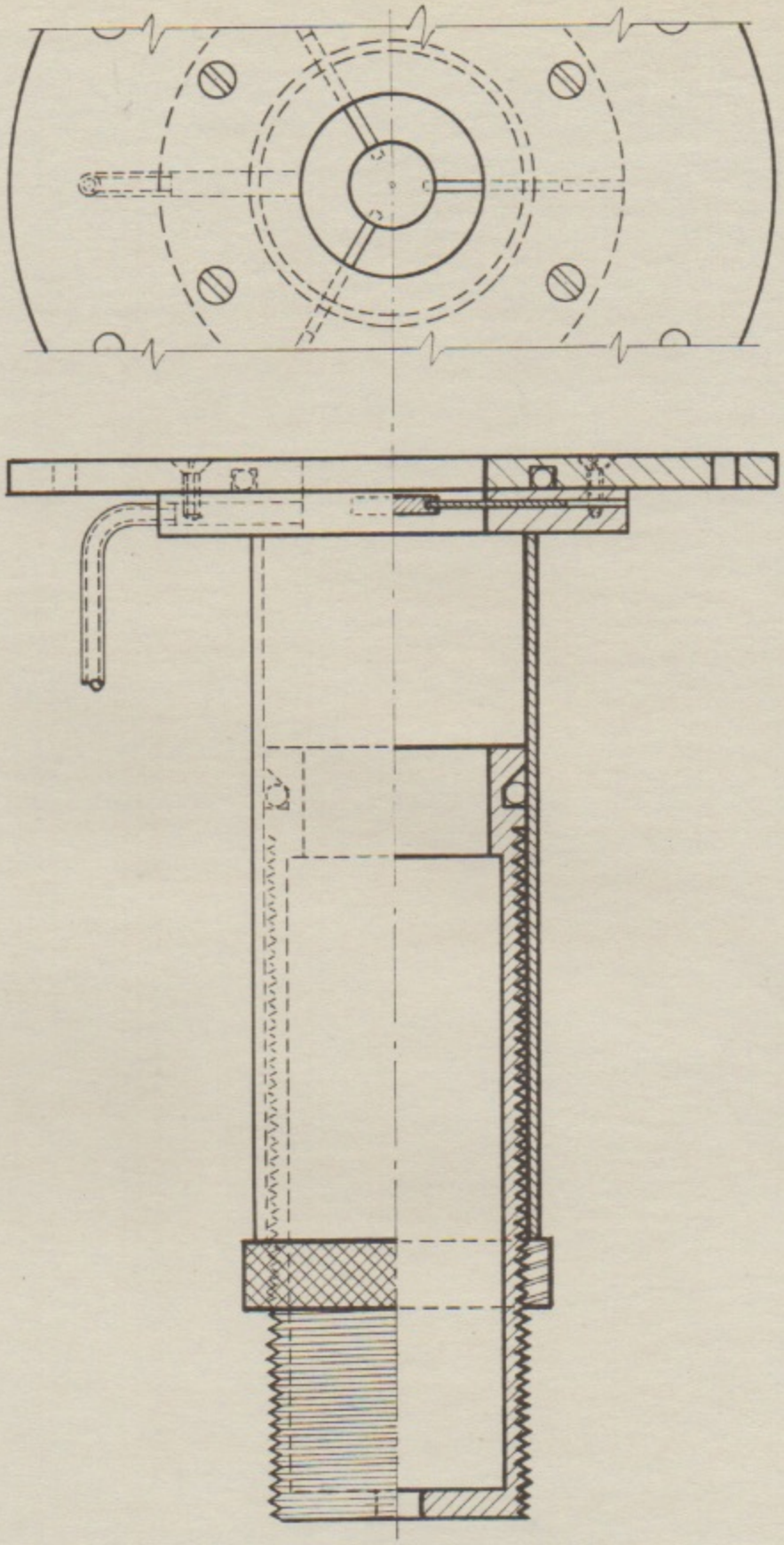

ADJUSTABLE VACUUM CHAMBER

It consists of two concentric brass tubes, the inner one being threaded on the outside except for the short length which contains an O-ring seal. A knurled keeping ring screws over this tube to hold it at the desired extension. The end plate is fitted to attach to the front of the annular slit diaphragm. The ¼" front hole is covered with an .8 mil mica window. The 1" rear opening has a ½" central support disc and is covered with 5 mil polyethylene. The combined transmission of the windows is .77 for Cu K-alpha radiation. The chamber is evacuated through the side tube in the end plate by a mechanical fore-pump. It is necessary to break the vacuum for each re-setting of the chamber length. The space between the front end of the vacuum chamber and the sample, occupied by the guard ring plug, is filled with helium by attaching a small polyethylene bag between the front face of the chamber and a brass plate which seals against the guard ring support.

d. The Slide

The slide on which the annular slit diaphragm and proportional counter are mounted is a 4" x 8" x ½" piece of brass with two vertical extensions at the ends of one side and one centered longer one (not visible in Figure 4) on the other side. The bottom of the slide was ground and then milled to make contact with the way on ½" wide by 2" long surfaces at each corner. The two vertical side pieces are 2" long and are ground and fitted to the side of the way. A spring housed in the central extension on the opposite side

keeps these side pieces in contact with the way. A block of brass secured laterally to the front of the top face of the slide acts as a support to which the annular slit diaphragm is screwed and also as the front piece of a cradle in which the proportional counter is strapped. An index at the front edge of the slide is set at the desired scale reading.

e. Annular Slit Diaphragm

The annular slit diaphragm is constructed in the same way as the pinhole diaphragm shown in Figure 7. It is 4½" in diameter and its adjustable steel ring contains a large conically bevelled hole to take the annular slit brass conical inserts. These inserts are about 1-3/4" in diameter and have a 1" center hole. The annular slits are made of 1/16" thick steel. An outer ring and an inner disc are made to fit concentrically and provide the desired slit diameter and width. A 1/16" center hole is bored in the disc for later use in aligning the system. The disc is accurately positioned inside the ring with the aid of a special jig. The two are then bridged with scotch tape and mounted on the end of their brass insert. The mounting holes are drilled with the aid of a jig to assure central alignment of the annular slit. The opening at the rear of the diaphragm is covered with 2 mil polyethylene which has a transmission of about .97 for Cu K-alpha radiation.

f. Proportional Counter Detector

The proportional counter[2], replaces the usual Geiger counter tube and Ross filters for detection and monochroma-

tization of the scattered radiation. Its advantages are the larger diameter windows obtainable and the elimination of the double count required with Ross filters. The counter was constructed by R. H. Neynaber. It is 3" in diameter, 9" long and has a window of .3 mil nickel foil 1" in diameter. The pre-amplifier[3], M in Figure 4, is attached directly to the detector. The output of the pre-amplifier is directed to an amplifier[4], and then to a single channel differential discriminator.[5] The output pulses of the discriminator are recorded by a conventional scalar after being inverted. The operating characteristics of the proportional counter will be discussed in paragraph D 3.

The .3 mil nickel window differentially attenuates Cu K-beta over Cu K-alpha radiation so that only about 8 per cent of the transmitted radiation is Cu K-beta.

6. Alignment Procedure

The steel way was bolted in place on the I-beam and its alignment checked and corrected as follows. To check for horizontal deviation from linearity a 1.5 mil molybdenum wire was stretched the length of the way and a few inches above it. A travelling microscope was then secured to the slide in a position to measure horizontal displacement from the wire. The slide was moved over the length of the way and readings of the relative positions of the wire were taken every 5 cm. This was repeated and the results plotted. The horizontal deviation was found to be less than 1 mil, so no corrective measures were taken. To check vertical

alignment two methods were used. In the first, the same wire used above was viewed from the side and readings were taken as before. The resulting curves were compared to the theoretical catenary for the wire, which was under a known tension, to determine deviations of the way alignment. The second method employed a telescope with a Gaussian eyepiece. The telescope was mounted a few feet from the end of the way with its axis parallel to the way. A plane mirror was fixed to the slide with its face perpendicular to the line of motion of the slide on the way. With the slide at an extreme end of the way, the telescope, focused on infinity, was accurately pointed at the mirror to bring the cross-hairs and their reflected image into alignment. The displacement of the horizontal cross-hair image then gave a relative measure of the slope of the way for different positions of the slide. A curve plotted from these readings was integrated graphically to give the displacement curve. The results for the two methods were in good agreement. The maximum deviation found was 5 mils. Shims were then introduced under the appropriate supports to neutralize the deviations and a re-check of the alignment indicated that the way was then straight to within less than 1 mil.

To align the pinholes and annular slit, a telescope, focused on infinity, was pointed toward the rear of the system from a position in front of the pinhole tube (see Figure 4) and the hole in the center of the annular slit was

illuminated with a sufficiently diffuse source of monochromatic light placed behind it. A guard ring aperture was then inserted in the guard ring support and the annular slit was positioned near its maximum distance from the guard ring. The point source of light from the center of the annular slit was diffracted by the guard ring aperture and the telescope was aligned to center the observed Fraunhofer diffraction pattern on the cross-hairs. This placed the axis of the telescope parallel to the center line through the annular slit and guard ring. The annular slit was then moved forward to nearly the minimum distance and the observed shift in the diffraction pattern used to correct the lateral position of the annular slit and telescope. The annular slit was then moved back to its former position and the process repeated until the pattern remained centered over the whole range of the annular slit positions. The axis of the telescope was then on a line through the center of the guard ring and parallel to the motion of the slide on the steel way. With the telescope still in place, the guard ring was removed and the .25 mm diameter second pinhole was inserted and adjusted until its diffraction pattern was centered. This was repeated with the first pinhole. It was observed that displacement of the pinhole due to less than 1/20th of a turn of the #28 set screws could be detected. This indicates an accuracy of alignment better than $\pm$ 2 mils.

7. Sample Holders

Sample holders required for x-ray scattering from solutions must have maximum transmission, maximum sample scattering, minimum background scattering and be leakproof.

The intensity of the transmitted scattered radiation from a sample will be proportional to the product of the thickness of the sample, t, and the absorption factor, $e^{-\mu t}$, where μ is the absorption coefficient for the sample. The optimum thickness of the sample holders is quickly found from the derivative of $te^{-\mu t}$ to be $1/\mu$. For protein solutions in water this is very nearly 1 mm and small deviations from this are not critical. Sample holders have been constructed from 3" x 3/4" x 1/16" Lucite strips. A 3/8" hole is bored through the center of the strip and counter bored on each side with a 9/16" bore to give a 1 mm thickness. Discs 9/16" in diameter are cut from low scattering, high transmission mica .015 mm thick and cemented in the insets to form the chamber windows. A hole is drilled into the chamber from one side of the strip using a #73 drill. The holders are filled with a hypodermic with a #25 needle through this hole. The holders are thoroughly flushed with distilled water between fillings. The transmission of the empty sample holder is 0.75 for Cu K-alpha radiation.

It was only after a considerable amount of testing of 16 different cements that a cold-hardening, truly waterproof cement was found for cementing the mica discs in place. The

only satisfactory cement found was Goodyear Pliobond, though cold-hardening Araldite 101 may be adaptable for use. No cellulose base cements are waterproof and the heat-hardened cements could not be used because of the tendency to warp the mica or damage the relatively low melting point Lucite. Attempts to use glass holders were generally unsatisfactory.

D. Operation and Performance of the Apparatus

In general, the pinhole collimating system performs with all the advantages that were expected from the design. In comparisons of data taken with it to data taken with a slit collimating system, the same information could be obtained in less time or with better statistics with the pinhole system. There is excellent agreement between direct pinhole data and slit corrected data. Furthermore, some experiments with relatively large spherical particles indicate that the peak resolution is better than that obtained with slits of comparable width resolution. The following discussion will provide more specific operational information.

1. Cathode Assembly (see B in Figure 5)

It was found that the heat from the filament conducted up the steel cathode support tube raised the temperature of the top brass plate considerably. To protect the O-ring seal, therefore, an arrangement has been provided which directs a continual stream of air on this plate.

The top of the anode in the annular region exposed to

the electron beam becomes slightly etched after a few hundred hours exposure. So far this has been easily removed with light polishing, but it indicates that at 2400 watts the tube is operating near its power limit.

2. Intensity

The alignment and transmitted radiation flux have been well established for the slit collimating system which uses the vertical focal line (see Figure 5). Therefore, it was useful to compare the intensities obtained with the pinhole collimating system to those of the slit collimating system. The expected ratio of these intensities can be calculated from the geometries of the two systems. Assume that the total radiation entering the system is the same in both cases, i.e., that both see the same proportion of the focal spot at the same values of tube voltage and current. Then, the following factors must be considered: the ratio of the solid angles intercepted by the sample in the pinhole and slit systems, ω_1/ω_2, the ratio of the solid angles intercepted by the detector slits, ω_3/ω_4, and the ratio of detector sensitivities, B. The final ratio, $\frac{\omega_1 \omega_3 B}{\omega_2 \omega_4}$, can be calculated from the geometry and experimental determination of B. It can be expressed as

$$\frac{I_p}{I_s} = \frac{\pi^2 D t a_1^2 (d_2 + 12.5)^2 L_2^2 B}{4 (a_2 h_2)^2 (d_1 + 10)^2 L_1^2}$$

where a_2 and h_2 are the slit width and height, respectively, and the other terms are as defined previously. The experi-

mental ratio was determined from carbon scattering reference intensities for the two systems. Each system has a separate standard scatterer adaptable to its sample holder. However, since reference readings are taken at 12 x 10^{-3} radians on the slit system and at 6 x 10^{-3} radians on the pinhole system, a conversion factor nad to be experimentally determined to compare references. It was found that standard pinhole scatterer values multiplied by 37.5 were equivalent to standard slit scatterer values. An intensity comparison was made under conditions for which the geometries established the calculated ratio as 29.4 to 1. The reference intensity obtained under these conditions on the pinhole system was 75 c/s. The slit system gave 100 c/s. Therefore, the actual experimental intensity ratio was 37.5 x 75/100 or 28.1. This compares very favorably with the calculated ratio of 29.4.

3. Proportional Counter

The proportional counter prepared by the original designers[2] was operated at 1500 to 2100 volts with a circuit amplification factor of from 10^3 to 10^5. They obtained a relative mean pulse height difference for Cu K-alpha and Fe K-alpha radiation of 20.7 per cent and a relative standard deviation of 7.5 per cent for the spread of the Cu K-alpha pulse height distribution. The counter used in these experiments was operated at 1800 to 2100 volts with an amplification factor of about 10^4. The response of the discriminator circuit to the Cu K-alpha pulse height distribution for

different counter voltages and amplifier settings is shown in Figure 10. A point on any one curve indicates the relative number of pulses received with an amplitude equal to that channel setting, D. The width of the channel used in obtaining these curves was 1.2 volts. In practice, the counter voltage and amplifier setting were adjusted to place the maximum somewhere between 12 and 16 on the differential bias abscissa, and a channel width of 4.0 volts was used. The small peaks at lower D values than the Cu K-alpha peaks are in the correct position to indicate the presence of a small amount of Fe flourescence. The resolution of the instrument was approximated from individual peak determinations under normal operating conditions for Fe flourescence and Cu K-alpha scattering. The relative pulse height difference for Cu - Fe was about 22 per cent. Assuming that pulse height is a linear function of λ in this region, the dispersion is about 0.11 Å per volt change in bias setting. Thus, the normal channel width used was .44 Å wide. The theoretical band width obtainable with balanced Ross filters is .11 Å. However, the additional spread introduced by the proportional counter statistics requires the use of the larger effective channel width to obtain comparable intensity. Because of the high intensity ratio of Cu K-alpha radiation to other wave lengths received, this has not been serious. The proportional counter output has been checked against Ross filters for various channel widths to verify this. The ratio

Figure 10

Curves showing the response of the discriminator circuit to the Cu K-alpha pulse height distribution for different combinations of counter voltage and amplifier setting. The total amplification for which each curve was obtained increases to the right.

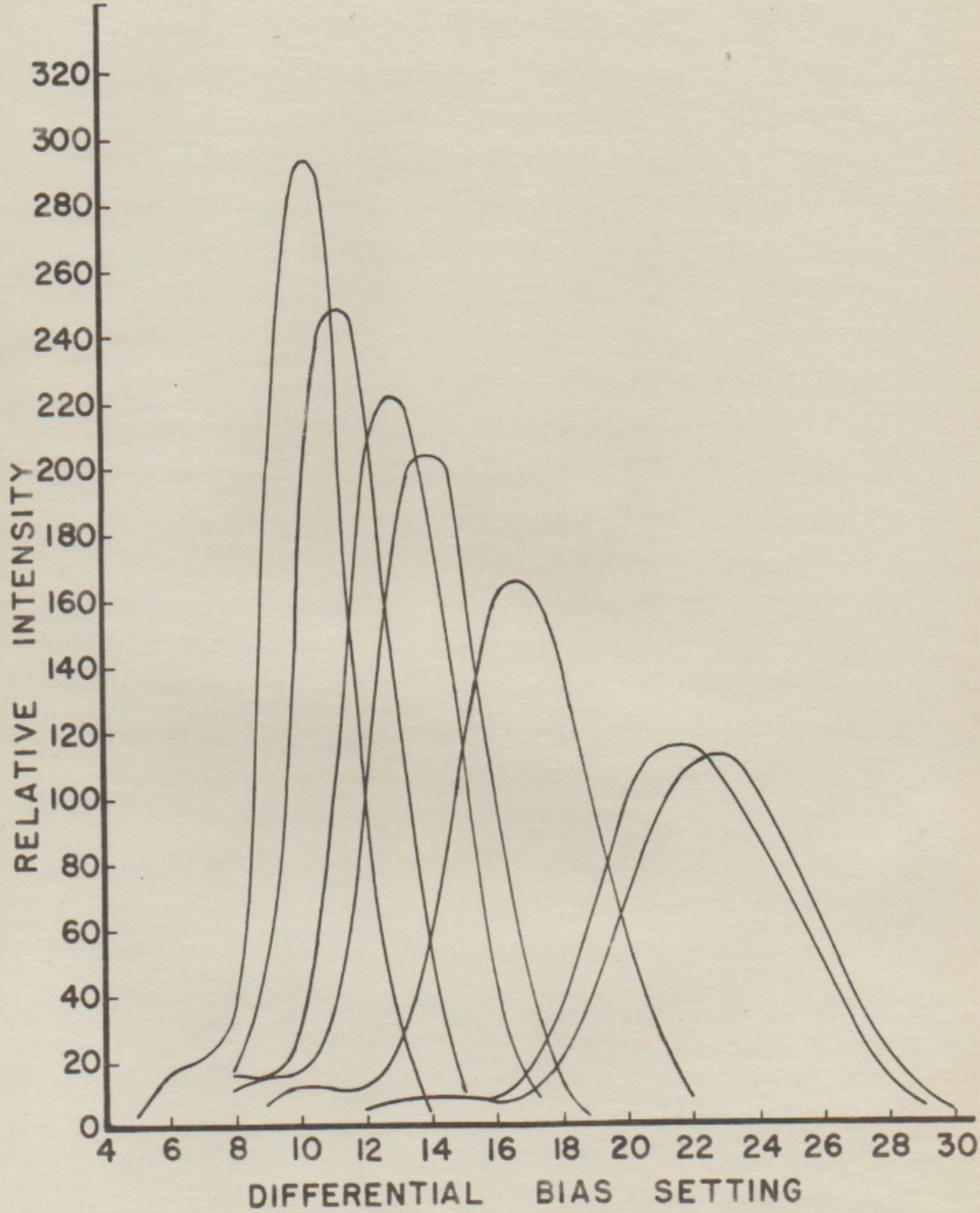
RELATIVE INTENSITY
320
300
280
260
240
220
200
180
160
140
120
100
80
60
40
20
0
4
6
8
10
12
14
16
18
20
22
24
26
28
30
DIFFERENTIAL BIAS SETTING

of intensities measured with and without filters remained constant to within 3 per cent for channel widths varying from 1.2 to 6.7 volts, indicating that the widest channel could be used without much loss of monochromatization. The statistical spread of the impulses by the ionization processes in the counter can be estimated from the average number of ion pairs produced per photon. Assuming 33 ion pairs per kv, this is 264 ion pairs per Cu K-alpha photon. The relative standard deviation, σ/N is then $\frac{\sqrt{264M}}{264}$, where M is a factor introduced to account for the effect of gas multiplication. M is not known very well but lies between 1 and 2. Thus, σ/N = 6.2 per cent to 8.7 per cent. The experimental deviation for the counter is found, from half-widths at .607 maximum intensity, to be about 11 per cent. This is outside the range expected and greater than the value obtained by the designers. This may be explained by the fact that a larger window is used on this counter than specified. This could cause field distortions which affect the linearity enough to give the observed increase in spread.

When the proportional counter is operated as an integral counter using the total integrated output with Ross filters, it is about 10 per cent less efficient than a Phillips Geiger tube. At the normal operating channel width of 4.0 volts, with maximum channel setting at 14.0 volts and without Ross filters, the proportional counter was only about 7 per cent more effecient than the Geiger counter because of the statistical spread. The use of a channel width of 6.7

volts increases the advantage to 55 per cent. Since the transmission of the Ross filters is about .5 for Cu K-alpha radiation, a theoretical advantage of 90 per cent is obtainable.

4. Helium Bellows

Despite the precautions taken to make the helium bellows a leak-proof system it was found necessary to keep helium flowing into the bellows at a constant rate of about a liter per minute. This rate was determined experimentally by observing the intensity loss rate for various flow rates. As a further precaution the bellows was flushed out periodically when in use.

5. Background

The room background depended upon the discriminator channel width used. For the normal 4.0 volt channel this background was 0.40 c/s compared to 0.36 c/s for a Phillips Geiger counter. The background due to pinhole edge scattering and helium scattering from in front of the stop depended upon the sizes of the components used.. For .5 mm pinholes and a 2 cm diameter annular slit with 2 mm slit width this background increased from about 1 c/s to 2 c/s over the range of the helium bellows from maximum to minimum extension. In the vacuum chamber the background was larger, going from about 2 c/s to 4 c/s over its range. However, when the $1/r^2$ factor is taken into account, the pinhole system backgrounds are of about the same magnitude or smaller than those for the

slit system under equivalent conditions. It can be expected that the background will be significantly reduced with the incorporation of a vacuum chamber extending the full distance from sample holder to annular slit for all angles.

II. Theory of X-ray Scattering from Macromolecules

A. General Theory

In this section a general theory will be developed for the intensity distribution of x-ray scattering from particles with rotational symmetry and uniform electron density. Only the coherent scattering will be considered since the incoherent Compton scattering is important only for higher energy radiation or larger scattering angles.

Consider a particle of matter of arbitrary shape which contains n electrons. If it is placed at a given orientation to a collimated beam of x-rays it can be shown[6] that the intensity distribution of the coherent scattering is given by

$$I = I_e n^2 f^2 \tag{1}$$

In this expression I_e is the Thompson scattering distribution for a single electron and f is the electronic structure factor defined by

$$f = \frac{1}{n} \sum_{j=1}^{n} e^{i\delta_j} \tag{2}$$

where δ_j is the phase difference between scattering from an electron at the origin and the jth electron. Also, f can be put in integral form by introducing the probability, PdV,

that an electron be found in volume dV, where enP is just the charge density and e the electronic charge. Then f is given by

$$f = \int_V e^{i\delta} P dV \tag{3}$$

In this application, x-rays will be assumed scattered from a large number of identical particles randomly oriented with respect to the beam. In this case the total scattered intensity is found by averaging the intensity for an arbitrary orientation over all possible orientations of the particle and multiplying by the number of particles. Since only rotationally symmetric particles will be considered, only two angles are necessary to describe the particle orientation. In addition, by choosing the Z axis of the laboratory system as the bisector of the supplement to the scattering angle, the phases of the scattering from the electrons in any given plane perpendicular to this axis are equal. This makes the scattering from the particle independent of the particle orientation about the laboratory Z axis. Therefore, it is only necessary to average the intensity over the angle between the axis of symmetry of the particle and the laboratory Z axis. Since for any increment of this angle, $d\gamma$, an increment of solid angle of $2\pi \sin\gamma d\gamma$ is subtended, the weighted average of the intensity becomes

$$I = I_e N n^2 \int_0^{\frac{\pi}{2}} f^2 \sin\gamma d\gamma \tag{4}$$

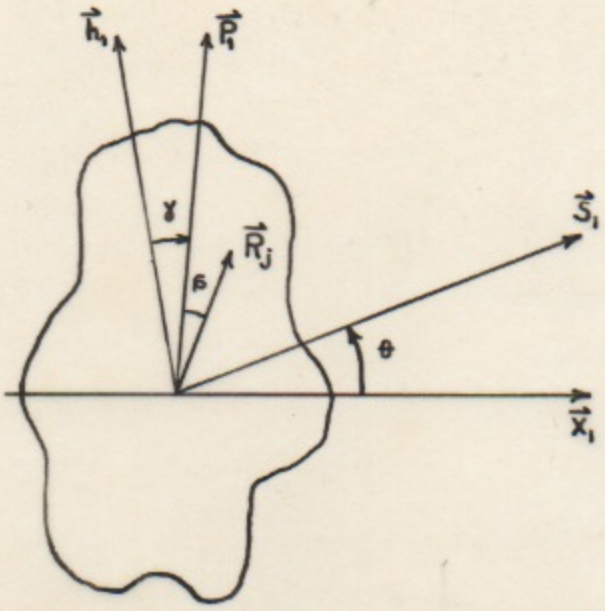

The figure to the left represents a particle of arbitrary shape in a beam of x-rays. All vectors with the subscript "1" are unit vectors. The vector $\vec{x}_1$ is the direction of the incident x-rays. $\vec{P}_1$ defines the Z axis of the particle coordinate system. $\vec{S}_1$ is the direction of radiation scattered at an angle, Θ. For convenience, $\vec{h}_1$ is chosen to bisect the supplement of the scattering angle, Θ. Also, $\vec{h}_1$ will be taken as the Z direction of the reference or laboratory coordinate system. As a result of this choice for the direction of $\vec{h}_1$, scattering at the same angle will be in phase from all the electrons in any plane perpendicular to $\vec{h}_1$. The vectors $\vec{h}_1$, $\vec{x}_1$, and $\vec{S}_1$ are in the same plane. $\vec{R}_j$ is the position vector of the jth electron in the laboratory coordinate system. The phase of the radiation scattered from the jth electron relative to the origin is given by

$$\delta_j = k(\vec{R}_j \cdot \vec{h}_1) \quad \text{where } k = \frac{4\pi}{\lambda} \vec{h}_1 \cdot \vec{x}_1 = \frac{4\pi \sin \Theta/2}{\lambda}$$

Let $\vec{\rho}$ be the radius vector of any point in the particle coordinate system, then

$$f = \int_V e^{ik[M]\vec{\rho}\cdot\vec{h}_1} \rho dV \qquad (5)$$

[M] is the necessary matrix to make the transformation

$$\vec{R} = [M]\vec{\rho}$$

It is given by

$$[M] = \begin{bmatrix} l_1 & l_2 & l_3 \\ m_1 & m_2 & m_3 \\ n_1 & n_2 & n_3 \end{bmatrix}$$

where the l, m, n are the appropriate direction cosines of each P axis (1,2,3) with respect to the x,y,z (l,m,n,) axes of the laboratory coordinate system.

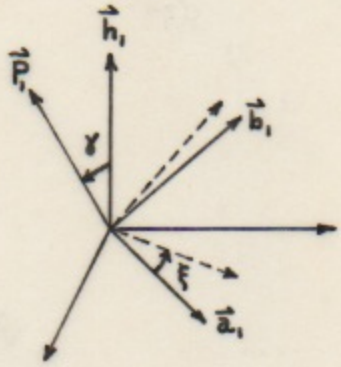

Referring to the diagram to the left, the laboratory coordinate system is represented by $\vec{h}_1$ and the unlabeled axes perpendicular to it. The particle system of coordinates is represented by $\vec{P}_1$, $\vec{a}_1$, $\vec{b}_1$. The direction of $\vec{a}_1$ in the plane perpendicular to $\vec{P}_1$ is arbitrary, so take it such that

$$\vec{a}_1 = [\vec{h}_1 \times \vec{P}_1]$$

Expanding $[M]\vec{\rho}\cdot\vec{h}_1$

$$\vec{R}\cdot\vec{h}_1 = [M]\begin{bmatrix} \rho_x \\ \rho_y \\ \rho_z \end{bmatrix}\cdot\vec{h}_1 = (\vec{b}_1\cdot\vec{h}_1)\rho_x + (\vec{a}_1\cdot\vec{h}_1)\rho_y + (\vec{P}_1\cdot\vec{h}_1)\rho_z$$

Introducing the angle of rotation of the $\vec{P}_1$ coordinate systems about $\vec{P}_1$, ξ, this becomes

$$\vec{R}\cdot\vec{h}_1 = \rho_x \sin\gamma\cos\xi + \rho_y \sin\gamma\sin\xi + \rho_z\cos\gamma$$

Now introduce cylindrical coordinates (r,α, z) into the particle coordinate system

$$\rho_x = r\cos\alpha\,,\quad \rho_y = r\sin\alpha\,,\quad \rho_z = z \qquad (r = \rho\sin\phi\,).$$

If the origin is chosen at the center of mass of the particle and it is rotationally symmetric about $\vec{P}_1$, then all orientations of the particle can be represented by γ and either α or ξ. Choose $\xi = 0$. Then

$$\vec{R}\cdot\vec{h}_1 = r \sin\gamma \cos\alpha + z \cos\gamma$$

PdV is obviously

$$\frac{r\,dr\,d\alpha\,dz}{V}$$

so

$$f = \frac{1}{V}\int_0^{2\pi} d\alpha \int_0^a r\,dr\, e^{ikr\sin\gamma\cos\alpha} \int_{-F(r)}^{F(r)} e^{ikz\cos\gamma}\, dz \qquad (6)$$

where $z = F(r)$ is the equation of the curve which is rotated to give the symmetric partical form.

Since

$$J_o(x) = \frac{1}{\pi}\int_0^{\pi} e^{ix\cos\phi}\, d\phi$$

f can be written

$$f = \frac{4\pi}{Vk\cos\gamma}\int_0^a r \sin\left[k\cos\gamma\, F(r)\right] J_o(kr\sin\gamma)\, dr \qquad (7)$$

This, then, is an expression for the electronic structure factor of a particle of rotational symmetry whose axis of rotation makes an angle of γ with a fixed laboratory axis. It is expressed as an integral over the particle coordinate system.

This integration will now be performed and the final expression for the intensity distribution will be obtained

for a few special cases. In most cases the final integration over γ cannot be performed.

1. Spheres

$$F(r) = \sqrt{a^2 - r^2}$$

There is no need to average over γ so

$$I = Nn^2 I_e f^2$$

and taking $\gamma = 0$, $J_o(0) = 1$, so

$$f = \frac{3}{a^3 k}\int_o^a r \sin\left[ka\sqrt{a^2 - r^2}\right] dr \qquad (8)$$

The proper transformations make this

$$f = \Phi(ka) = \frac{3}{(ka)^3}\int_o^{(ka)} x \sin x dx = 3\frac{\sin(ka) - (ka)\cos(ka)}{(ka)^3} \qquad (9)$$

and

$$I = Nn^2 I_e \Phi^2(ka) \qquad (10)$$

Note that $\Phi(u) = 3\sqrt{\frac{\pi}{2}}\frac{J_{3/2}(u)}{u^{3/2}}$

2. Cylinders

$$F(r) = H, \quad (0 \leq r \leq a), \quad F(r) = 0, \quad (r > a)$$

where the length of the cylinder is 2H, its radius a. Then

$$f = \frac{2\sin(kH\cos\gamma)}{ka^2 H\cos\gamma}\int_o^a rJ_o(kr\sin\gamma)dr \qquad (11)$$

Using

$$\int_o^a rJ_o(r)dr = aJ_1(a)$$

and substituting in (4), the scattered intensity from cylinders is given as

$$I = I_e N n^2 \int_0^{\frac{\pi}{2}} \frac{\sin^2(kH\cos\gamma)}{(kH\cos\gamma)^2} \cdot \frac{J_1^2(ka\sin\gamma)}{(ka)^2\sin\gamma}\, d\gamma \qquad (12)$$

3. Ellipsoids of Revolution

$$F(r) = v\sqrt{a^2 - r^2}\,, \qquad (0 \leq r \leq a)$$

Let $r = a\sin\beta$, $dr = a\cos\beta\, d\beta$, $F(r) = va\cos\beta$

Then

$$f = \frac{3}{kav\cos\gamma} \int_0^{\frac{\pi}{2}} \sin\beta\cos\beta\sin(kav\cos\gamma\cos\beta) J_0(ka\sin\gamma\sin\beta)\, d\beta \qquad (13)$$

Now

$$J_0(ka\sin\beta\sin\gamma) = \sum_{j=0}^{\infty} \frac{(-1)^j (ka)^{2j}}{\Gamma^2(j+1)2^{2j}} (\sin\beta\sin\gamma)^{2j}$$

$$\sin(kav\cos\gamma\cos\beta) = \sum_{i=0}^{\infty} \frac{(-1)^i (kav)^{2i+1}}{\Gamma(2i+2)} (\cos\gamma\cos\beta)^{2i+1}$$

so

$$f = \sum_i \sum_j \int_0^{\frac{\pi}{2}} \frac{(-1)^{i+j} (ka)^{2(i+j)} v^{2i} \sin^{2j}\gamma\cos^{2i}\gamma}{2^{2j}\Gamma^2(j+1)\Gamma(2i+2)} \cdot \sin^{2j+1}\beta\cos^{2i+2}\beta\, d\beta \qquad (14)$$

Since

$$\int_0^{\frac{\pi}{2}} \sin^{2j+1}\beta\cos^{2i+2}\beta\, d\beta = \frac{\Gamma(j+1)\Gamma(i+3/2)}{2\Gamma(i+j+5/2)}$$

and

$$\Gamma(i+3/2) = \frac{\sqrt{\pi}\,\Gamma(2i+2)}{2^{2i+1}\Gamma(i+1)}$$

then

$$f = \frac{3\sqrt{\pi}}{4} \sum_i \sum_j \frac{(-1)^{i+j} (ka)^{2(i+j)} \sin^{2j}\gamma\, (v\cos\gamma)^{2i}}{2^{2(i+j)}\Gamma(i+j+5/2)\Gamma(i+1)\Gamma(j+1)} \qquad (15)$$

Noting that

$$C^{i+j}_{i \text{ or } j} = \frac{\Gamma(i+j+1)}{\Gamma(i+1)\Gamma(j+1)}$$

and letting

$$x = \sin^2\gamma, \quad y = v^2\cos^2\gamma, \quad A_{(i+j)} = \frac{(-1)^{i+j}(ka)^{2(i+j)}}{2^{2(i+j)}\Gamma(i+j+5/2)\Gamma(i+j+1)}$$

then

$$f = \frac{3\sqrt{\pi}}{4} \sum_i \sum_j A_{(i+j)} C^{i+j}_{i \text{ or } j} \; x^j y^i \tag{16}$$

The terms of this series can be represented by an array of ordered pairs:

(0,0)	(1,0)	(2,0)	(3,0)	(4,0)	. . .
(0,1)	(1,1)	(2,1)	(3,1)	⋮	
(0,2)	(1,2)	(2,2)	⋮		
(0,3)	(1,3)	⋮			
(0,4)	⋮				
⋮					

It can be shown that this repeated series is absolutely convergent. Therefore the order of the summation may be changed. It is apparent that all the terms of this series are available by rearranging the summation to add the terms diagonally

$$f = \frac{3\sqrt{\pi}}{4} \sum_{i+j=0}^{\infty} \sum_{i \text{ or } j=0}^{i+j} A_{(i+j)} C^{i+j}_{i \text{ or } j} \; x^j y^i \tag{17}$$

For $i + j = n$

$$f = \frac{3\sqrt{\pi}}{4} \sum_{n=0}^{\infty} \left[A_n \sum_{i=0}^{n} C^n_i \; x^{n-i} y^i \right] \tag{18}$$

where the terms in the bracket are just those for the nth diagonal. Then, since

$$\sum_{i=0}^{n} C_i^n x^{n-i} y^i = (x + y)^n ,$$

$$f = \frac{3\sqrt{\pi}}{4} \sum_{n=0}^{\infty} A_n (x + y)^n$$

or

$$f = \frac{3\sqrt{\pi}}{4} \sum_{n=0}^{\infty} \frac{(-1)^n (ka)^{2n} (\sqrt{x + y})^{2n}}{2^{2n} \Gamma(n+5/2) \Gamma(n+1)} \tag{19}$$

Since

$$\Phi(u) = 3\sqrt{\frac{\pi}{2}} \frac{J_{3/2}(u)}{u^{3/2}} = \frac{3\sqrt{\pi}}{4} \sum_{\lambda=0}^{\infty} \frac{(-1)^\lambda u^{2\lambda}}{2^{2\lambda} \Gamma(\lambda+1) \Gamma(\lambda+5/2)}$$

Then

$$f = \Phi(ka\sqrt{x + y}) = \Phi(ka \sqrt{\sin^2\gamma + v^2 \cos^2\gamma}) \tag{20}$$

and

$$I = I_e N n^2 \int_0^{\frac{\pi}{2}} \Phi^2(ka \sqrt{\sin^2\gamma + v^2 \cos^2\gamma}) \sin\gamma d\gamma \tag{21}$$

Equations (10), (12), and (21) are all in agreement with expressions derived previously by different methods.[7]

B. Approximate Theory

1. Guinier[8] has shown that in the central region of the scattering curve a good approximation to the exact function is provided by

$$I = N n^2 I_e e^{-\frac{k^2 R^2}{3}}$$

where $k = \frac{4\pi \sin \theta/2}{\lambda}$, R equals the radius of gyration of

the particle about its center of mass, and θ is the scattering angle. The angular range of usefulness of this approximation depends upon the particle shape. It is generally more limited for very asymmetric particles, but is most extensive for slightly asymmetric particles rather than for spheres. For spheres the approximation is accurate to an error of less than five per cent out to angles where the intensity is 0.45 of the central maximum. Since θ is generally very small, $\sin \theta/2 \simeq \theta/2$ and

$$I = I_e N n^2 e^{-5.556 R^2 \theta^2}$$

evaluating for the Cu K-alpha line. The radius of gyration can easily be determined from a plot of log of intensity versus angle squared.

$$\frac{d \ln I}{d\theta^2} = - 5.556 R^2$$

2. A method has been developed for using $\ln \frac{I}{\Lambda}$ vs. θ^2 plots in regions where the exact function deviates from the Guinier approximation by not more than a few per cent. Accuracy is thus gained by using a more extended range of the experimental data. The actual theoretical curve on a ln I vs. θ^2 plot over this extended range deviates slightly from a straight line. The statistical spread of the experimental points exceeds this variation, however, so the experimental curve is easily approximated by a straight line. But the slope in this region may deviate slightly from the slope at zero angle by an amount which depends on the shape

of the particle. From the complete scattering curve an estimate of shape is obtained and from the theoretical scattering curve for this shape is calculated a correction to the experimental radius of gyration. The observed slope must be corrected first for certain systematic errors in the method of measurement.. For serum albumin the correction is accidentally negligible, but for hemoglobin it amounts to about 3 per cent.

3. An approximation with any desired accuracy can be obtained by expanding the perfectly general Debye relationship. The Debye relationship gives the scattering averaged over all orientations of a particle consisting of a group of electrons arranged at fixed distances from each other. This expression is

$$I = I_e \sum_{m=1}^{n} \sum_{l=1}^{n} \frac{\sin k|\vec{r}_{lm}|}{k|\vec{r}_{lm}|} , \qquad k = \frac{4\pi \sin \theta/2}{\lambda}$$

where $|\vec{r}_{lm}|$ = the distance from the lth to the mth electron,

θ = the scattering angle, and

n = the number of electrons.

Substituting

$$\frac{\sin k|\vec{r}_{lm}|}{k|\vec{r}_{lm}|} \equiv \sum_{j=0}^{\infty} \frac{(-1)^j}{(2j+1)!} (k|\vec{r}_{lm}|)^{2j}$$

rewriting in terms of distances from an origin at the center of mass

$$|\vec{r}_{lm}| = |\vec{r}_l - \vec{r}_m|, \quad |\vec{r}_{lm}|^2 = (r_l^2 - 2\vec{r}_l \cdot \vec{r}_m + r_m^2)$$

this becomes

$$I = I_e \sum_{l=1}^{n} \sum_{m=1}^{n} \sum_{j=0}^{\infty} \frac{(-1)^j k^{2j}}{(2j+1)!} (r_l^2 - 2\vec{r}_l \cdot \vec{r}_m + r_m^2)^j$$

Expanding and dropping sums which are zero because of symmetry or from choosing the origin at the center of mass, and multiplying by N, the number of particles,

$$I = Nn^2 I_e \left[1 - \frac{1}{3}(kR_2)^2 + \frac{k^4}{60}(R_4^4 + R_2^4 + 2T) - \frac{k^6}{42 \cdot 60}(R_6^6 + 3R_2^2 R_4^4 + 12U) + \ldots\right]$$

where (for particles with reflection symmetry in each of the coordinate planes)

$$nR_j^j = \sum_{i=1}^{n} r_i^j , \quad T = (R_2^2 - R_{xx}^2)^2 + (R_2^2 - R_{yy}^2)^2 + (R_2^2 - R_{zz}^2)^2$$

R_{xx}^2 = (radius of gyration about X axis)^2, etc.

$$U = \left[(R_2^2 - R_{xx}^2)\ (R_2^2 - R_{yy}^2)\ (R_2^2 - R_{zz}^2)\right] \begin{bmatrix} R_{x^4} & R_{x^2y^2} & R_{x^2z^2} \\ R_{x^2y^2} & R_{y^4} & R_{y^2z^2} \\ R_{x^2z^2} & R_{y^2z^2} & R_{z^4} \end{bmatrix}$$

$$nR_{x^2y^2} = \sum_{i=1}^{n} x_i^2 y_i^2 , \text{ etc.} \quad R_2^2 = \tfrac{1}{2}(R_{xx}^2 + R_{yy}^2 + R_{zz}^2)$$

Since it is difficult to expand this sufficiently to approach the accuracy of the Guinier approximation, the first few terms can be used to determine correction coefficients for the Guinier approximation

$$I = Nn^2 I_e e^{-\frac{k^2R^2}{3}} \left[1 + c_1 u^4 + c_2 u^6 + \ldots\right]$$

This has been done through c_2 for spheres and c_1 for ellipsoids. Defining new parameters $u = ka$ or $u' = kR_2$ (a = radius of symmetry at origin) one gets

$$I \text{ (spheres)} = Nn^2 I_e e^{-\frac{1}{3}u^2}\left[1 - \frac{1}{350}u^4 - \frac{2}{(15)^3 \cdot 7}u^6 + \cdots\right]$$

$$I \text{ (ellipsoids)} = Nn^2 I_e e^{-\left(\frac{2+v^2}{5}\right)\frac{u^2}{3}}\left[1 + \frac{1}{350}\left(\frac{19v^4 - 68v^2 + 4}{45}\right)u^4 + \cdots\right]$$

$$I \text{ (ellipsoids)} = Nn^2 I_e e^{-\frac{u'^2}{3}}\left[1 + \frac{1}{630}\left(\frac{19v^4 - 68v^2 + 4}{v^4 + 4v^2 + 4}\right)u'^4 + \cdots\right]$$

where v is the axial ratio.

The following table gives a few comparative values:

Spheres				Ellipsoids v = 2			
u	Guinier	I	Exact	u'	Guinier	I	Exact
1	.819	.817	.816	1	.717	.718	.717
2	.449	.426	.427	2	.264	.270	.274
3	.165	.117	.119				
3.5	.086	.032	.042				
4	.041	-.003	.008				

These values give some idea of the ranges of validity of the Guinier approximation and of the more exact approximation just developed. It is seen that these ranges are quite dependent on the particle shape.

C. Interparticle Interference Effect

Since the theories derived above all assume infinite dilution or separation of the particles, the actual experimental curves for finite concentrations would be expected to differ from the predicted ones.. This matter has been treated by Fournier for spheres.[9] The expression which he gives for the intensity is

$$I = Nn^2 I_e f^2 \frac{1}{1 + Kc\,\Phi(ks)} \qquad (A)$$

$Nn^2I_ef^2$ = infinite dilution intensity $\equiv I_o$

$K = \frac{V\rho_s N_o}{M}$

V = particle volume

ρ_s = density of solvent

M = molecular weight of particle

c = concentration of particles, gms/cc.

$\Phi(ks)$ = f, the square root of the scattering function, for spheres with radius s. The radius appearing here is the effective collision radius of the molecules and may be much greater than their diameter.

It is seen from this expression that for angles where $\Phi(ks)$ becomes very small, interparticle interference effects are negligible. Thus it is expected that the positions of minima and maxima will be unaffected for reasonable values of Kc.

The effect on the slope of the lnI vs. θ^2 curve can be found by taking the derivative of the corrected expression for I, using the following substitutions and approximations:

$$V = \frac{4}{3}\pi(\alpha a)^3, \quad s = \alpha a = 2a \text{ for hard spheres.}$$

$$\Phi(ks) \simeq \Phi(k\alpha a) = e^{-\frac{5.556\alpha^2R^2\theta^2}{2}}$$

$$K = \alpha^3 B, \quad B = \frac{4\pi\rho_s a^3 N_o}{3M}$$

Then

$$\frac{d \ln I}{d\theta^2} = -5.556R^2\left[\frac{1 - Bc\alpha^3(\frac{\alpha^2}{2} - 1)\Phi(k\alpha a)}{1 + Bc\alpha^3\Phi(k\alpha a)}\right] = -5.556R'^2$$

This can be written

$$R'^2 = R^2\left[\frac{1 - (\frac{\alpha^2}{2} - 1)x}{1 + x}\right] \simeq R^2\left(1 - \frac{\alpha^2 x}{2}\right), \text{ if } x \ll 1$$

where

$$x = Bc\Phi(k\alpha a)\alpha^3$$

Thus, for small c a plot of R' vs. c will give a straight line with slope,

$$-\frac{\alpha^2 x}{4c}R = -\frac{B\alpha^5\Phi(k\alpha a)}{4}R$$

and which extrapolates to R at c = 0. This provides a method for getting the true R despite interparticle interference effects. However, practical considerations place a limit on the lowest value of c available, so for too large B and α this particular method will be unsatisfactory. It is also apparent that if there is much non-linearity in the ln I vs. θ^2 curves, and this is the case for concentrations and angles of observation sometimes used, one must be careful to take the slope at the same angle for any series of concentrations.

D. Inherent Experimental Errors

1. Misalignment of the Collimating System

Since perfect alignment is unobtainable in practice, it is desirable to consider the effect of taking data with the center of the annular detector slit off the axis of the x-ray beam. Take the center of the beam at O and the center of the annular slit at a distance of Δz from it. Using the Guinier

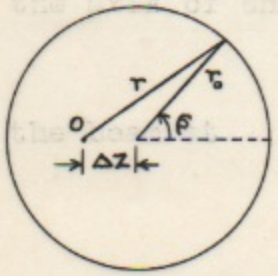

approximation,

$$I = I_o e^{-bR^2\theta^2}$$

where $\theta = \frac{r}{L}$, and b = 5.556 evaluating for the Cu K-alpha line. Let

$$\frac{r_o}{L} = \theta_o \, , \quad \frac{\Delta z}{r_o} = \epsilon$$

then

$$\theta^2 = \frac{1}{L^2}\left(r_o^2 + 2r_o\Delta z \cos\phi + (\Delta z)^2\right) \simeq \theta_o^2(1 + 2\epsilon\cos\phi)$$

The average intensity measured by the annular slit is

$$I = \frac{I_o}{\pi}\int_o^{\pi} e^{-bR^2\theta^2} d\phi = \frac{I_o}{\pi} e^{-bR^2\theta_o^2}\int_o^{\pi} e^{-c\cos\phi}\, d\phi$$

where

$$c = 2\epsilon bR^2\theta_o^2$$

Since

$$J_o(iy) = \frac{1}{\pi}\int_o^{\pi} e^{-y\cos\phi}\, d\phi$$

then

$$I = I_o J_o(ic) e^{-bR^2\theta_o^2}$$

$$\ln I = \ln I_o + \ln J_o(ic) - bR^2\theta_o^2$$

$$\frac{d \ln I}{d\theta_o^2} = -bR^2\left(1 + i2\epsilon \frac{J_1(ic)}{J_o(ic)}\right) \, , \text{ for } \epsilon \neq f(\theta_o)$$

$$\frac{J_1(ic)}{J_o(ic)} = \frac{ic}{2}\left[\frac{1 + \frac{c^2}{2\cdot 4} + \frac{c^4}{3\cdot 64} + \frac{c^6}{4\cdot 36\cdot 64} + \cdots}{1 + \frac{c^2}{4} + \frac{c^4}{64} + \frac{c^6}{36\cdot 64} + \cdots}\right] \leq \frac{ic}{2}$$

So

$$R'^2 = R^2(1 - b\epsilon^2) \quad , \quad b \leq 2bR^2\theta_o^2$$

The error in measuring R is thus $\leq -(bR^2\theta_o^2)\epsilon^2$. For the apparatus used in these experiments $\epsilon < 10^{-2}$ and the error $< .005$ per cent. Since this approximation was made for the portion of the curve with rapidly changing I, it can be expected that the error in the peak region will be even less.

2. Effect of Imperfect Resolution

a. On Value of Radius of Gyration

The observed intensity at any nominal setting, θ, can be calculated by integrating the product of the angular distribution of radiation incident on the sample times the Guinier scattering function. This integration cannot be carried out for even the simplest distributions. However, using tabulated values of the error function and assuming constant effective incident intensity over the range, $\theta - \Delta\theta$ to $\theta + \Delta\theta$, it is easily shown that with the resolution and samples used here the observed radius of gyration cannot be in error by more than 0.5 per cent from imperfect resolution.

b. On Positions of Minima and Maxima

An analytical solution of this problem for the general case is very difficult even to approximate. However, a fairly well known geometrical method is very simple to use. Assuming constant effective incident intensity over the range, $2\Delta\theta$, the measured intensity at the angular setting, θ, is the area under the scattering curve from $\theta - \Delta\theta$ to $\theta + \Delta\theta$. No shift in the positions will result unless the minima and maxima are asymmetric as shown in the diagram

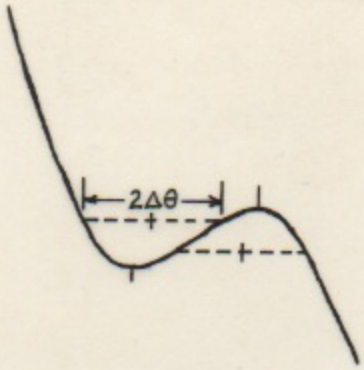

to the left of a hypothetical scattering curve. The experimentally measured minima and maxima are found by bridging the dips and peaks, as shown, with horizontal lines of length $2\Delta\theta$. It is apparent that a shift of these lines in either direction will measure more intensity for the minimum and less for the maximum. The error is then just the difference between the exact values on the curve and the centers of the $2\Delta\theta$ lines.

E. Scattering from Particles in Solution

In studying biological particles with x-ray scattering it is usually necessary or desirable to use them in aqueous solution. The scattered intensity from a particle is then proportional to the square of the electron density difference between the particle and the solvent.

The coeffecient of the angular part of the scattering function is then given by

$$Nn^2 I_e \left[1 - \left(\frac{\gamma}{\alpha\beta}\right)\right]^2$$

where the ratios of mass density, electrons per molecule, and molecular weight, of particle to solvent are given by, respectively, α, β, and γ. N is the number of particles irradiated, n the number of electrons per particle. To get

the total scattered intensity from the solution, the scattering from the solvent must be added to the differential scattering from the particles. At the small angles used the solvent scattering is generally small.

It is of interest to compare the zero angle scattering intensities expected from particles of different molecular weight.. For a given kind of particle the following parameters are needed:

N = number of particles irradiated

n = number of electrons per particle

η = number of electrons per unit volume

ρ = mass per unit volume

M = molecular weight

c = concentration

v = irradiated volume

Then

$$Nn^2 = \frac{cv}{N_o} \cdot \left(\frac{\eta}{\rho}\right)^2 M$$

If it is assumed that two different particles have equal electron and mass density, then if equal concentrations of them are similarly irradiated, the factor $\frac{cv}{N_o}\left(\frac{\eta}{\rho}\right)^2$ will be the same for both. This also makes the $\frac{\gamma}{\alpha\beta}$ ratios equal, so the ratio of intensities will just be

$$\frac{I_1}{I_2} = \frac{M_1}{M_2}$$

The assumptions for this result are quite valid for protein molecules.

III. Protein Experiments

A. Introduction

A protein is a polypeptide linkage of amino acids. All amino acids have the structure shown in the diagram below. The R is a variable which defines the particular type of amino acid and consists of various combinations of some or all of the elements, C, H, N, O, S, Fe, and P. Some rare proteins contain I and Cu. The structure at the left is in a dipolar ionic form which is the form in which proteins exist at the isoelectric point rather than as non-polar isomers.

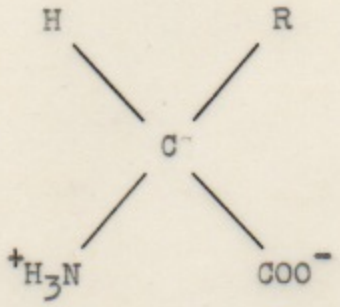

These amino acids combine by the affinity of the amino groups ($^{+}H_3N$) for the carboxyl groups (COO^{-}) and unite with the elimination of water to form chains as in the diagram below..

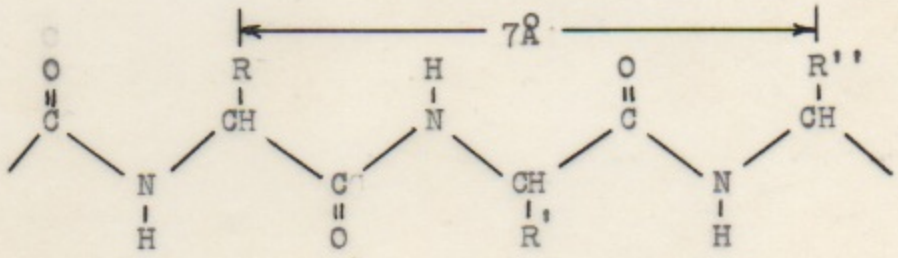

The properties of a given protein are determined by its characteristic sequence of amino acids. These chains then take on various shapes. A suggestion by Pauling and Corey[10] is that they are twisted in helices and that these in turn, in fibrous molecules, are joined like strands of rope.[11]

The helices coil up in some more complicated way in the globular molecules. The presence of many ions at large distances of separation gives all protein molecules a strong dipolar moment of the order of 10^3 Debye units. This moment, by producing high dielectric constants and other effects, can appreciably influence the chemical reactions of cells..

All living cells contain proteins. In the blood they carry oxygen to the tissues and participate in immune reactions. They are the elements of muscle fiber and form hormones and viruses.

Specifically, bovine serum albumin acts to maintain the plasma volume by increasing the osmotic pressure so the liquid in the bloodstream is not forced through the walls by the blood pressure. It also transports materials other than fats. Since this protein is readily available, it has been one of the most widely studied. The principal methods of determining size and shape characteristics of proteins are from dielectric dispersion measurements, double refraction of flow, sedimentation and diffusion, viscosity, and x-ray diffraction studies. The results of most of these methods indicate a molecular weight for bovine serum albumin of about 69,000 and a shape approximated by a prolate ellipsoid of axial ratio between 3 and 4 to 1. Recently Anderegg[12] has obtained evidence from small-angle x-ray scattering that it may have the shape of an oblate ellipsoid with an axial ratio of 1 to 3.5 at the isoelectric pH, and with ionic strength,

$\Gamma/2$ = .05. The volume he obtains for the molecule would require an internal hydration of .31 gms. of water per gram of protein to bring the molecular weight into agreement with previous results.. Scatchard[13] has proposed that the shape of bovine serum albumin may change with pH due to an internal Donnan pressure from unequal distribution of diffusable ions across the molecular surface. This would lead to swelling and distortion of the molecular shape.

Hemoglobin is the predominant component of red blood cells.. It is thought to be slightly aspherical in shape. Bragg and Perutz[14], using single crystal x-ray diffraction methods, describe it as an approximate prolate ellipsoid with dimensions 54 x 54 x 70 Ångstroms. The molecular weight of hemoglobin is quite unambiguously known to be 67,000.

Fibrinogen is an important component in the process of blood clotting. It is known to be quite asymmetric and is rod-like in shape. Estimates of its axial ratio are in poor agreement, varying from 2 to 1 to 20 to 1. Anderegg[15] has obtained a scattering curve for fibrinogen which suggests an axial ratio of between 10 and 20 to 1, but the data were subject to large corrections for slit effects. The molecular weight of fibrinogen is not too well known, but an average of the estimates places it at 340,000.

The purpose of the experiments described here was to study the size and shape of bovine serum albumin over a range of pH's and ionic strengths and to obtain information about

the size and shape of hemoglobin and fibrinogen at their isoelectric points. Where the data overlap, the present measurements with pinhole collimation have served to confirm earlier data taken with slit collimation.

B. Experimental Methods

The information on the radius of gyration and shape of the proteins under each given set of conditions was obtained in a series of runs. Except for some preliminary runs on bovine serum albumin, these consisted of two runs each, at four different concentrations in the angular range, 5×10^{-3} to 16×10^{-3} radians, and one or more runs at higher concentration in the extended range 6×10^{-3} to 40 or 61×10^{-3} radians. The short runs were averaged and used to obtain the radius of gyration from an extrapolated plot of R vs. c. The extended runs gave information on the shape of the particles from comparison with theoretical curves. Pinholes .5 mm in diameter were used for all runs. For the extended angular runs the maximum diameter (20 mm) annular slit was used with a 6.7 mm diameter beam stop. For short runs 50 per cent more intensity was obtained by using the 10 mm diameter annular slit with its 3.6 mm beam stop. Settings of the annular slit and beam stop were made using tables of distance opposite angle prepared for the two annular slits. The stabilized x-ray tube power supply was allowed to warm up for about an hour before taking data. The discriminator alignment, channel width, channel setting, and focal spot align-

ment were checked each day. The power supply was stabilized to a fraction of a per cent against variations in the 220 volt supply, but the control circuits and counter circuits were insufficiently stabilized against the abnormal variations sometimes noticed in the 110 volt lines. The resultant intensity variations, indicated by meters, were as high as 3 per cent at these times, but were manually corrected as efficiently as possible. A check for intensity variation in the x-ray beam was made by taking periodic carbon scattering references. Usually, 6400 counts were taken for each point, or averages were made to bring most of the data to at least this statistical accuracy. Points were usually taken every 10^{-3} radians for the extended runs and every 5×10^{-4} radians for the short runs. All data were standardized to the same intensity level. The background scattering from the collimating system, the sample holder, and the solvent was determined from the averages of several runs with the sample holder in place, containing only the solvent. This background was then subtracted from the protein runs to obtain the net protein scattering. No correction for absorption was necessary since only relative intensities were needed. The data were corrected for the $1/r^2$ effect before plotting. The necessary multiplying factor observed experimentally for equating the data taken with one annular slit to data taken with the other was in good agreement with the calculated value. This permitted extrapolation of the ex-

tended runs to low dilutions by fitting on the short run data.

The solution samples were kept in polyethylene bottles at 5° C when they could be used within a week after preparation. They were frozen if it was necessary to use them later than that. The solutions were introduced into the sample holders with a hypodermic needle and allowed to come to room temperature before use as a precaution against air bubble formation. No one sample was used longer than eight hours.

Salt or other gegenions are usually added to protein solutions for x-ray studies to reduce interparticle interference effects by electrically shielding the protein ions from one another.

The bovine serum albumin was obtained in powder form from the Armour Laboratories. Dipolar ions, such as proteins, can be converted into ions carrying a net charge by addition of acids or bases to the colloidal suspension. This net charge varies with the pH and the ionic strength of the material. At limiting high (about 12) and low (about 2) values of pH the protein denatures. The charge on the proteins is due to the neutralization of dipole ions by the excess OH^- or H^+ in solution which is present due to the usual hydrolysis effects.

Solutions of bovine serum albumin for the preliminary runs were prepared in acetate and glycine buffers to give a wide range of acid pH's and an ionic strength of .05. Extended runs were made at concentrations of 5 or 10 per cent,

short runs at concentrations of 3 and 1 per cent.. All pH's were measured on a Beckman Model G pH meter, standardized against pH 4.00 or pH 7.00 standard buffers..

The solutions for the regular runs on bovine serum albumin were prepared in 10 or 20 per cent concentration (by weight) in distilled water and then thoroughly electrodialyzed in an apparatus designed and constructed by Prof. R. M. Bock of the Biochemistry Department.[16] The desired concentrations, pH's and ionic strengths were obtained by proper dilution with solutions of the necessary molarity in HCl or NaOH and NaCl. The molarity of HCl or NaOH required for the desired pH's was predicted from titration curves for serum albumin.[16, 17] Most of the extended runs were made at concentrations of 5 per cent and the short runs were made at concentrations of 3, 2.2, 1.4 and 0.6 per cent. The dilutions were made by adding only salt solution of the necessary ionic strength (usually .05) to keep the same ratio of moles of acid or base to grams of protein. This maintained a fairly constant pH over the range of concentrations. All solutions added to the original electrodialyzed solution were prepared using conductance water. The usual precautions were taken to rinse burettes, pipettes, bottles, etc. in conductance water before use.

The rat hemoglobin sample was prepared by Professor H. F. Deutsch of the Physiological Chemistry Department and the bovine hemoglobin was prepared under his direction. The rat hemoglobin was obtained as a twice crystallized, 2.2

per cent solution in .3M potassium phosphate buffer. Its pH was 7.90. Extended runs were made at this concentration and short runs at 2.2, 1.4, and 0.6 per cent. Dilutions were made with buffer solution. The bovine hemoglobin was prepared from beef blood. The whole blood was centrifuged to separate the plasma into the supernatant which was removed and discarded. The red cells were then rinsed three times with a hypertonic 1.2 per cent NaCl solution, centrifuging each time. Distilled water was added in a ratio of about 3 to 1 to burst the cells, and the cell walls were centrifuged off. The supernatant remaining was estimated to be 99 per cent pure oxyhemoglobin and had a concentration of 7.1 per cent. The concentrations of the hemoglobin solutions were measured by Dr. Deutsch on a spectrophotometer using the pyridine hemochromagen method. Extended runs were made at 7.1 per cent and 3 per cent and short runs at 4, 3, 2, and 1 per cent. The runs were made at the isoelectric pH and at an ionic strength of 0.05.

The bovine fibrinogen was obtained from I. Billick of the Department of Chemistry as a 2.64 per cent solution in 0.45 M sodium phosphate buffer with pH 6.2. Extended runs only were made at 2.64 and 1.32 per cent.

C. Results of Experiments

1. Bovine Serum Albumin

Fourteen preliminary runs were made in a survey of the approximate effects to be found at various acid pH's. From

near the isoelectric point at about pH 4.8 down to nearly pH 2 most of the H^+ ion added to a protein solution of the concentrations used is bound by the protein. This results in a net charge per molecule which, e.g., is about + 70 electron charges at pH 3.0. Thus, interparticle interference would be expected to increase with increasingly acid or basic pH's. This would tend to lower the intensity at small angles according to equation (A) in section II C. This is supported very graphically by Figure 11 which is a composite of the curves obtained at the five different pH's listed. All of these protein solutions had an ionic strength of .05 which actually shielded out a large part of the interference. The curves were taken from 5 per cent solutions. The effects decrease for lower concentrations, but they were still found to introduce considerable non-linearity in the ln I vs. θ^2 curves even at the lowest concentrations, for the lower pH's. For this reason, and also because no large changes in extrapolated radii of gyration were apparent, it was decided to limit careful study to pH's between 4.0 and 6.0.

a. The Radius of Gyration

Series of runs were made under the following five conditions:

1. pH $\simeq$ 4.0, $\Gamma/2$ = .05
2. pH $\simeq$ 4.4, $\Gamma/2 \leq$ .005 (minimum due to acid only)
3. pH $\simeq$ 5.0, $\Gamma/2$ = 0 (isoionic)
4. pH $\simeq$ 5.25 $\Gamma/2$ = .05 (NaCl only)
5. pH $\simeq$ 6.0 $\Gamma/2$ = .05

Figure 11

A composite of the relative intensity vs. scattering angle curves obtained at five different pH's for bovine serum albumin with an ionic strength of .05 in 5 per cent solution. The lower-angle portions of the curves are depressed at pH's away from the isoelectric point because of interparticle interference effects.

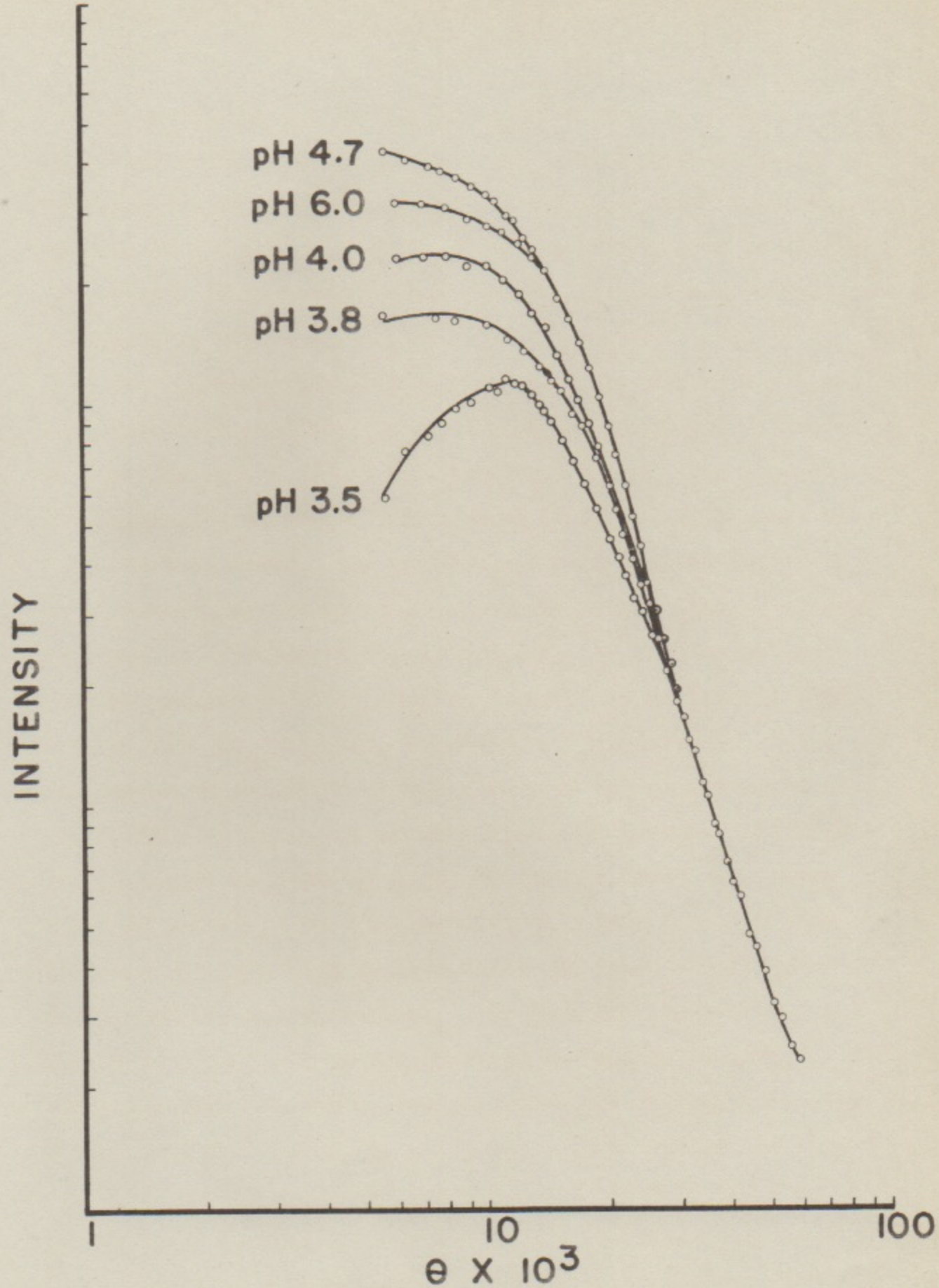
pH 4.7
pH 6.0
pH 4.0
pH 3.8
pH 3.5
INTENSITY
1
10
100
θ X 10³

A representative set of ln I vs. θ^2 curves is shown in Figure 12 for series 4. At the extreme pH's interparticle interference made the first part of the curve turn down and, at the pH 5.0 isoionic point, what are interpreted as aggregation effects made the curves turn up. Examples of these are shown in Figure 13.

The extrapolation curves of R vs. c for the five series are shown in Figure 14. Each of these extrapolated values is the uncorrected experimental value. Taking into account the previously described corrections, 0.5 per cent should be added to each value. The total error in R estimated from a consideration of intensity fluctuations, statistics, and comparisons of reproducibility is ± 0.4 R. It will be noticed that the spread in R for different series is definitely correlated with pH. However, since the differences are of the same order of magnitude as the error, no definite conclusions can be made on the basis of this information alone. In Figure 15 a plot is given of R vs. pH for different concentrations of protein. The less dependable values from the preliminary runs are included and lines are drawn which appear to approximate the variations. The line for the extrapolated values of R is drawn on the basis of the values from Figure 14 only, but vertical extrapolations using the values at the intersections with the 5, 3, and 1 per cent lines produce values which are in very good agreement with this line. This result seems to lend further support to the idea that the

Figure 12

A representative set of ln I vs. θ^2 curves for bovine serum albumin. Straight lines have been drawn through the points. The slope of each line is proportional to the square of the apparent radius of gyration at that particular concentration.

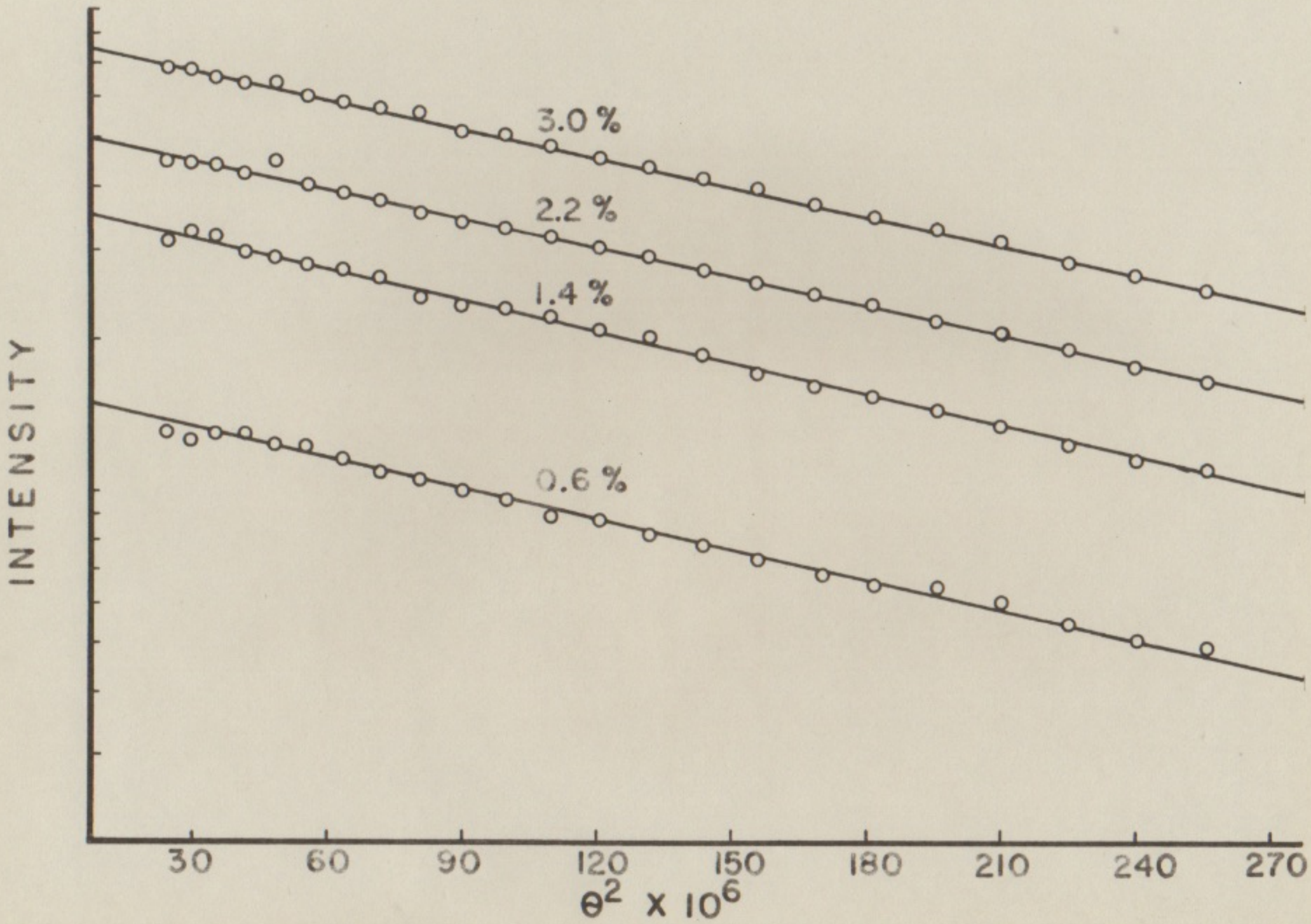
3.0 %
2.2 %
1.4 %
0.6 %
INTENSITY
30
60
90
120
150
180
210
240
270
θ² x 10⁶

Figure 13

Two ln I vs. θ^2 curves for bovine serum albumin showing deviations from linearity. The upper curve is depressed at lower angles because of interparticle interference effects. The lower curve is raised because of aggregation effects.

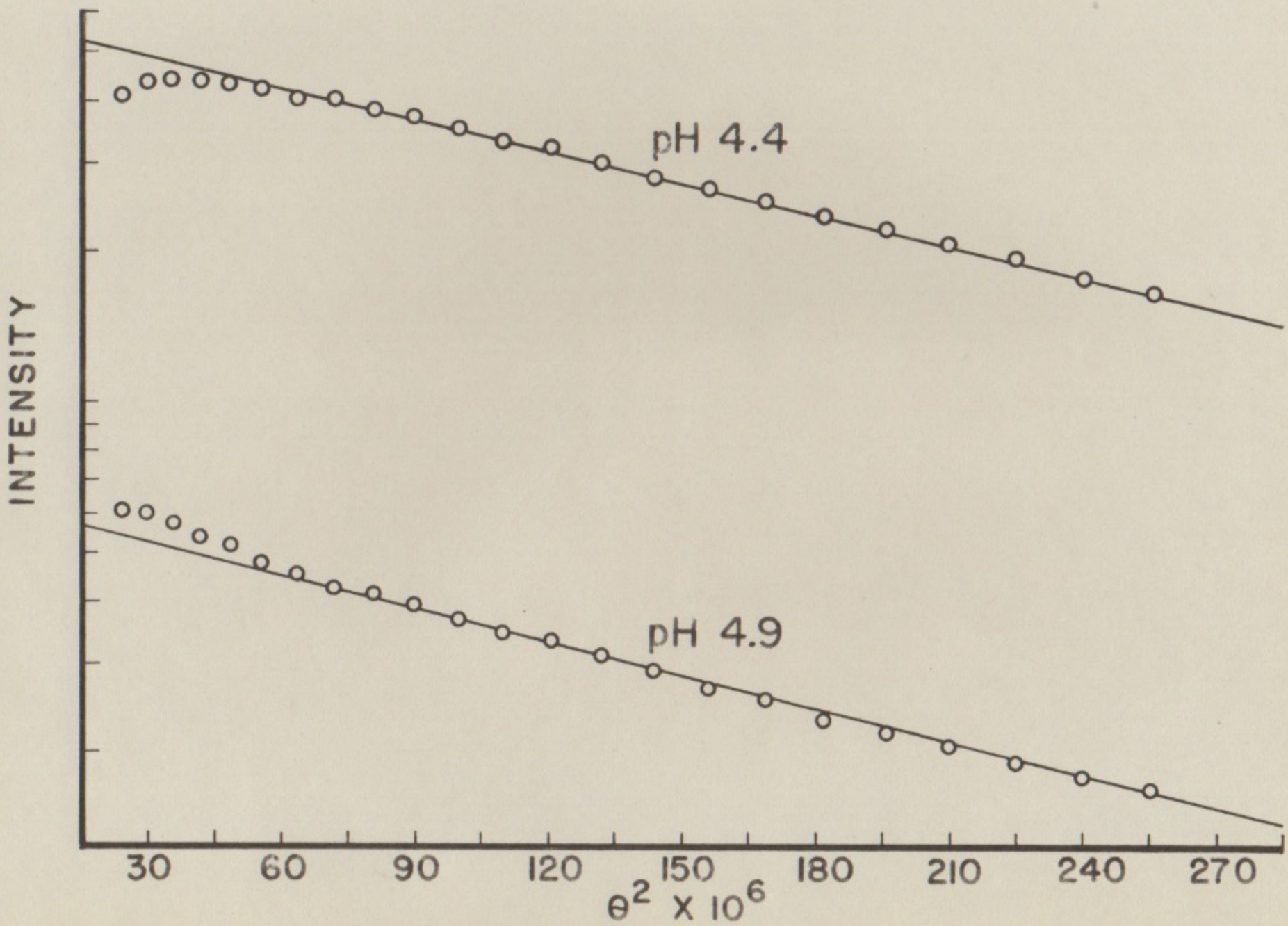
pH 4.4
pH 4.9
INTENSITY
30
60
90
120
150
180
210
240
270
θ² X 10⁶

Figure 14

The extrapolation curves of radius of gyration vs. concentration for the five series of runs made with bovine serum albumin. Each extrapolation is labeled with the pH and ionic strength used for the series.

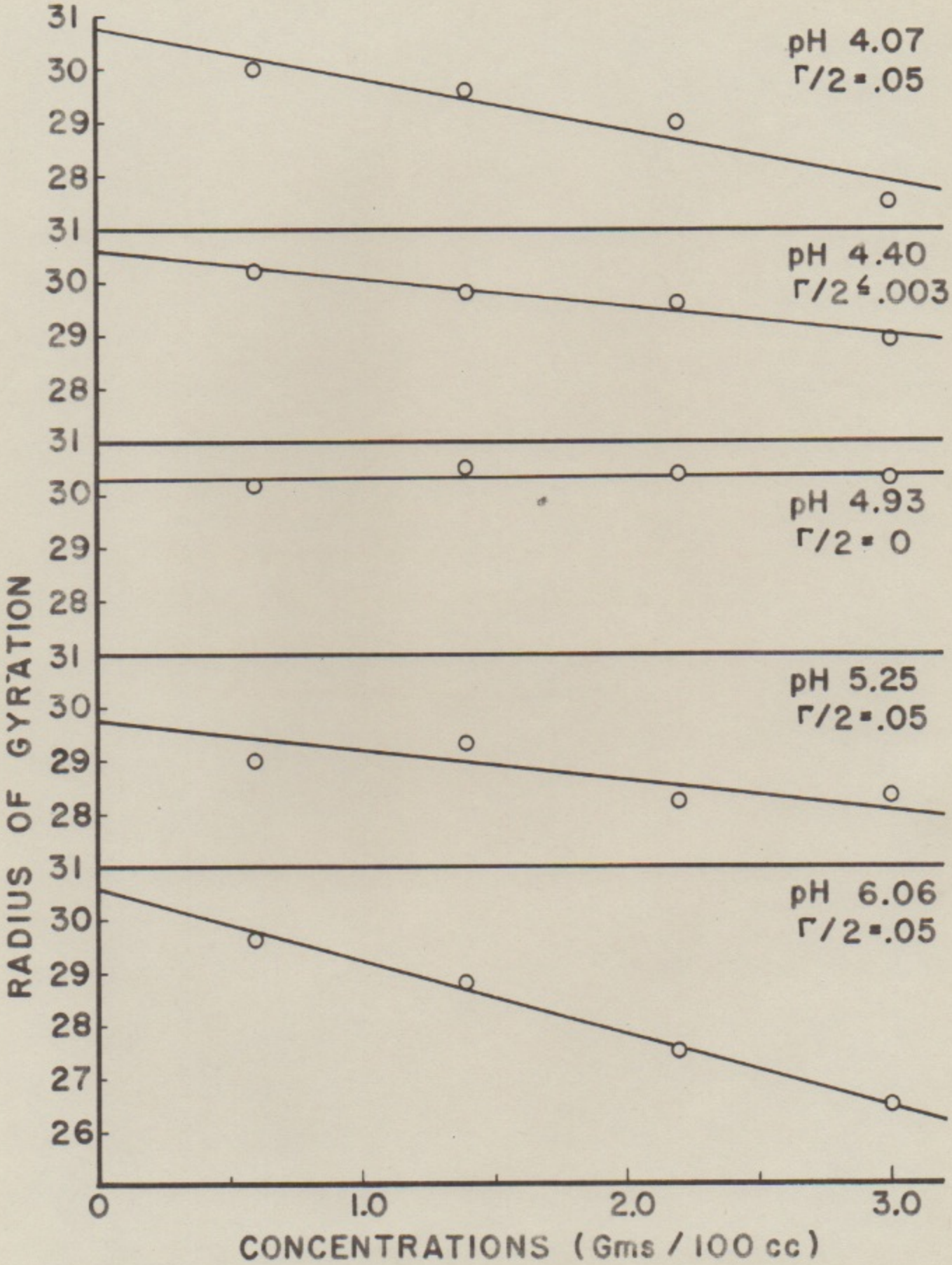
pH 4.07
Γ/2 = .05
pH 4.40
Γ/2 = .003
pH 4.93
Γ/2 = 0
pH 5.25
Γ/2 = .05
pH 6.06
Γ/2 = .05
RADIUS OF GYRATION
31
30
29
28
27
26
0
1.0
2.0
3.0
CONCENTRATIONS (Gms / 100 cc)

Figure 15

A plot of radius of gyration vs. pH for bovine serum albumin at different concentrations. The straight lines are drawn as an approximation of the positions of the points for one concentration.

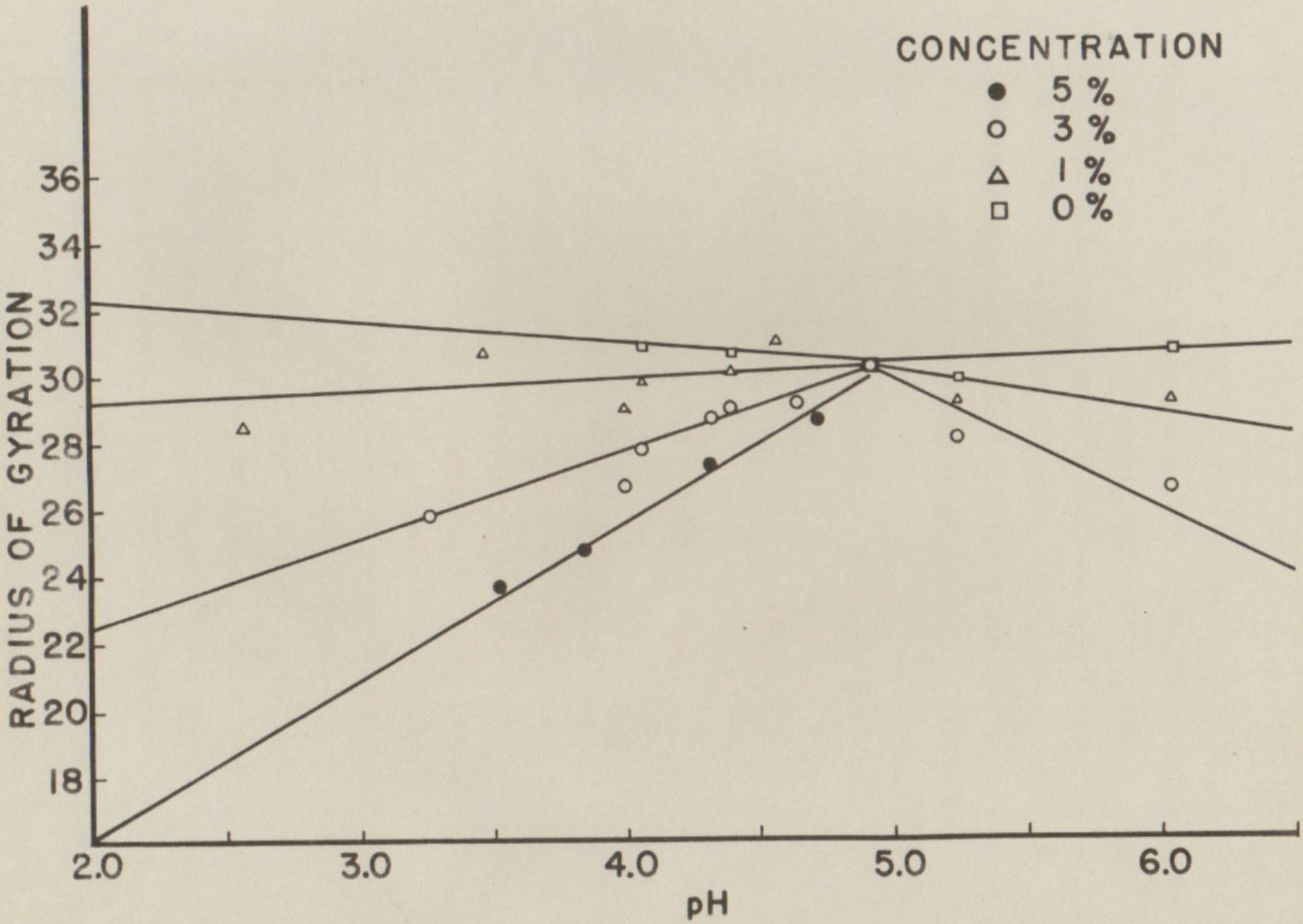
CONCENTRATION
5 %
3 %
1 %
0 %
RADIUS OF GYRATION
36
34
32
30
28
26
24
22
20
18
2.0
3.0
4.0
5.0
6.0
pH

molecule swells at pH's away from the isoelectric point. Though the effect would appear to be small, the relative volume increase goes as the cube of the relative radii of gyration and would result in an increase in volume of 13 per cent between pH 5 and pH 3 on the basis of this curve. The fact that the values for series 4 fall lower than one might expect may indicate some small effect due to the presence of salt alone or a different behavior at the basic pH's, but no definite conclusions can be made. Taking the best value for R as the average of the values at the two isoionic points (with and without NaCl), and making the required corrections, gives

$$R = 30.3 \pm 0.4 \text{ Angstroms}$$

b. The Axial Ratio

The scattering curve had no maxima or minima in the range of angles used. This indicates either that it is a much smaller particle than would be consistent with its radius of gyration, or more reasonably, that it is quite aspherical. Theoretical curves for spheroids of axial ratios from 1/10 to 10 are available,[18] and can be compared with the experimental curves. It is found that the only reasonably good fit is for an oblate ellipsoid with axial ratio of about 1 to 3.5. This fit is shown in Figure 16. A careful study of the average positions of the points shows that the fit is not precise along the whole curve. This could be due to experimental error or the presence of impurities. It is quite probable, of course, that the particle is not exactly an

Figure 16

A comparison of the experimental points obtained for bovine serum albumin with the theoretical curves for oblate ellipsoids with different axial ratios.

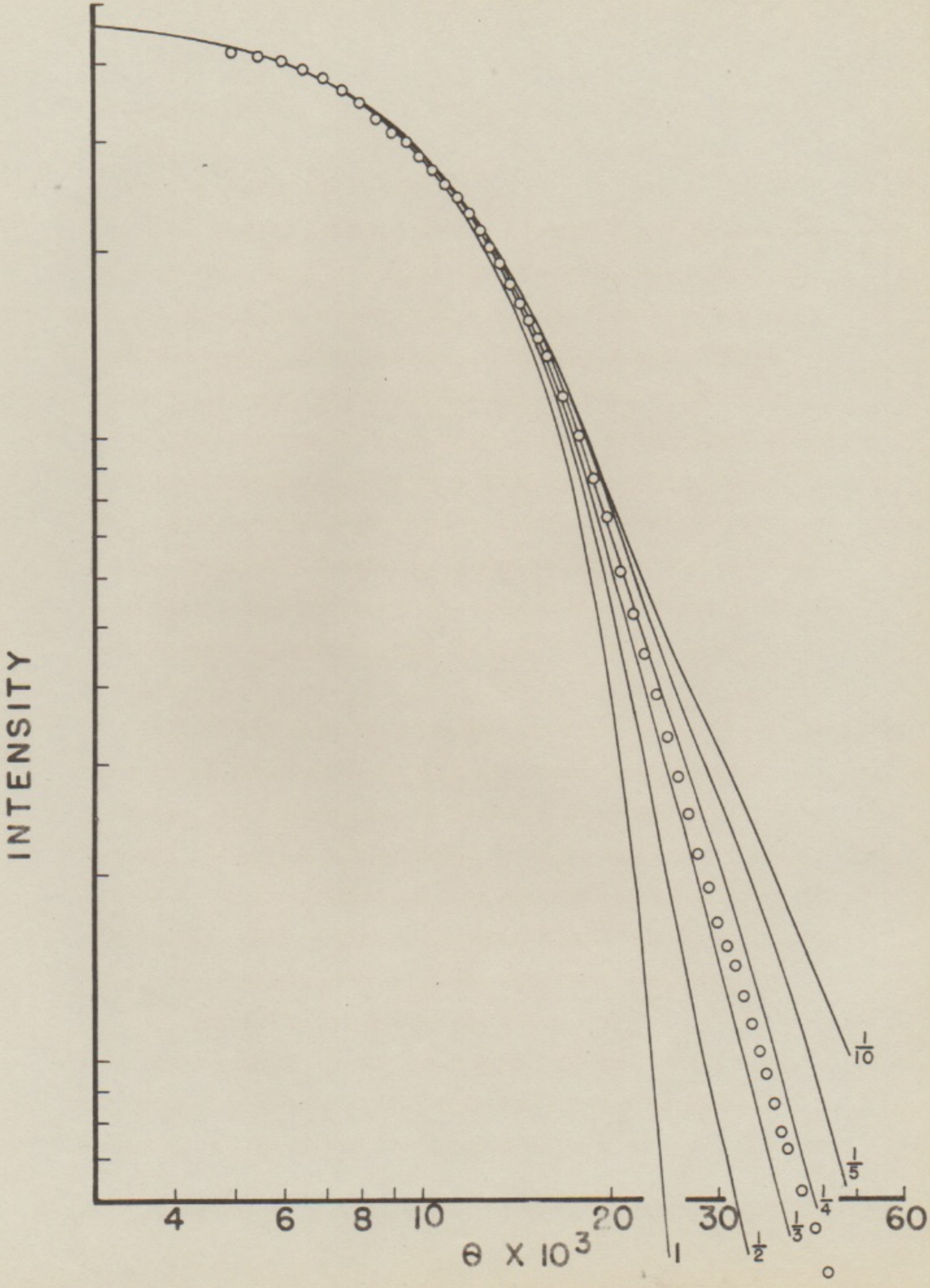
INTENSITY
4
6
8
10
20
30
60
θ X 10^3
1
1/2
1/3
1/4
1/5
1/10

oblate ellipsoid, but of a shape which is closely approximated by one.

c. Internal Hydration

The partial specific volume for most proteins in solution is about 0.75 cm^3/gm.[19] Using a molecular weight of 69,000 this gives a volume of 8.6×10^{-20} cm^3 for the dry bovine serum albumin molecule. From the values found in these experiments for R and the axial ratio, v, the volume of the molecule in solution becomes that of an oblate ellipsoid with dimensions 94 x 94 x 27 Å, or about 12.4×10^{-20} cm^3. This is considerably greater than the value found above. Following Anderegg, it can be assumed that the excess volume is due to internal hydration. The amount necessary to give agreement would be 0.33 gms of water per gm of protein.

All of the above results for the size and shape of bovine serum albumin are in good agreement with those of Anderegg. An alternative to assuming internal hydration to explain the larger volume found by small angle x-ray scattering is that the particle does not fit the assumptions of the theory, such as the requirement of uniform electron density. This alternative does not seem very probable.

d. Effects Near Isoelectric Point

Curves at 10, 5 and 2 per cent adjusted to the same equivalent intensity scale, and with average pH 4.8 are shown in Figure 17 for electrodialyzed bovine serum albumin

Figure 17

Scattering curves for bovine serum albumin obtained at the isoelectric point. Electrodialyzed bovine serum albumin was used at three different concentrations to get the curves for an ionic strength of zero. The other curve is for a .05 molar salt solution.

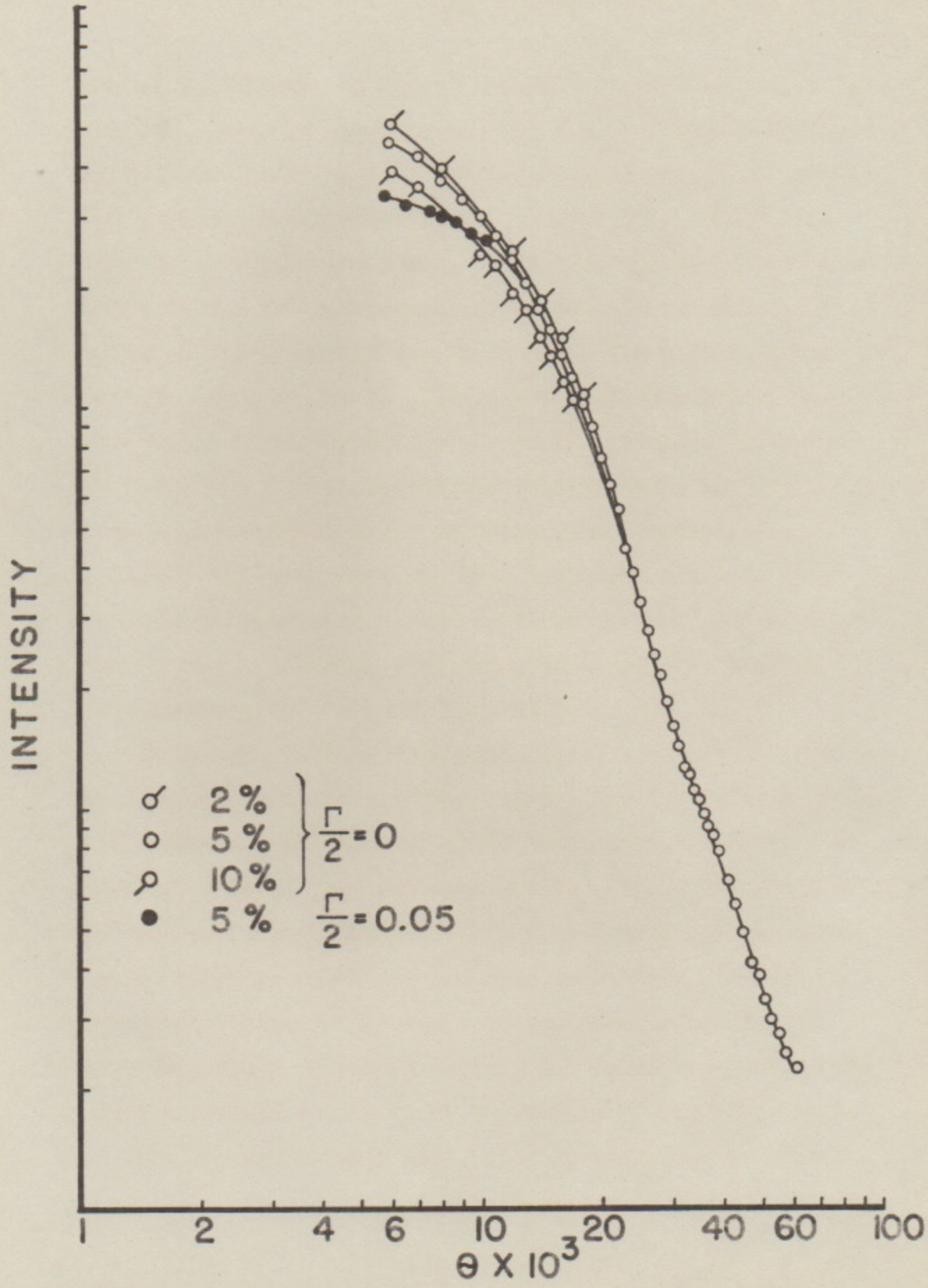
INTENSITY
2%
5%
10%
Γ/2 = 0
5%
Γ/2 = 0.05
1
2
4
6
10
20
40
60
100
θ X 10³

with no salt added, as compared with a curve taken at pH 4.7 with $\Gamma/2 = .05$. It is apparent that the pure electrodialyzed BSA contains quantities of large molecular weight particles that increase the average radius of gyration. Since this state is a most unstable one, it is quite probable that the effect is due to aggregation of the protein molecules. It was not noticed for any solutions which had a small ionic strength, even as low as .0006. The fact that the curves extrapolate to higher slopes for lower dilutions rules out the possibility of an attractive interparticle interaction, since such an effect would decrease with concentration. Light scattering experiments have indicated a strong tendency of serum albumin to aggregate with time[20] and of another globular protein, ovalbumin, to aggregate in salt-free solutions near the isoelectric point.[21]

It is also noticed that both of these curves exhibit negative and positive curvature in the low intensity region. This effect was noticed for these cases only, which were at about the same pH near the isoelectric point. The wings of the extended curves for all other runs agreed and lay along a curve which smoothed out the hump shown here. It can be shown that the curve of Figure 17 could be produced if a small percentage of the scattering particles had an approximately spherical volume about twice that of the BSA. Since all samples were equally pure, this could not be an impurity effect, but could be due to the formation of a small percen-

tage of dimers, which became negligible at pH's away from the isoelectric point where the molecules acquired charges and tended to repel one another.

e. Effect of Denaturing Protein

A sample of the pH 6.05 protein was denatured by heating just to the boiling point. The pH rose to 6.18 and a comparison of its curve with that of the normal curve for pH 6.05 is shown in Figure 18. The rise in the curve either indicates aggregation or the presence of other large radius of gyration particles such as might be produced by "unwinding" of the globular protein.

f. Effect of Poor Wave Length Resolution

In Figure 19 two curves are compared which were taken under different conditions of wave length resolution. The normal curve was taken with the differential discriminator set at the normal channel width. The integral counter curve was taken using the entire integrated output of the proportional counter except for pulses from photons with a wave length longer than about 3 Å. Since at 30 kv most of the continuous spectrum lies below the Cu K-alpha wave length of 1.54 Å, it would be expected, from $d \sim \theta/\lambda$, that for the integrated output an effectively larger particle would be indicated. This is just what occured, since the slope of the small angle region increased, as shown.

g. Time Run

A check on the practice of running the same sample for several hours was made by taking 16 points of a radius of

Figure 18

A comparison of curves obtained from a 5 per cent solution of bovine serum albumin at pH 6.05 and ionic strength .05 before and after heat denaturation.

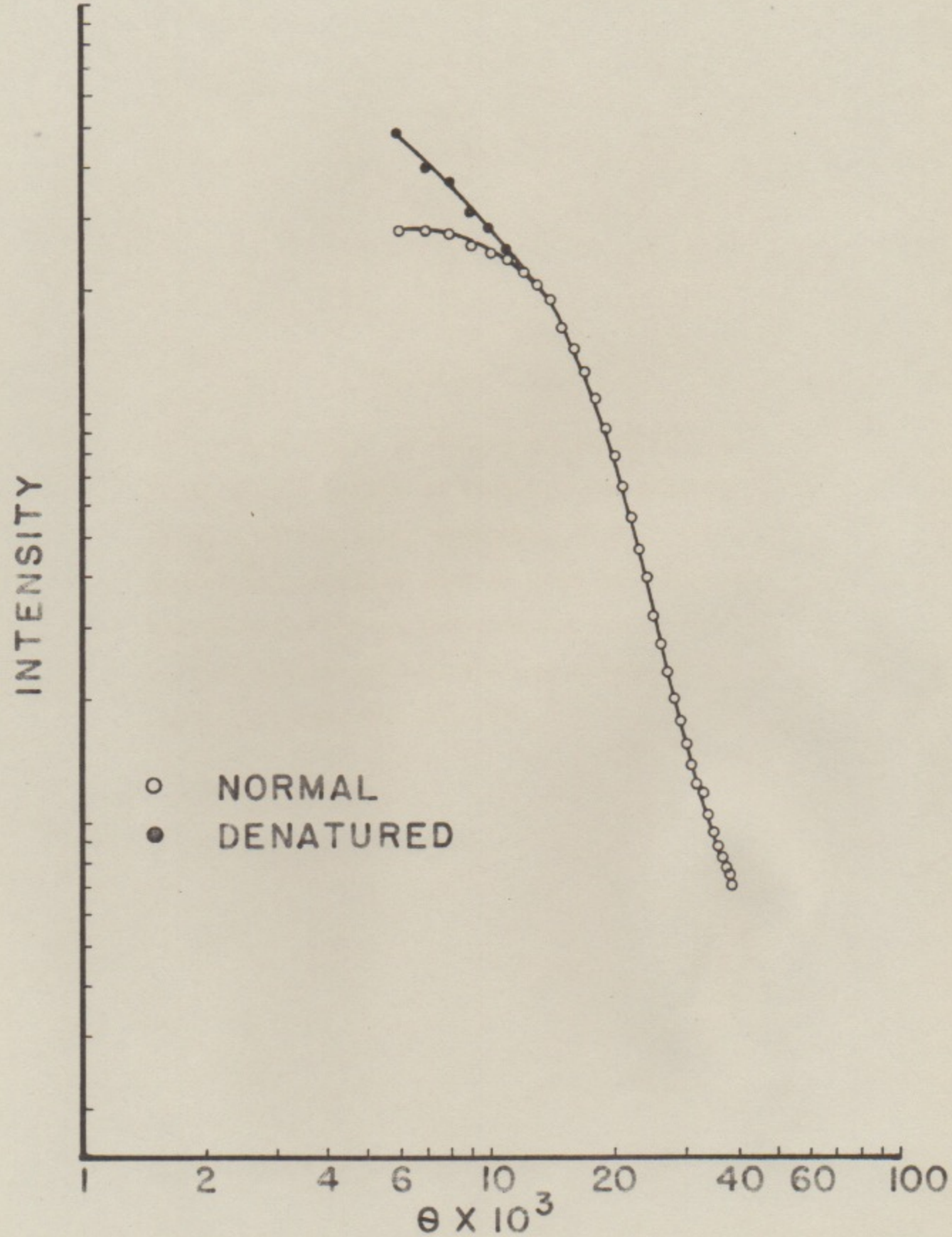
INTENSITY
NORMAL
DENATURED
1
2
4
6
10
20
40
60
100
θ X 10³

Figure 19

A comparison of curves obtained from a 5 per cent solution of bovine serum albumin at pH 6.05 and ionic strength .05 with the normal proportional counter wave length resolution and using an integral counter which counted nearly all the photons scattered by the sample into the detector.

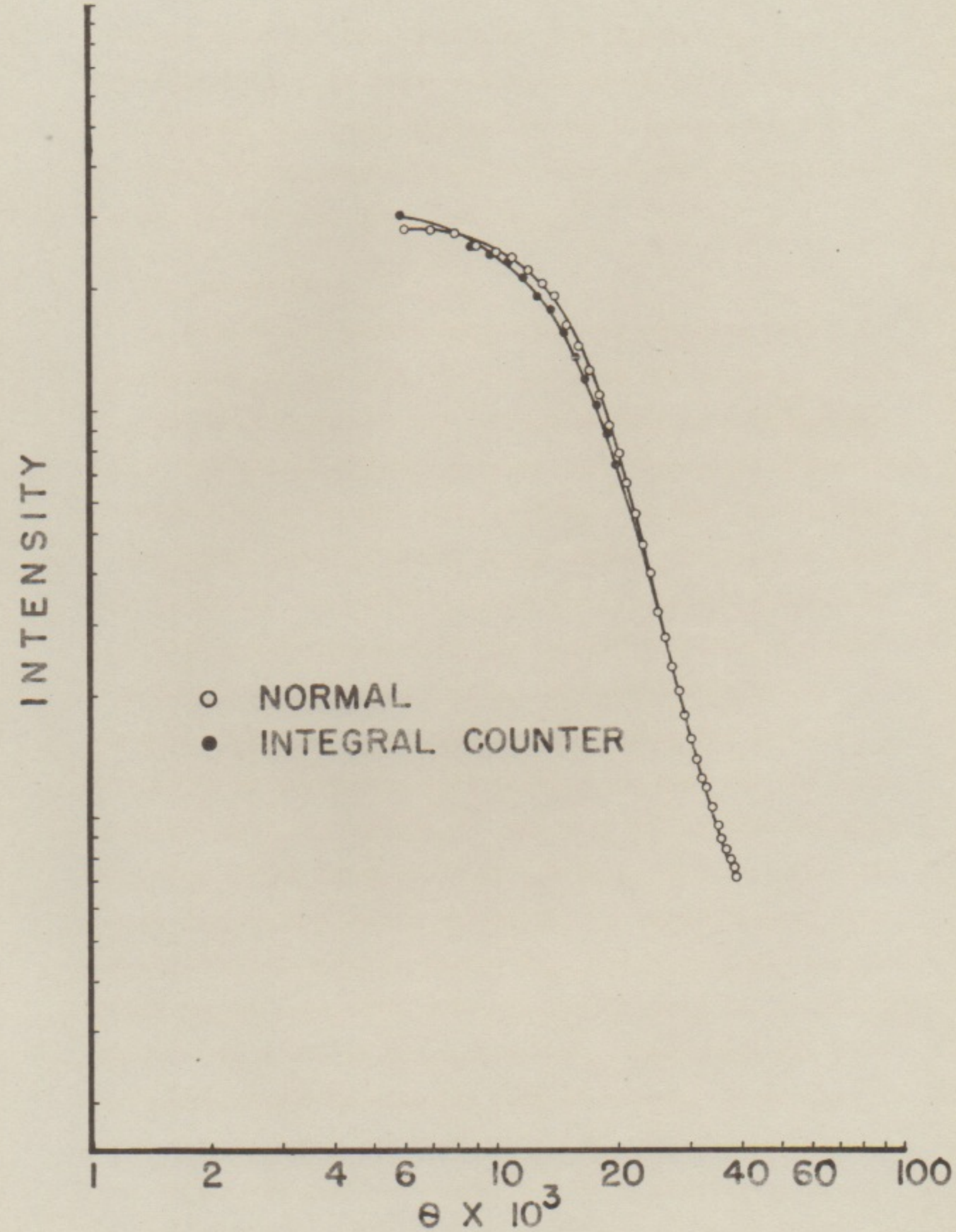
INTENSITY
NORMAL
INTEGRAL COUNTER
1
2
4
6
10
20
40
60
100
θ X 10³

gyration curve for BSA repeatedly for 12.5 hours.. The points were gone through 12 times and an analysis of the deviations indicated no continuous trend. It was therefore assumed that the serum albumin could be safely used at room temperature for periods of time less than this.

2. Hemoglobin

A plot of the bovine hemoglobin experimental curves for 7.1 per cent, 3 per cent, and 1 per cent are shown in Figure 20. The peak region is the average of four runs at 7.1 per cent. The effect of interparticle interference as a function of concentration is well displayed and, as shown previously, it decreases markedly toward large angles. It was not possible to obtain the extended curve for rat hemoglobin beyond 33×10^{-3} radians because of the low concentration and the high background from the buffer. The evaluation of the theoretical function through the peak region for prolate ellipsoids of revolution with axial ratio near one has been performed by P. W. Schmidt.[22] The best fit is obtained with the curve for an axial ratio of 1.5 to 1. The experimental points for rat and bovine hemoglobin are shown plotted with the theoretical curve in Figure 21. The large angle portion of the bovine hemoglobin curve is raised above the theoretical curve by a nearly constant amount. This could not be a resolution effect because the peak is raised. Since the curve for the purer rat hemoglobin does not seem to exhibit this difference over the range that it is available, it may

Figure 20

A composite of the intensity vs. scattering angle curves obtained for bovine hemoglobin at three different concentrations..

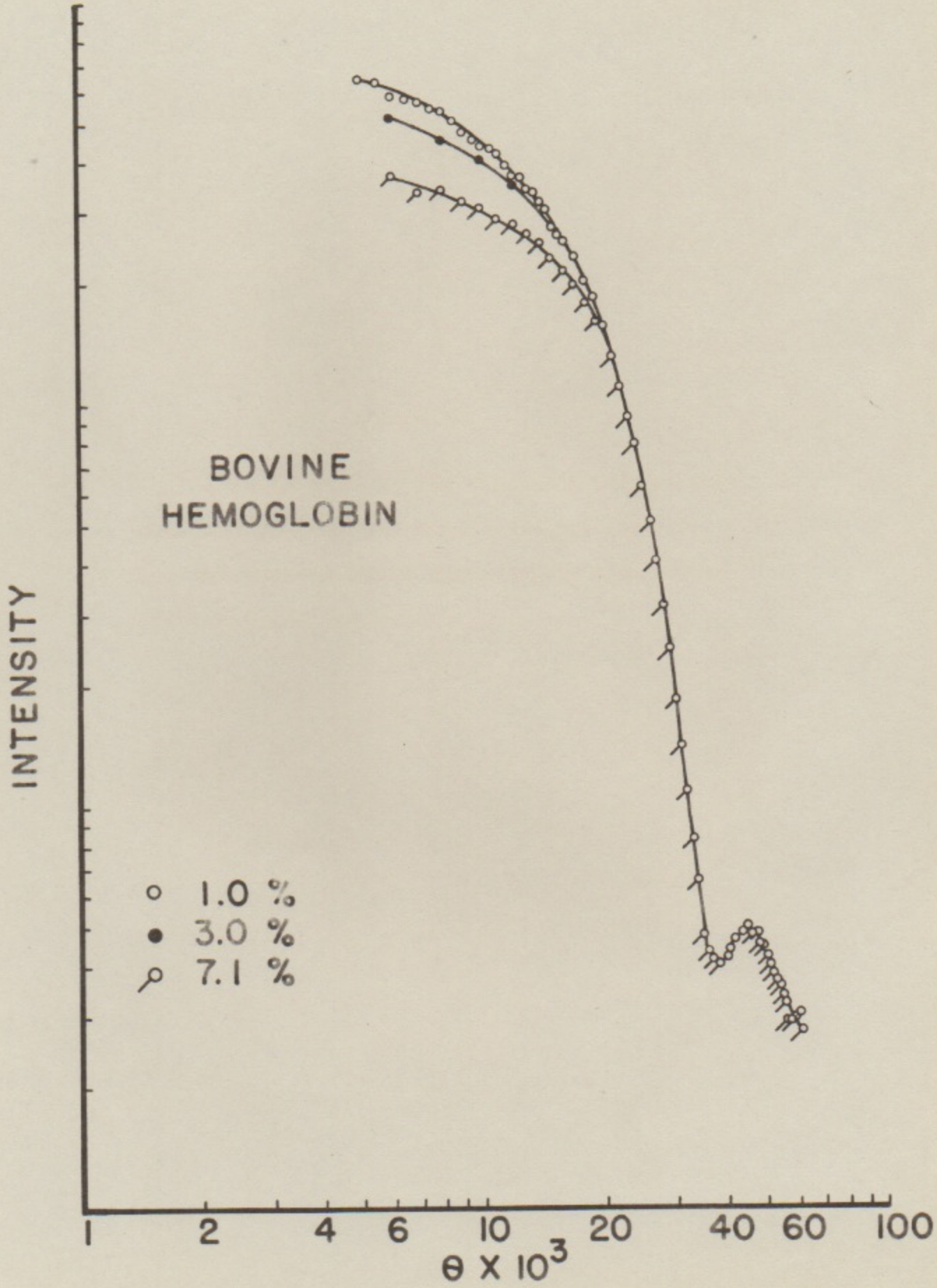
BOVINE
HEMOGLOBIN
INTENSITY
1.0 %
3.0 %
7.1 %
1
2
4
6
10
20
40
60
100
θ X 10³

Figure 21

A comparison of the experimental points obtained for rat and bovine hemoglobin and the theoretical curve for prolate ellipsoids with an axial ratio of 1.5.

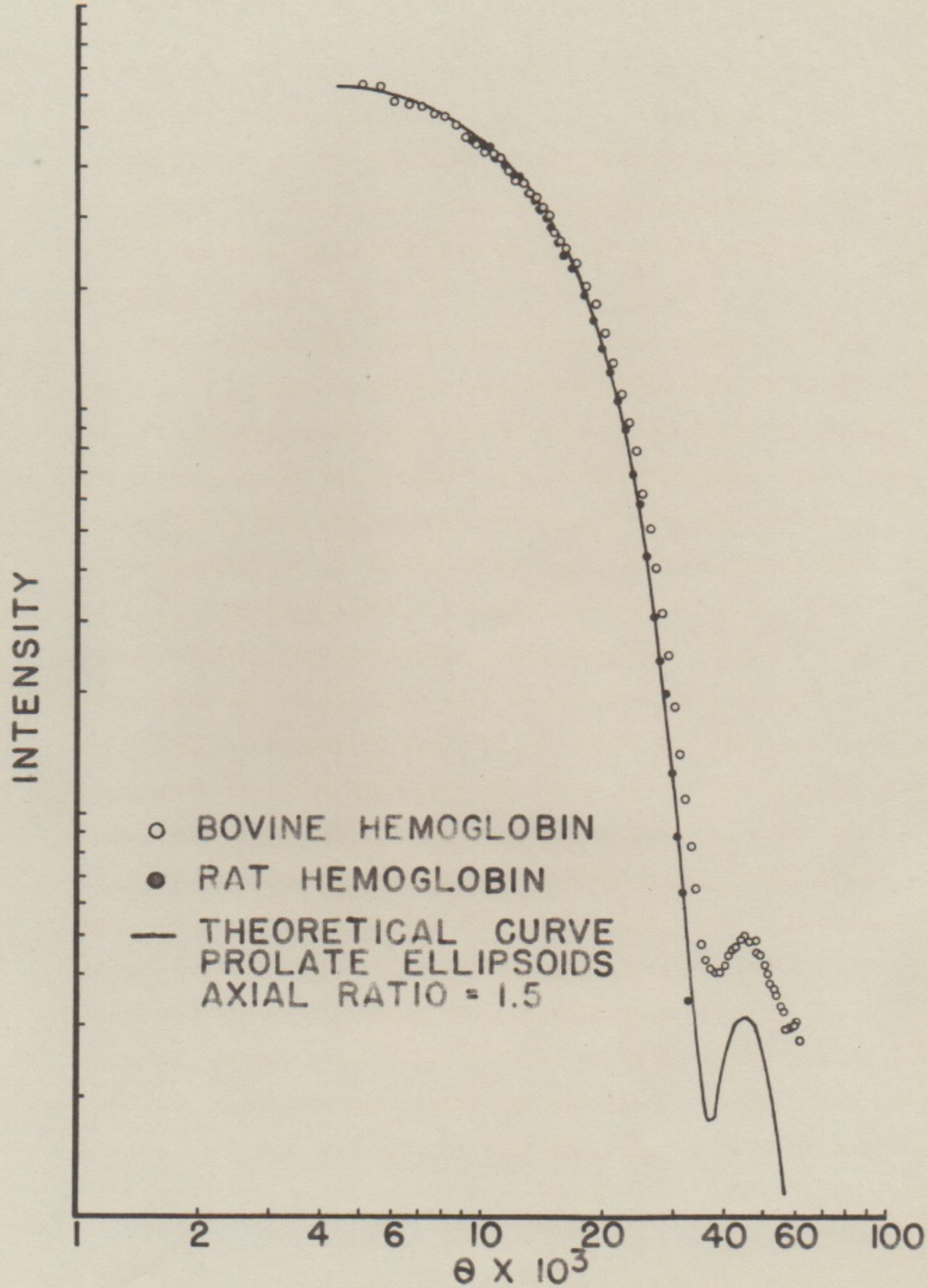
INTENSITY
BOVINE HEMOGLOBIN
RAT HEMOGLOBIN
THEORETICAL CURVE
PROLATE ELLIPSOIDS
AXIAL RATIO = 1.5
1
2
4
6
10
20
40
60
100
θ X 10³

be assumed that the bovine hemoglobin contained a small amount of low molecular weight impurity. This would have little effect on the positions of the minimum and maximum and, since the curves for both hemoglobins coincide at low angles, it is assumed that the radius of gyration is not seriously affected.

The maximum and minimum are shown more clearly in Figure 22. A comparison of the angles at which they occur with the theoretical curve permits the determination of the semi-minor axis, a, of the prolate ellipsoidal particle. This becomes 27.5 Å from the minimum and 28.0 Å from the maximum. Since the maximum is likely to be less affected by any errors, the weighted average is taken as 27.8 ± 0.3 Å. This makes the particle dimensions about 56 x 56 x 83 Å. A further check on the particle size is obtained from the radius of gyration. A plot of the R vs. c points for bovine and rat hemoglobin is shown in Figure 23. Only the bovine hemoglobin points are extrapolated since the strong tendency observed of rat hemoglobin to crystallize introduced large aggregation effects which made the data unreliable. The experimentally observed radius of gyration, corrected for resolution error and the deviation of the theoretical curve from a Gaussian, is then 25.9 ± 0.3 Å. The value of the radius of gyration, which one calculates for ellipsoids on the basis of a = 27.8 ± 0.3 Å, v = 1.5, is 25.6 ± 0.3 Å. This gives quite good agreement, though the mean R observed is slightly larger

Figure 22

A plot of the curve obtained for bovine hemoglobin in the angular range of the resolved minimum and maximum. The line is drawn through the experimental points.

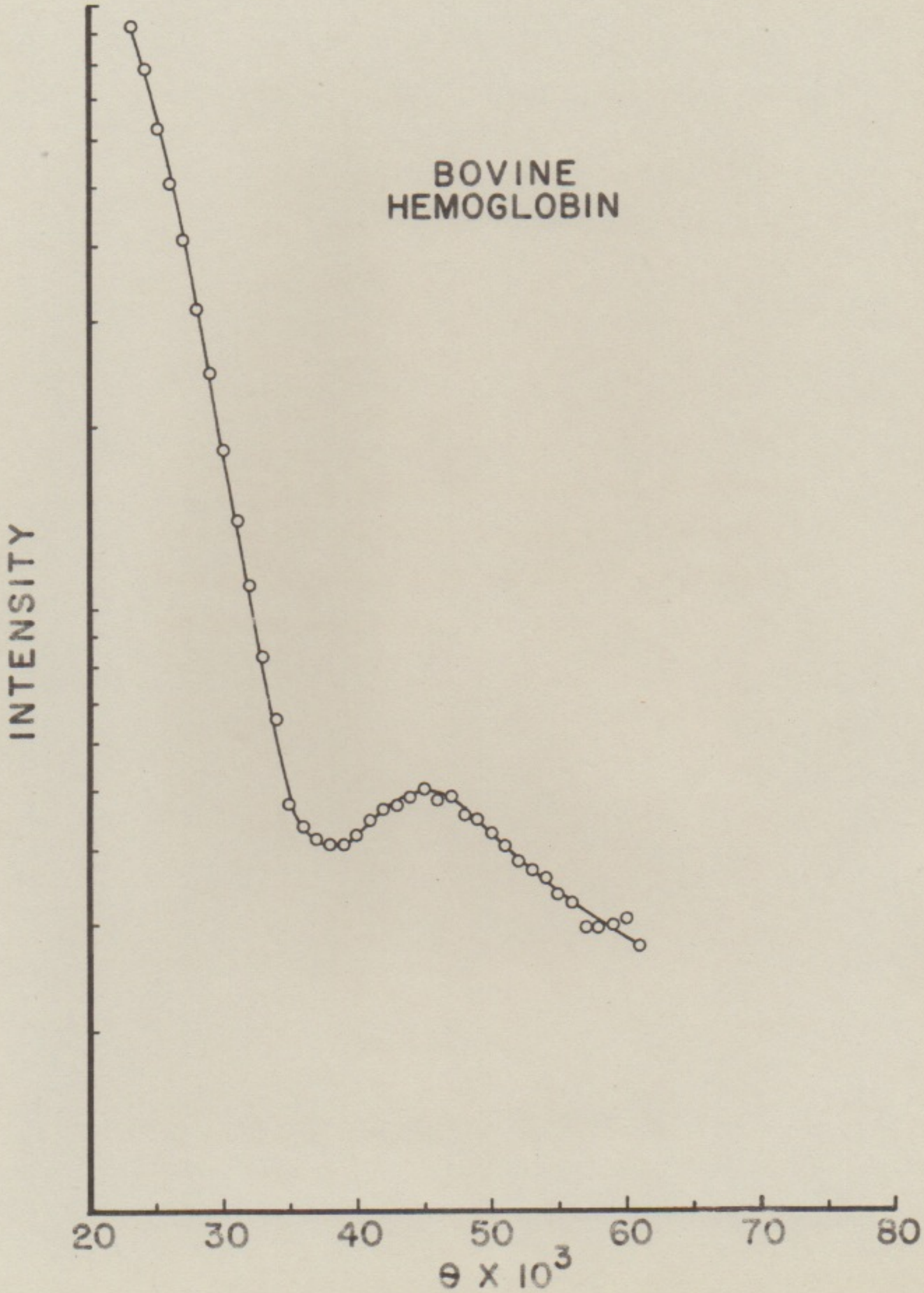
BOVINE
HEMOGLOBIN
INTENSITY
20
30
40
50
60
70
80
θ X 10³

Figure 23

A plot of radius of gyration vs. concentration for rat and bovine hemoglobin. The straight line extrapolation is drawn through the points for bovine hemoglobin..

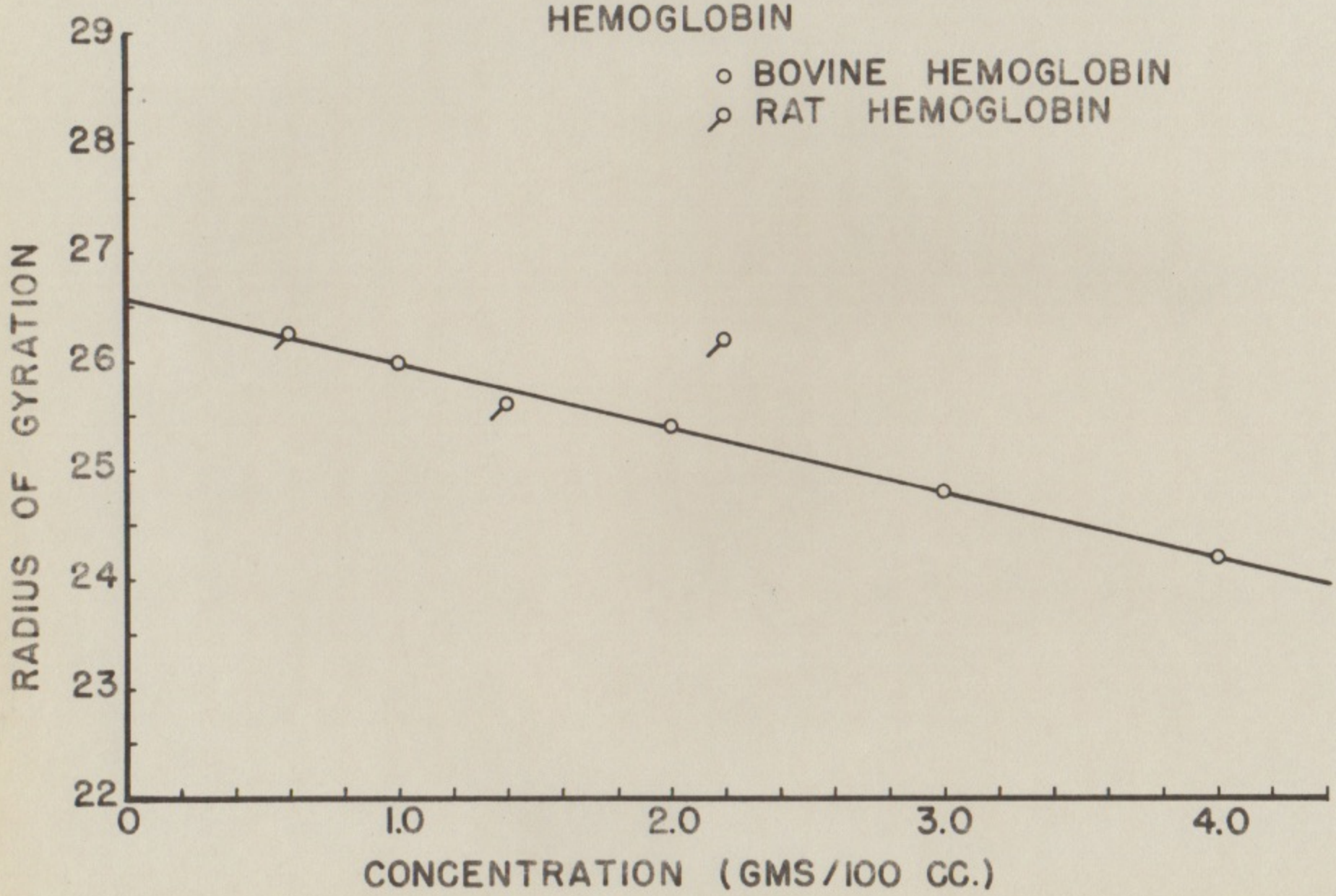
HEMOGLOBIN
BOVINE HEMOGLOBIN
RAT HEMOGLOBIN
RADIUS OF GYRATION
29
28
27
26
25
24
23
22
0
1.0
2.0
3.0
4.0
CONCENTRATION (GMS/100 CC.)

than that calculated from the particle dimensions. This could mean that the particle is not precisely a prolate ellipsoid but of a shape which distributes a little more mass at the extremities, though not enough to appreciably alter the theoretical curve. It should be mentioned that there is a possibility that the raised portion of the bovine hemoglobin curve is not simply due to impurities, but that it is real and represents the curve for a non-ellipsoidal particle. For example, a cylinder with a smaller axial ratio could have the same radius of gyration and the same radius, a. Until theoretical curves through the peak region for cylinders are available there must be some doubt as to the exact shape. Also, for molecules of this size the diameter of the polypeptide chains in the protein is only one order of magnitude less than the particle dimensions. This introduces variations in the internal electron density which will give slightly different theoretical curves.

If the parameters obtained are accepted, then the dimensions of the particle do not entirely agree with those proposed by Bragg and Perutz. The value for "a" is nearly in agreement, but the major axis is longer by about 19 per cent. This is assuming internal hydration of the protein, since Perutz's dimensions are for the hydrated molecule. Using Perutz's data on the form birefringence of hemoglobin molecules, Bragg and Pippard have recently shown[23] that an axial ratio of 1.45 is indicated for the hemoglobin molecule,

rather than 1.3 as found from the x-ray data of Bragg and Perutz. The axial ratio of 1.5 found here is in good agreement with this result.

The volume of a 56 x 56 x 83 Å prolate ellipsoid is $13.8 \times 10^{-20} cm^3$. On the basis of the accepted molecular weight for hemoglobin and the specific volume of proteins, this requires an internal hydration of 0.50 gms of water per gram of protein for agreement.

3. Fibrinogen

Due to the nature of the constants for this particle, the smallest angles obtainable with the pinhole collimating system did not permit obtaining high enough relative intensities on the fibrinogen curve to make accurate comparisons with theory. There was good agreement with most of the equivalent part of Anderegg's slit corrected curve, though a dip which appears in his curve starting just below the high intensity limit of these data did not appear to be reproduced. However, the general acceptability of the slit corrections, which are quite large for very asymmetric particles, was confirmed, and an axial ratio of between 10 and 20 to 1 is indicated on the basis of uniform cylinder theory.

A comparison of the types of curves expected from particles of different shapes but with the same molecular weight can be made by plotting the bovine serum albumin, bovine hemoglobin, and bovine fibrinogen data adjusted for differences in molecular weight. This is done in Figure 24. The

Figure 24

A comparison of the curves expected from particles with different shapes and equal molecular weight. The curves have been shifted vertically an amount determined by the relative molecular weight of the particles to eliminate the differences in zero angle intensity..

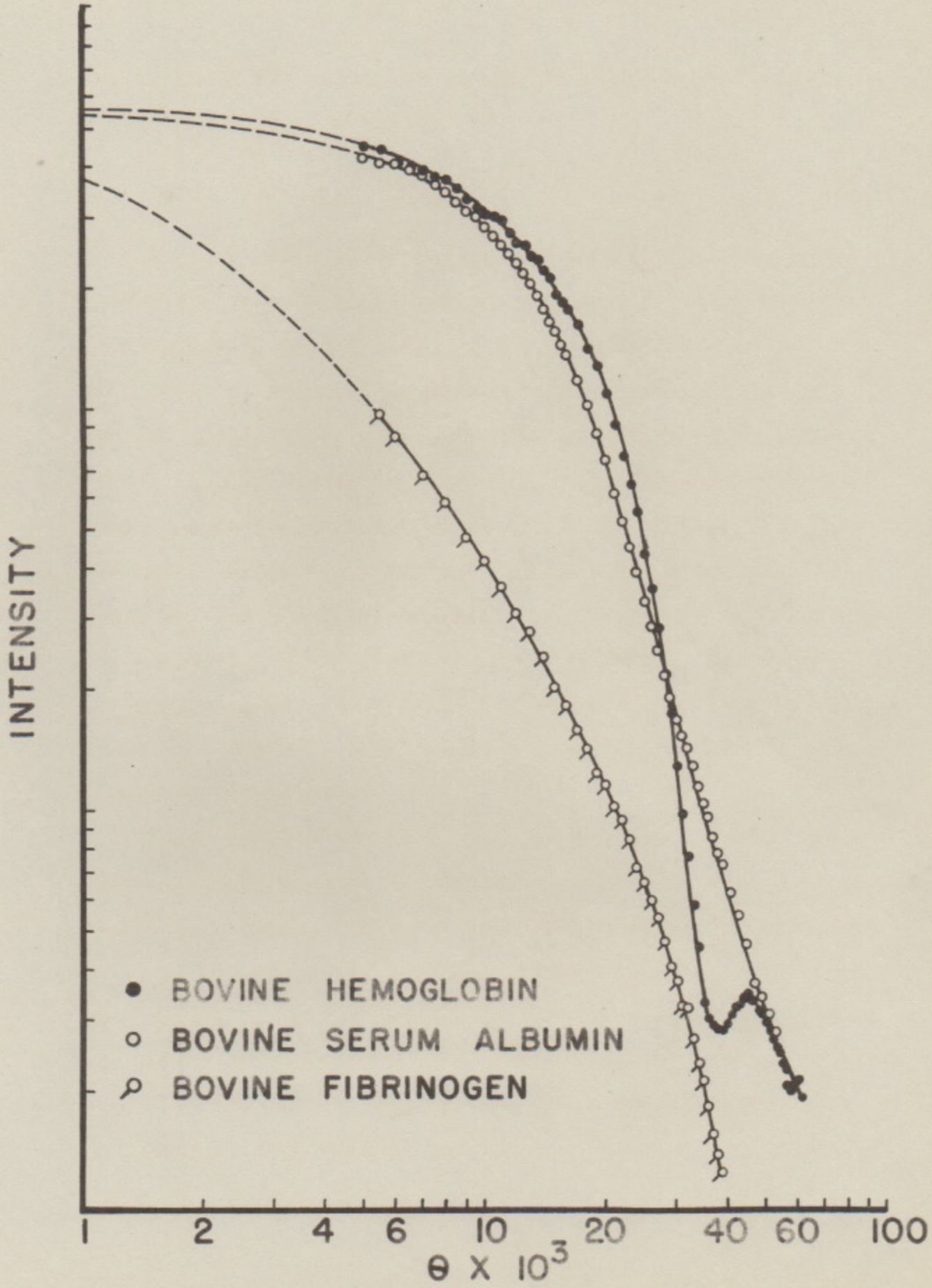
INTENSITY
BOVINE HEMOGLOBIN
BOVINE SERUM ALBUMIN
BOVINE FIBRINOGEN
1
2
4
6
10
20
40
60
100
θ X 10³

dotted lines are estimates of the extrapolations toward a common value at zero angle.

Summary

A small angle x-ray scattering collimating system has been built incorporating pinhole geometry. This represents an improvement over the slit geometry previously used for such systems, since it makes corrections for slit height effects unnecessary. The scattered radiation is detected with a fixed diameter annular slit. Its distance from the sample is varied and determines the angle of detection. The larger solid angle intercepted at the shorter distances increases the effective intensity at the larger angles where low scattering intensities are usually found. The system has been used to measure the size and shape of protein molecules in solution. The principal results of these experiments are as follows:

There is evidence that the bovine serum albumin molecule swells a small amount when in solution at pH's away from the isoelectric point. This has been inferred from determinations of the radius of gyration at various pH's. The radius of gyration of bovine serum albumin at the isoelectric point has been determined as 30.3 $\pm$ 0.4 Å. From comparison of the data with theoretical curves, the shape of the molecule is in agreement with that of an oblate ellipsoid with axial ratio of 1 to 3.5. These results set the dimensions of the

particle at 94 x 94 x 27 Å.

The radius of gyration of the hemoglobin molecule was found to be 25.9 ± 0.3 Å. The full experimental curve resolved the first minimum and maximum of the diffraction pattern and comparison with theoretical curves set the particle shape approximately as that of a prolate ellipsoid with axial ratio of 1.5 to 1 with minor axis equal to 55.6 ± 0.6 Å. The dimensions of the particle are then given as about 56 x 56 x 83 Å.

The total volumes for both molecules are greater than those predicted for dry molecules by quite well known values of molecular weights and protein densities. The difference is attributed to internal hydration of the particles in solution of .33 and .50 gms of water per gram of protein, respectively, for the bovine serum albumin and the bovine hemoglobin.

References

1. B. R. Leonard, Jr.; Ph.D. Thesis, Univ. of Wis. (1951)
2. Bernstein, Brewer, and Rubinson; Nucleonics 6, 2, 39 (1950)
3. Elmore and Sands; Electronics, McGraw-Hill (1949) p. 166
4. Bernstein, Brewer, and Rubinson; Nucleonics 6, 2, 41 (1950)
5. Elmore and Sands; Electronics, McGraw-Hill (1949) p. 235
6. Compton and Allison; X-rays in Theory and Experiment, Van Nostrand, (1948) p. 138
7. G. Fournet and A. Guinier; J. phys. et radium, 11, 516 (1950)
8. A. Guinier; Annals der Physik, 12, 16 (1939)
9. G. Fournet; Ph.D. Thesis, U. of Paris, Série A-No. 2384 (1950)
10. L. Pauling and R. B. Corey; Proc. U. S. Nat. Acad. Sci., 37 (1951) and 38 (1952)
11. L. Pauling and R. B. Corey; Nature 171, 59 (1953)
12. J. W. Anderegg; Ph.D. Thesis, p. 45, Univ. of Wis. (1952)
13. G. Scatchard; American Scientist, 40, 1, 61 (1952)
14. W. L. Bragg and M. F. Perutz; Acta Cryst. 5, 323 (1952)
15. J. W. Anderegg; Ph.D. Thesis, p. 63, Univ. of Wis. (1952)
16. R. M. Bock; Bachelor's Thesis, Univ. of Wis. (1949)
17. E. J. Cohn and J. T. Edsall; Proteins, Amino Acids, and Peptides, Reinhold (1943) p. 503
18. G. Porod; Acta Physica Austriaca, 2, 255 (1948)
19. E. J. Cohn and J. T. Edsall; Proteins, Amino Acids, and Peptides, Reinhold (1943) p. 377
20. Halwer, Nutting and Brice; J. Am. Chem. Soc. 73 (1951)
21. J. F. Foster and R. E. Rhees, Arch. Biochem. Biophys. 40 (1952)

22. P. W. Schmidt; Ph.D. Thesis, Univ. of Wis. (1953)

23. W. L. Bragg and A. B. Pippard; Acta Cryst. 6, 865 (1953)

Acknowledgements

I wish to thank the personnel of the University of Wisconsin machine shop for their work and assistance in the construction of the collimating system; Professor H. F. Deutsch for his work and assistance in preparing the hemoglobin samples; the Office of Naval Research and the Wisconsin Alumni Research Foundation for financial assistance; and Professor W. W. Beeman, under whose guidance this work was done.

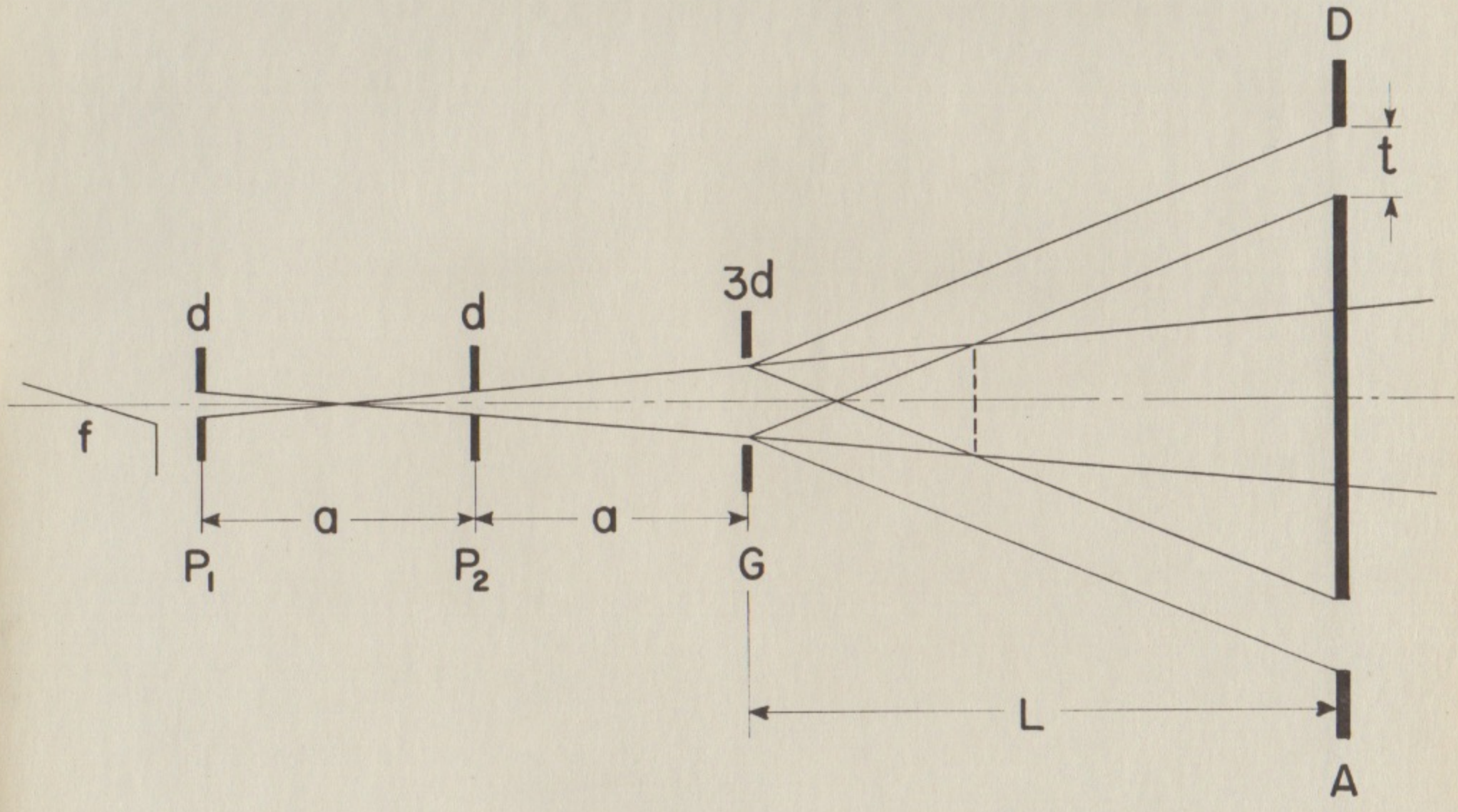
D
t
d
d
3d
f
a
a
P1
P2
G
L
A

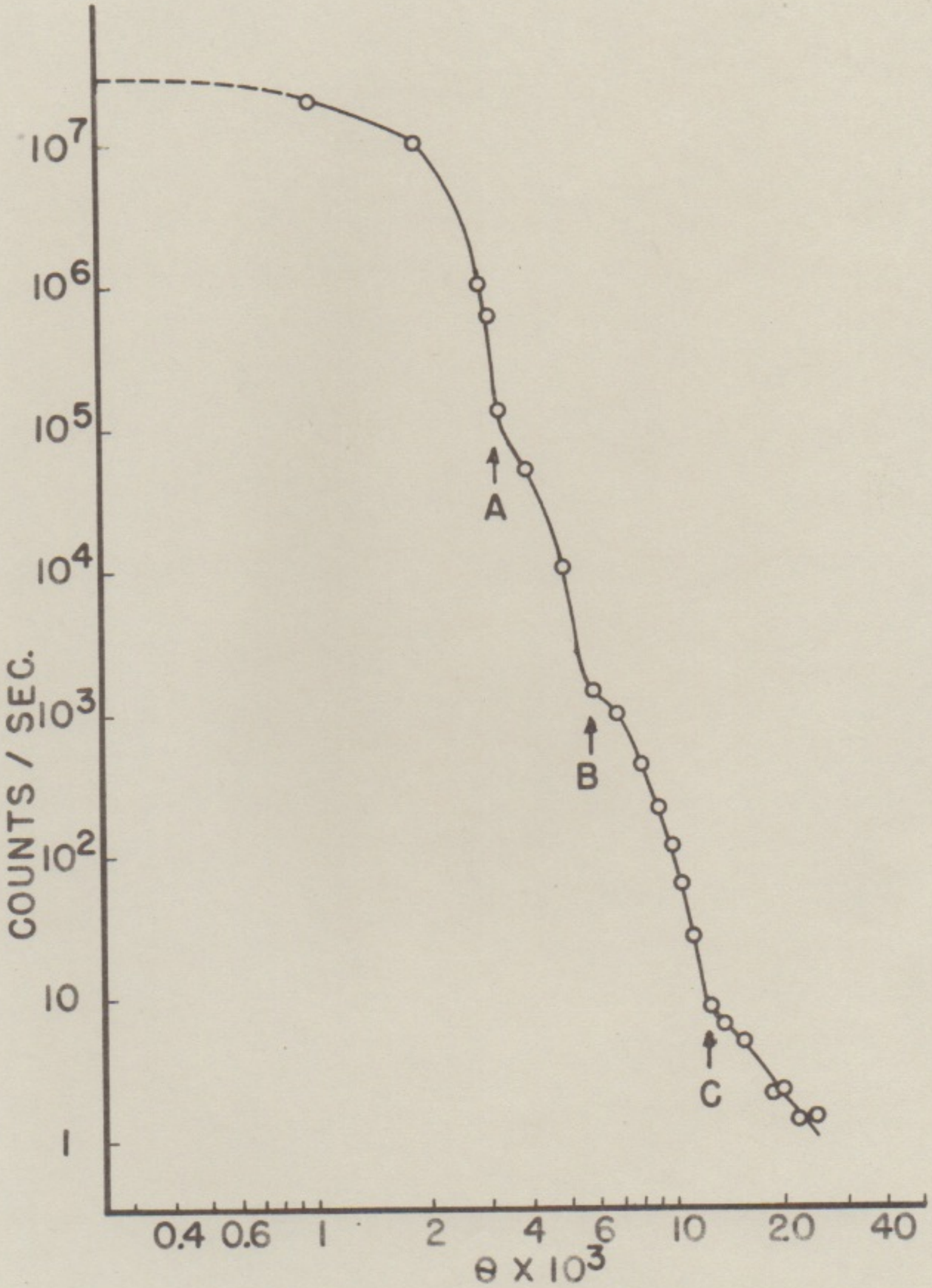
COUNTS / SEC.
10^7
10^6
10^5
10^4
10^3
10^2
10
1
A
B
C
0.4 0.6 1 2 4 6 10 20 40
$\theta \times 10^3$

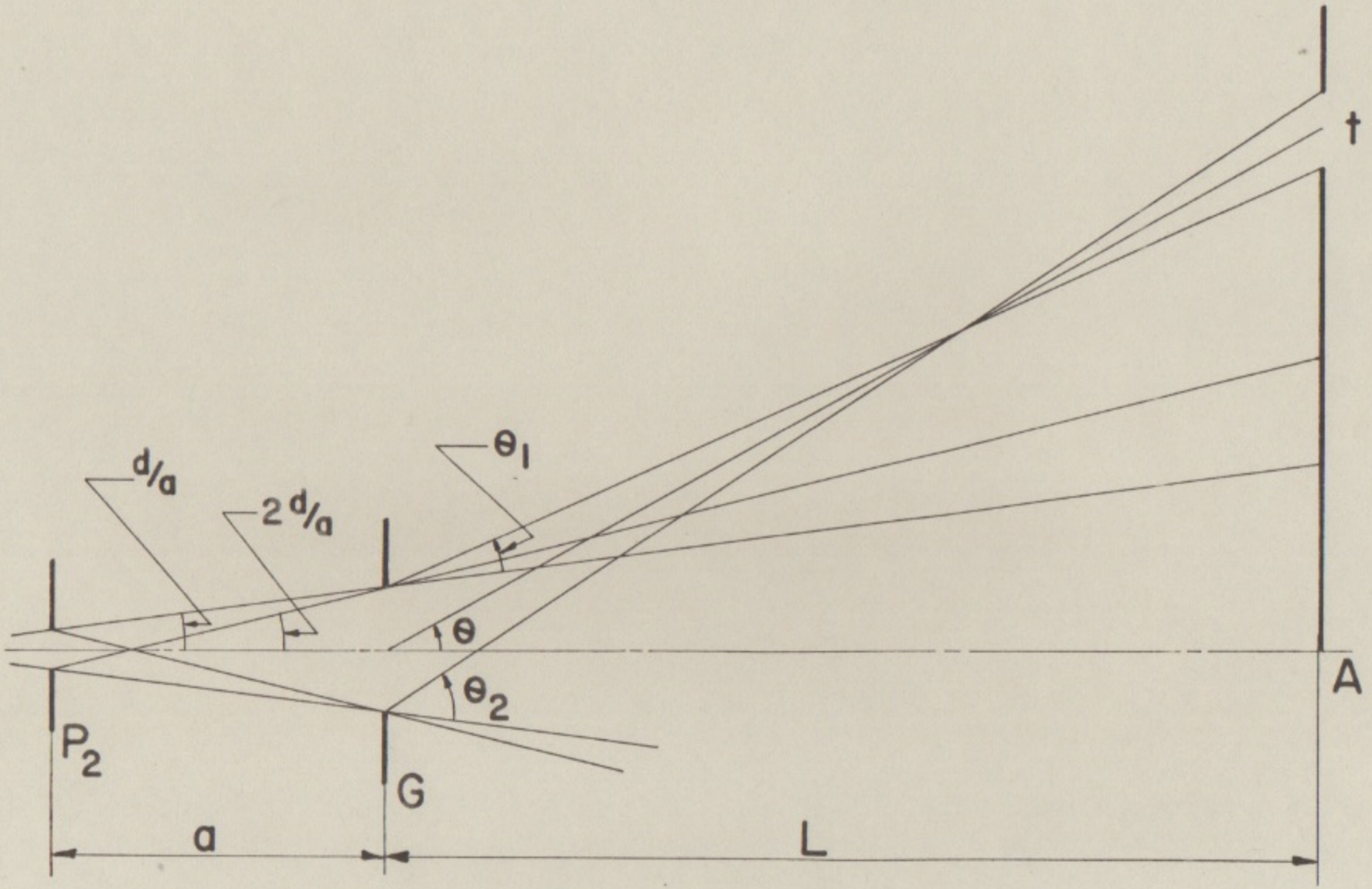
t
θ1
d/a
2 d/a
θ
θ2
A
P2
G
a
L

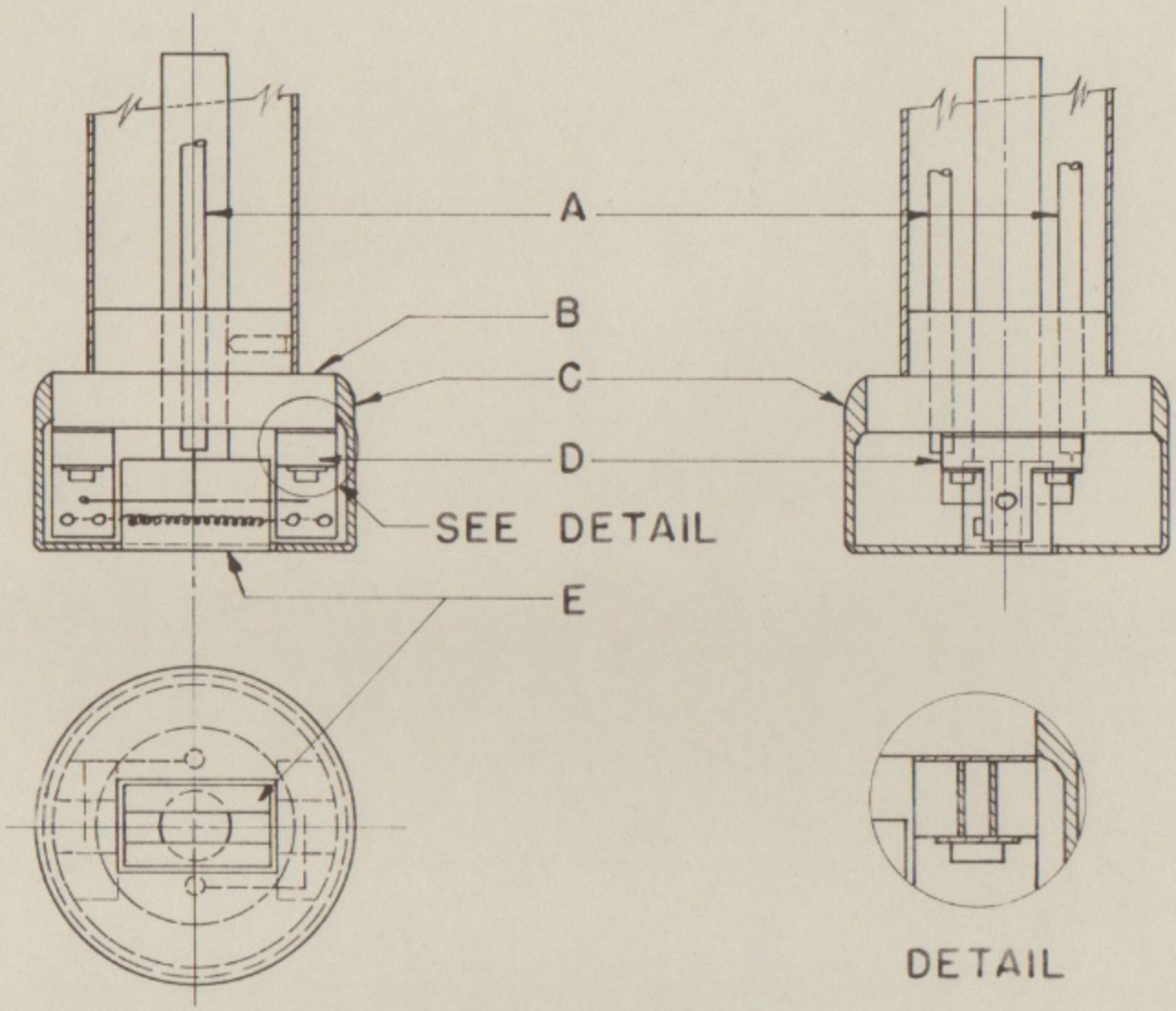

ELECTRON GUN

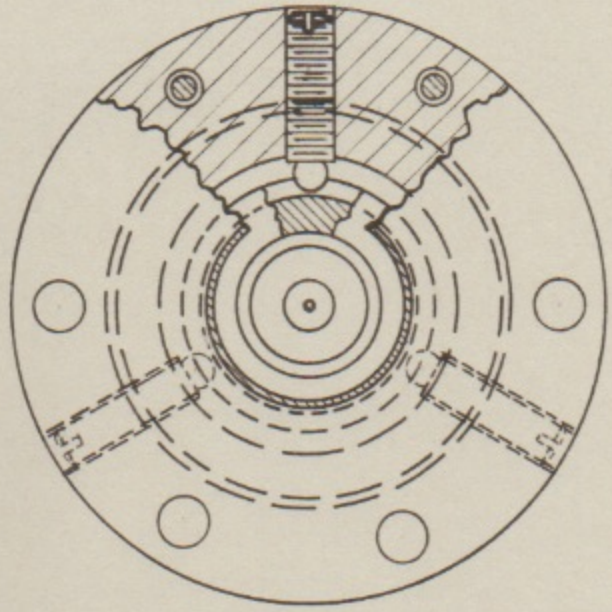

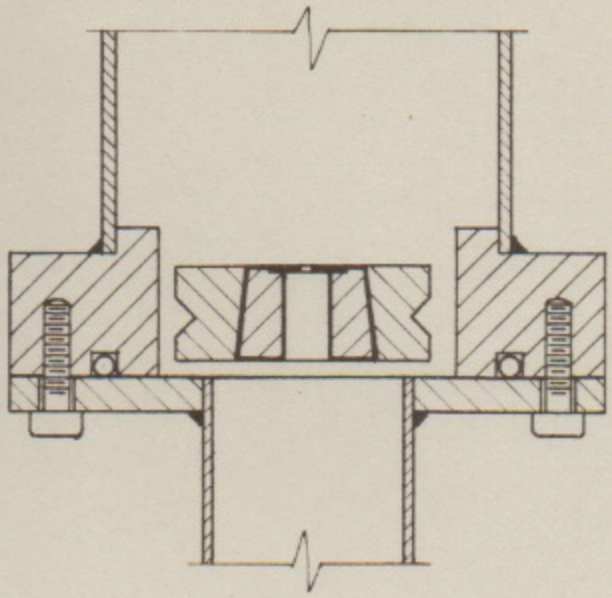

ADJUSTABLE PINHOLE DIAPHRAGM

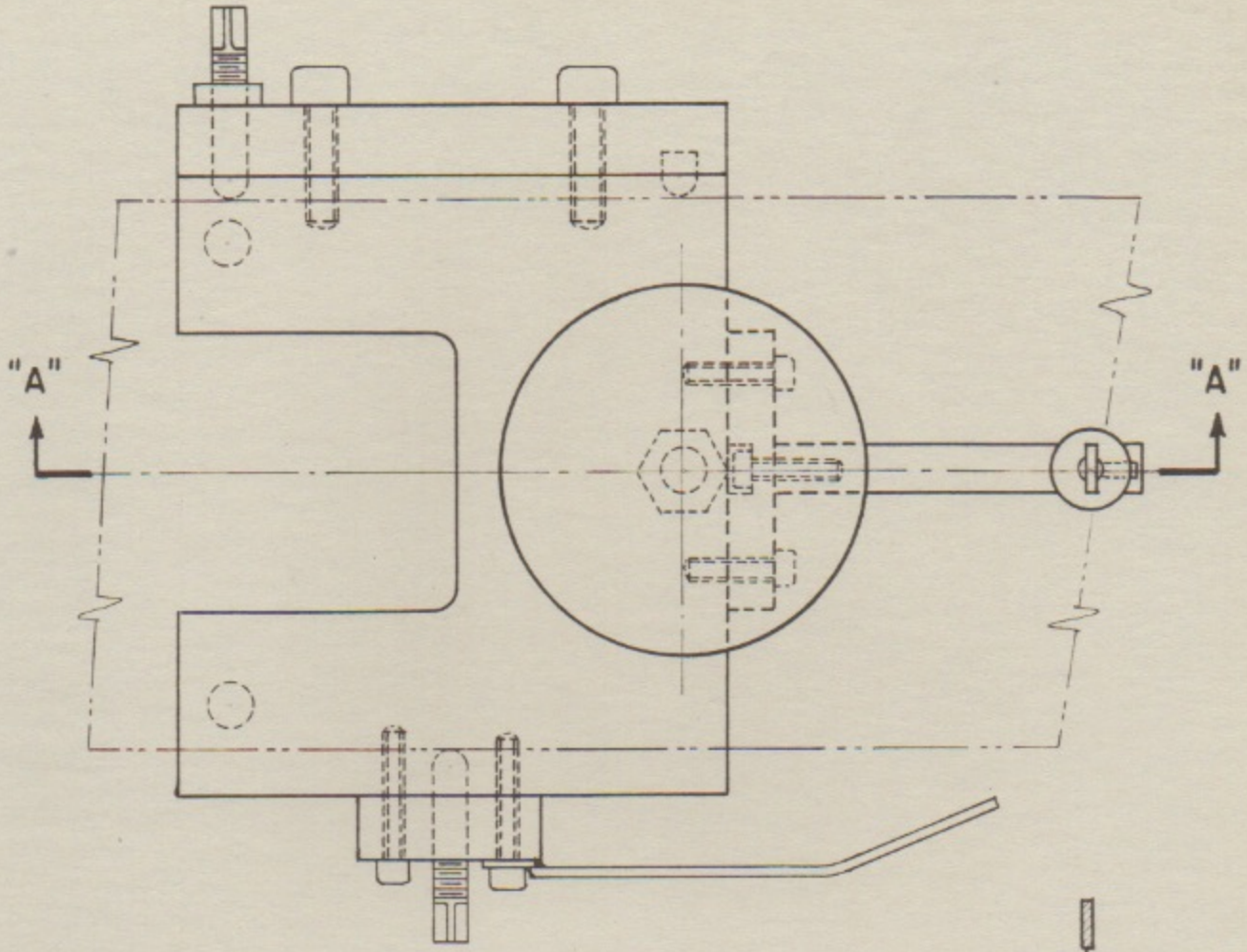

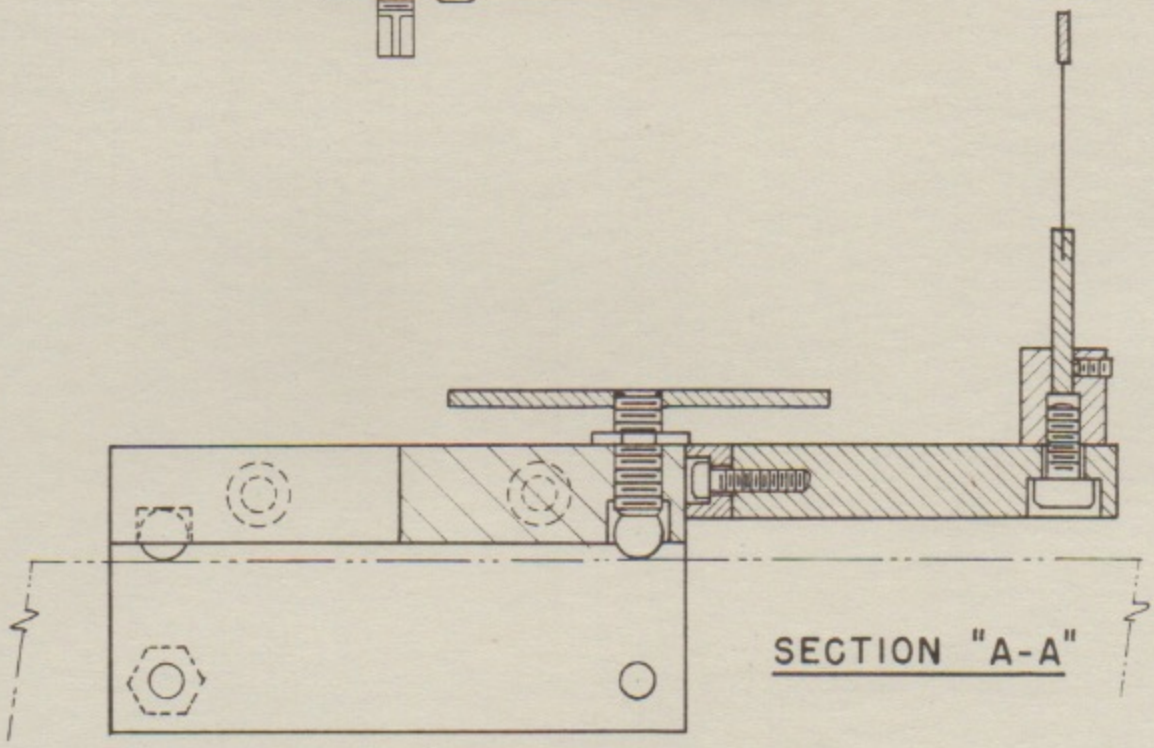

SECTION "A-A"

BEAM STOP SUPPORT

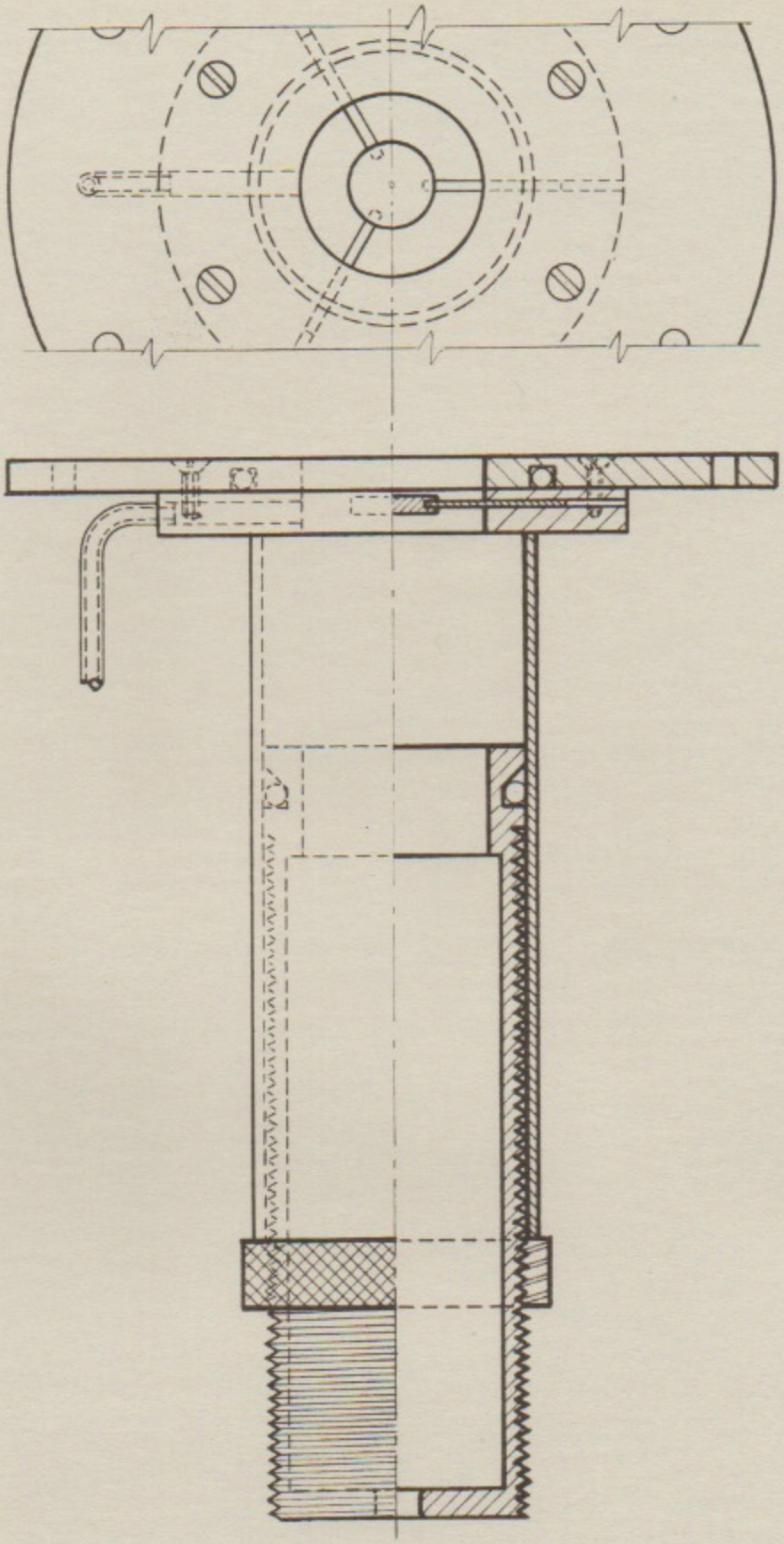

ADJUSTABLE VACUUM CHAMBER

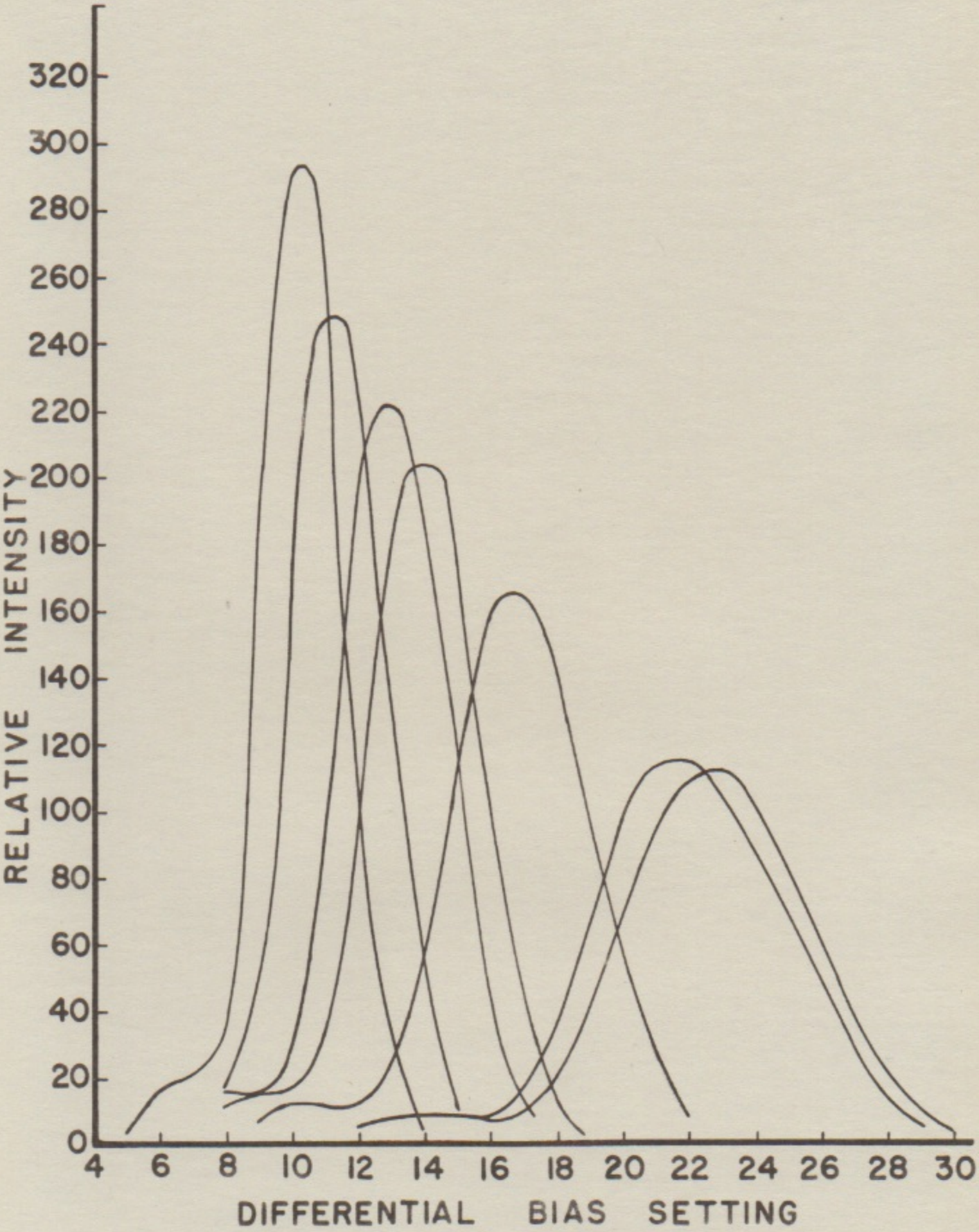
RELATIVE INTENSITY
320
300
280
260
240
220
200
180
160
140
120
100
80
60
40
20
0
4
6
8
10
12
14
16
18
20
22
24
26
28
30
DIFFERENTIAL BIAS SETTING

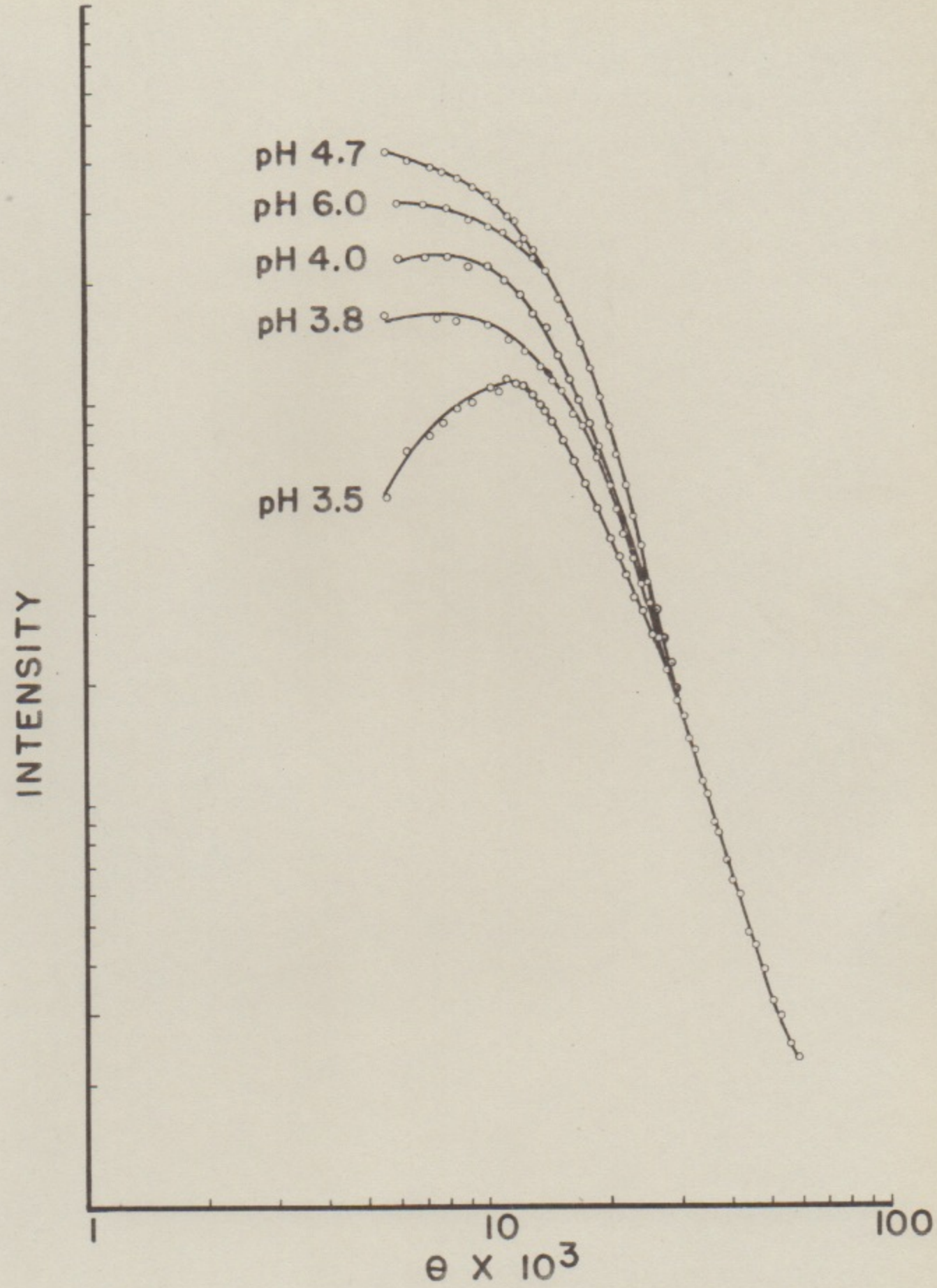
pH 4.7
pH 6.0
pH 4.0
pH 3.8
pH 3.5
INTENSITY
1
10
100
θ X 10³

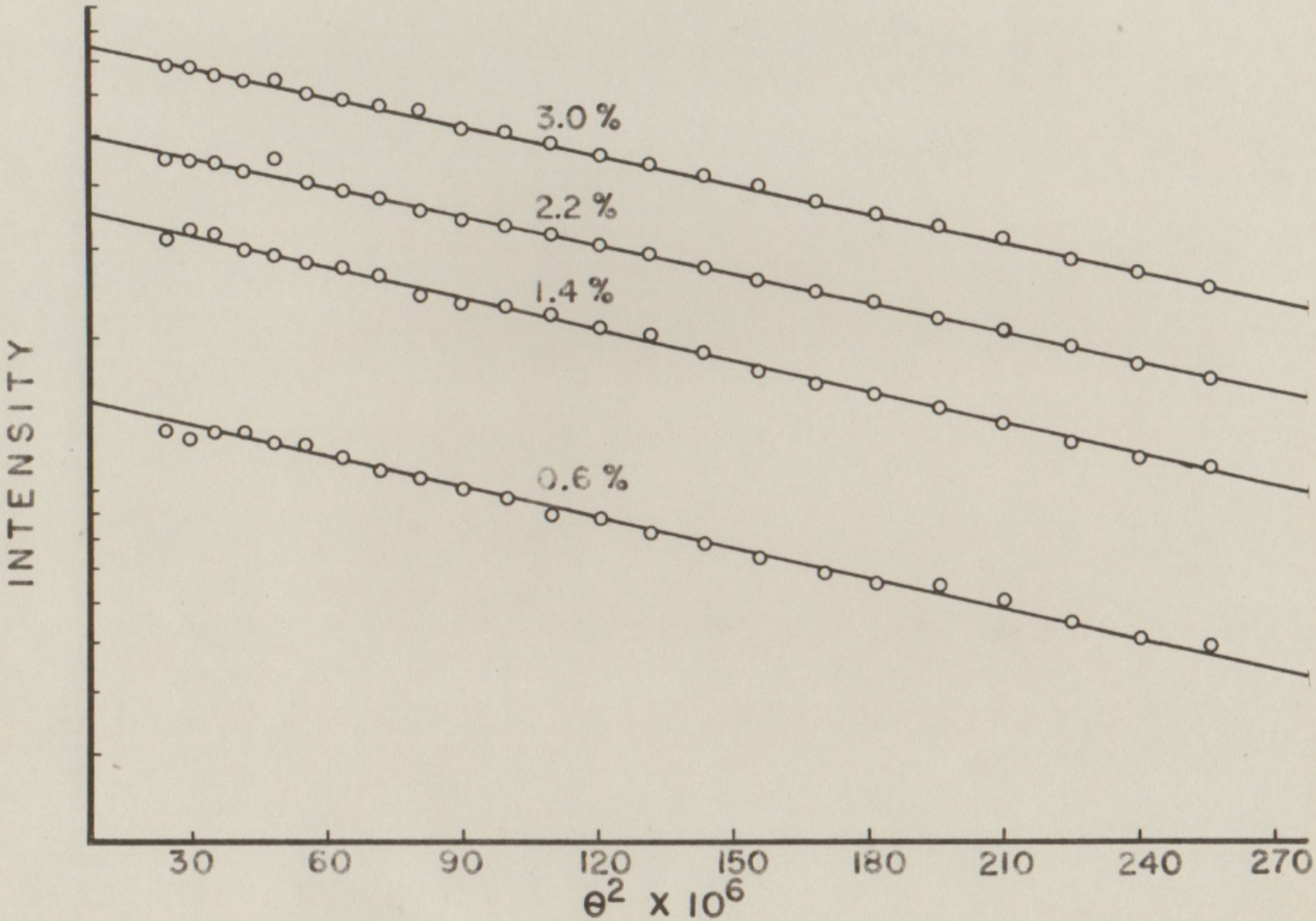
3.0 %
2.2 %
1.4 %
0.6 %
INTENSITY
30
60
90
120
150
180
210
240
270
θ² x 10⁶

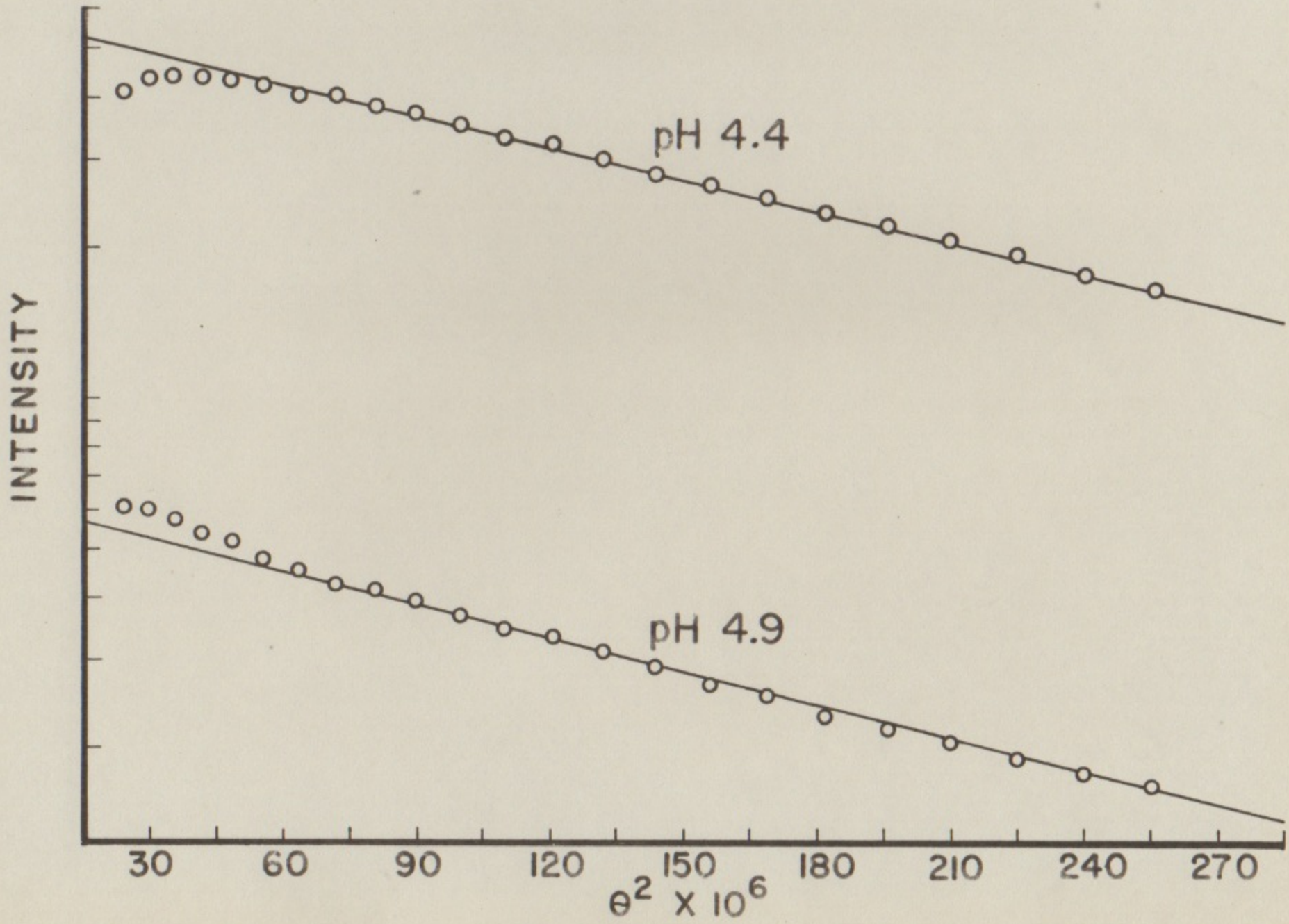
pH 4.4
pH 4.9
INTENSITY
30
60
90
120
150
180
210
240
270
θ² X 10⁶

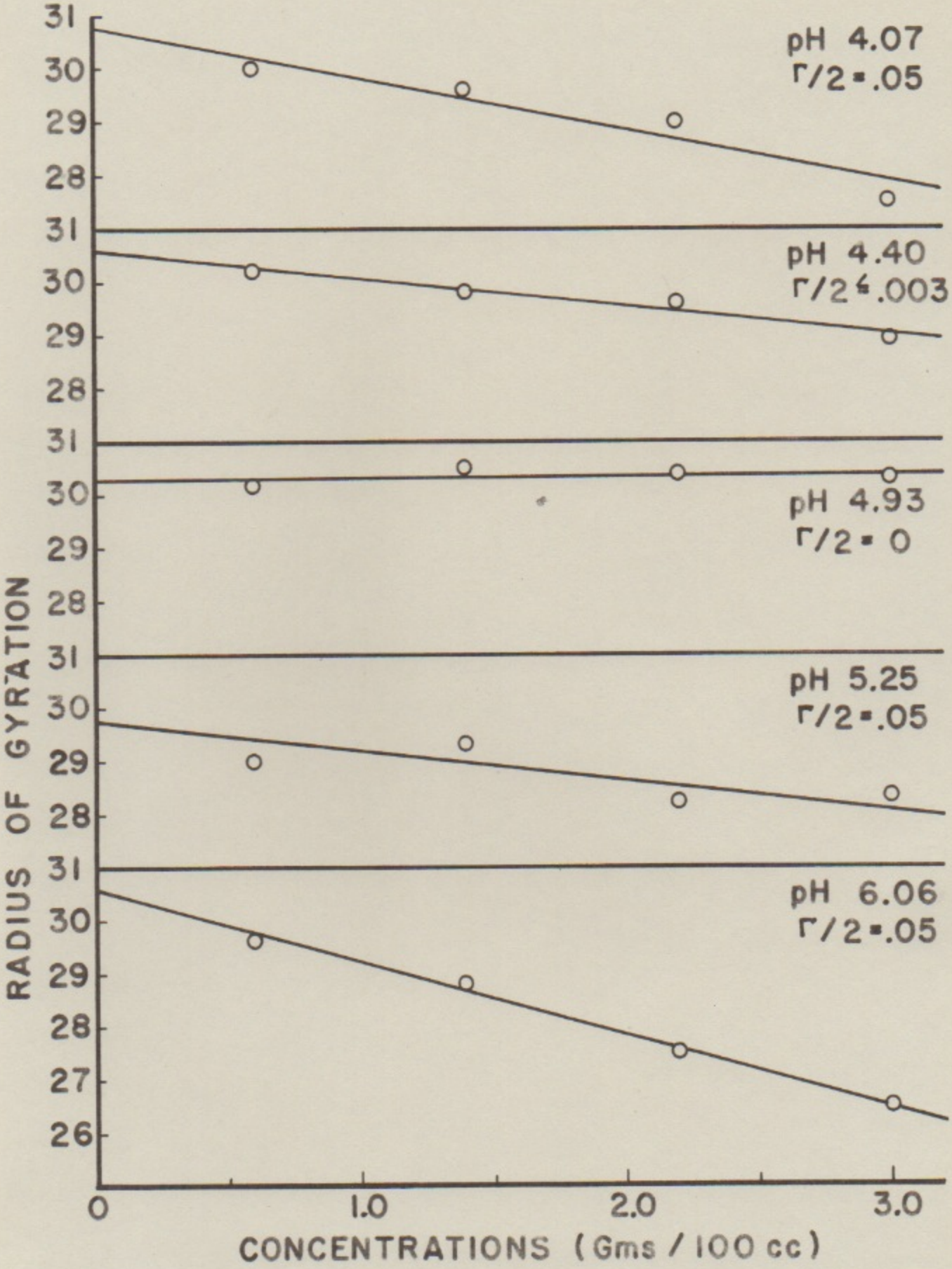
pH 4.07
Γ/2 = .05
pH 4.40
Γ/2 = .003
pH 4.93
Γ/2 = 0
pH 5.25
Γ/2 = .05
pH 6.06
Γ/2 = .05
RADIUS OF GYRATION
31
30
29
28
31
30
29
28
31
30
29
28
31
30
29
28
31
30
29
28
27
26
0
1.0
2.0
3.0
CONCENTRATIONS (Gms / 100 cc)

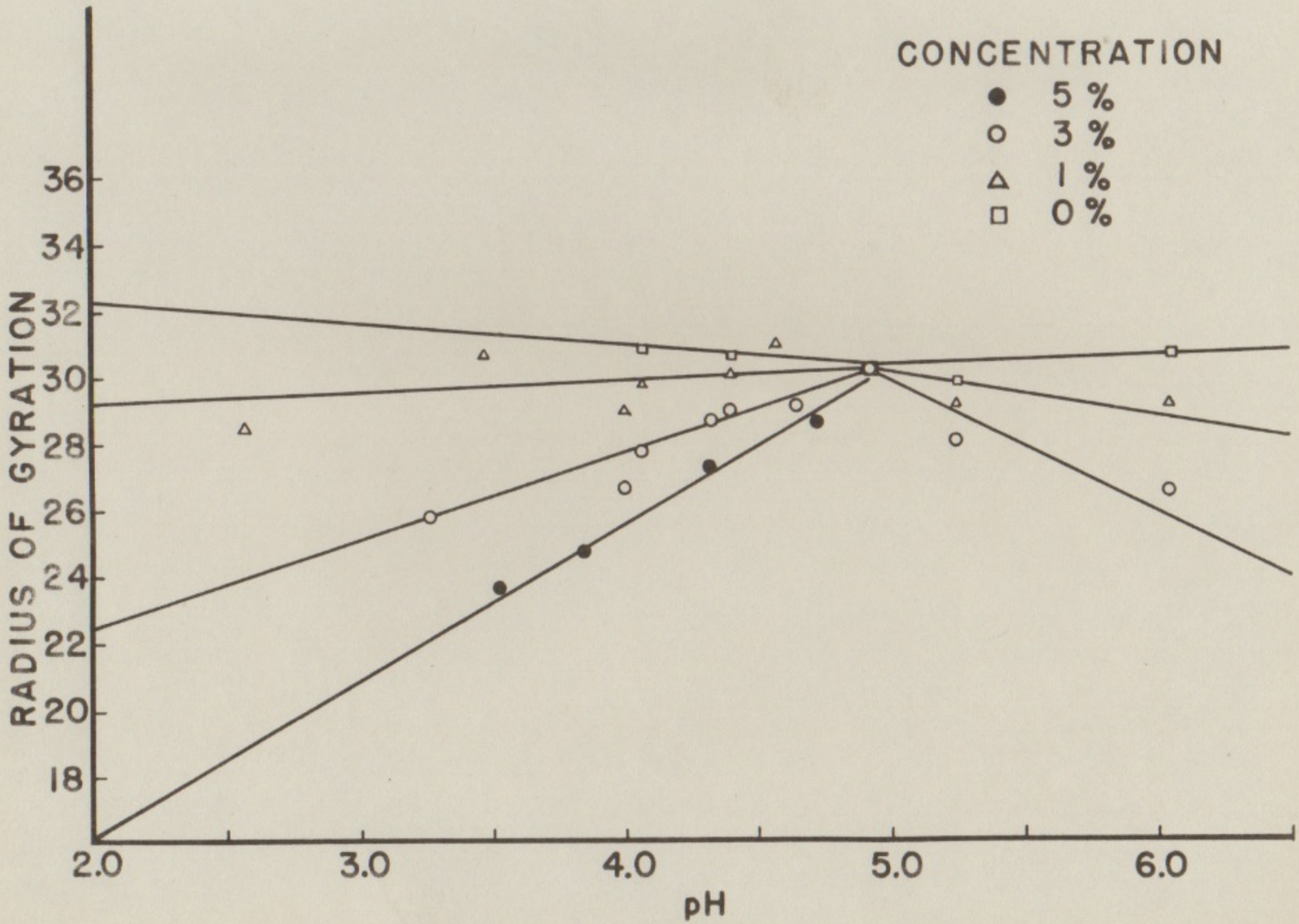
CONCENTRATION
5 %
3 %
1 %
0 %
RADIUS OF GYRATION
36
34
32
30
28
26
24
22
20
18
2.0
3.0
4.0
5.0
6.0
pH

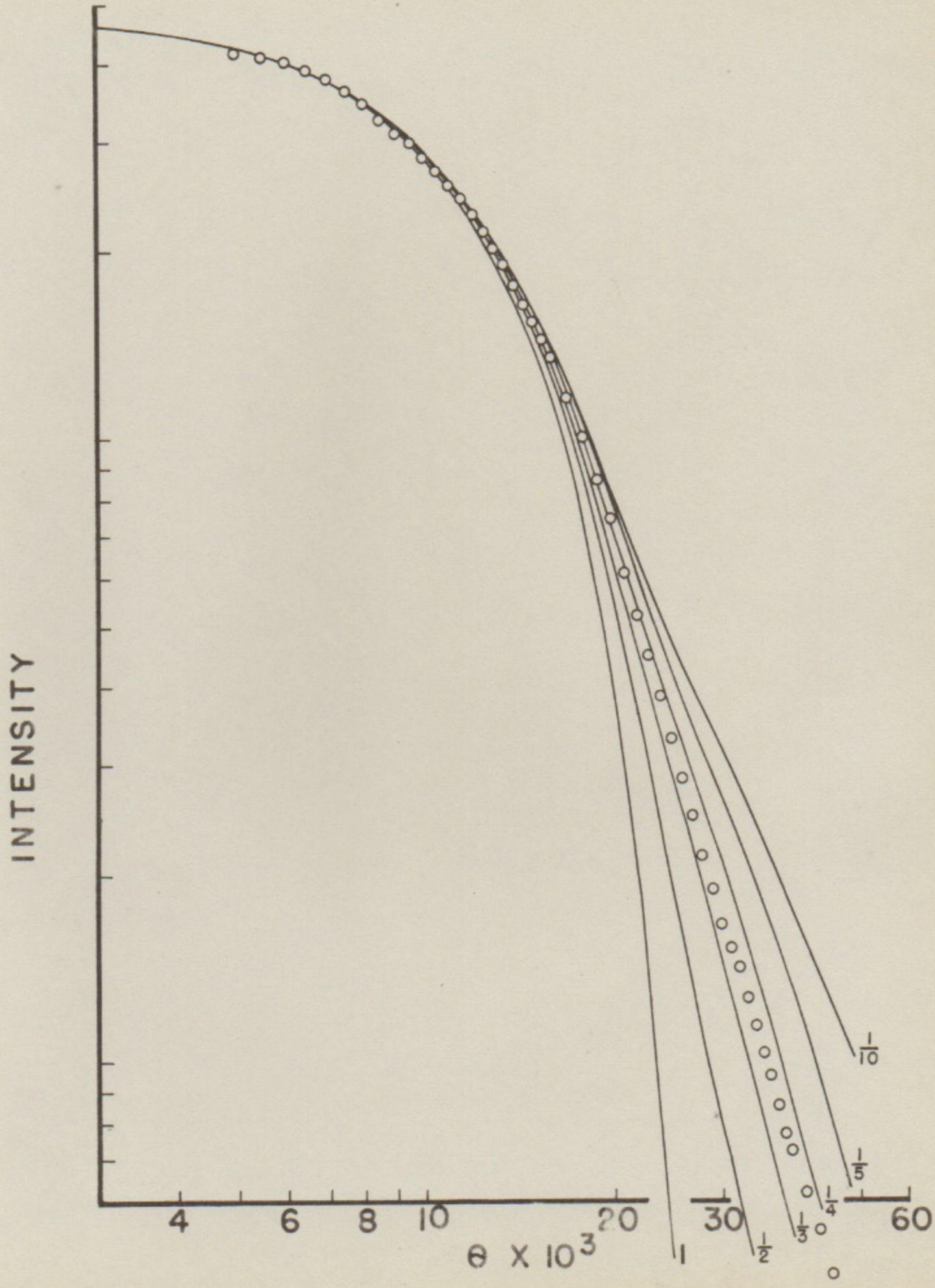
INTENSITY
4
6
8
10
20
30
60
θ X 10^3
1
1/2
1/3
1/4
1/5
1/10

INTENSITY
2 %
5 %
10 %
Γ/2 = 0
5 %
Γ/2 = 0.05
1
2
4
6
10
20
40
60
100
θ X 10^3

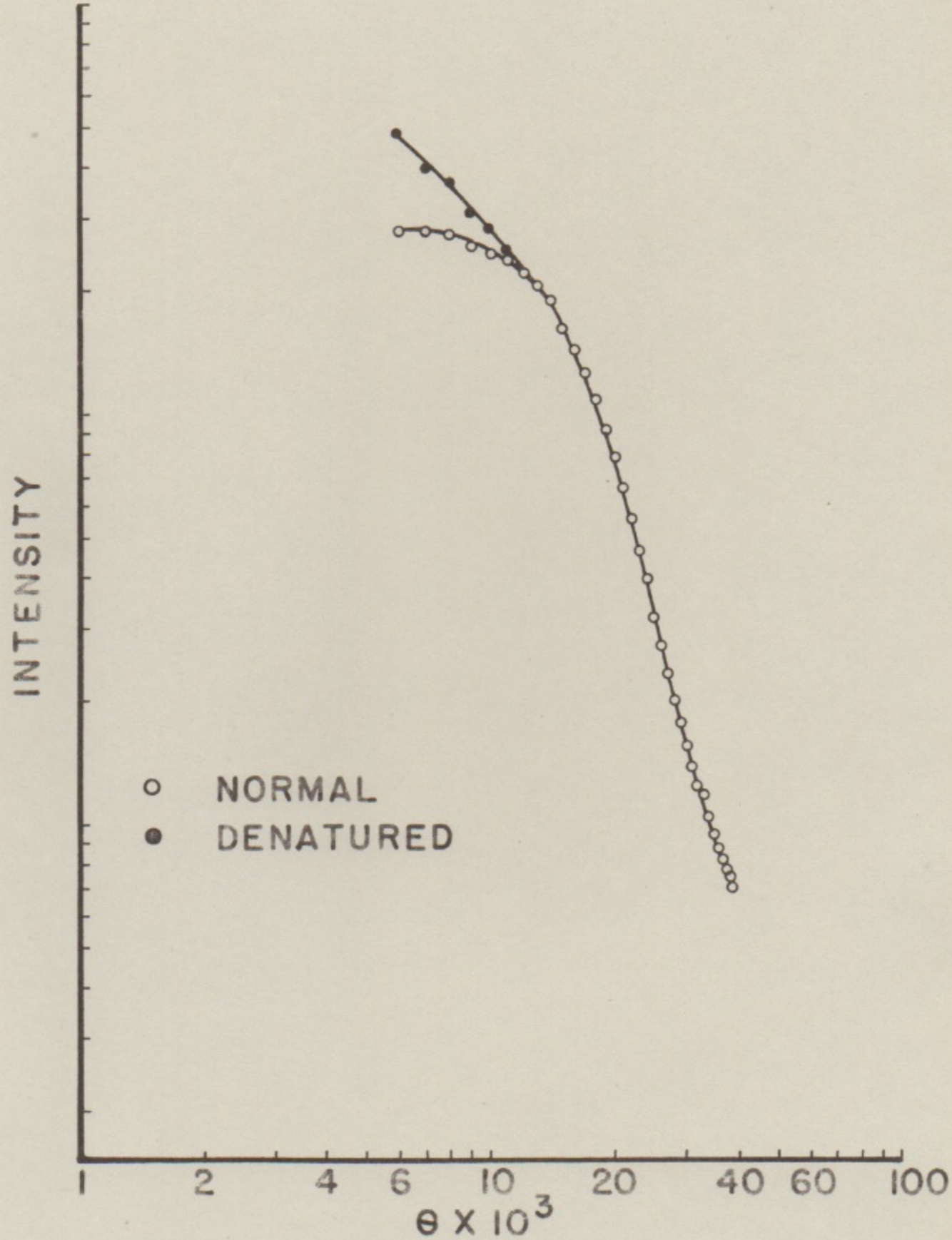
INTENSITY
NORMAL
DENATURED
1
2
4
6
10
20
40
60
100
θ X 10³

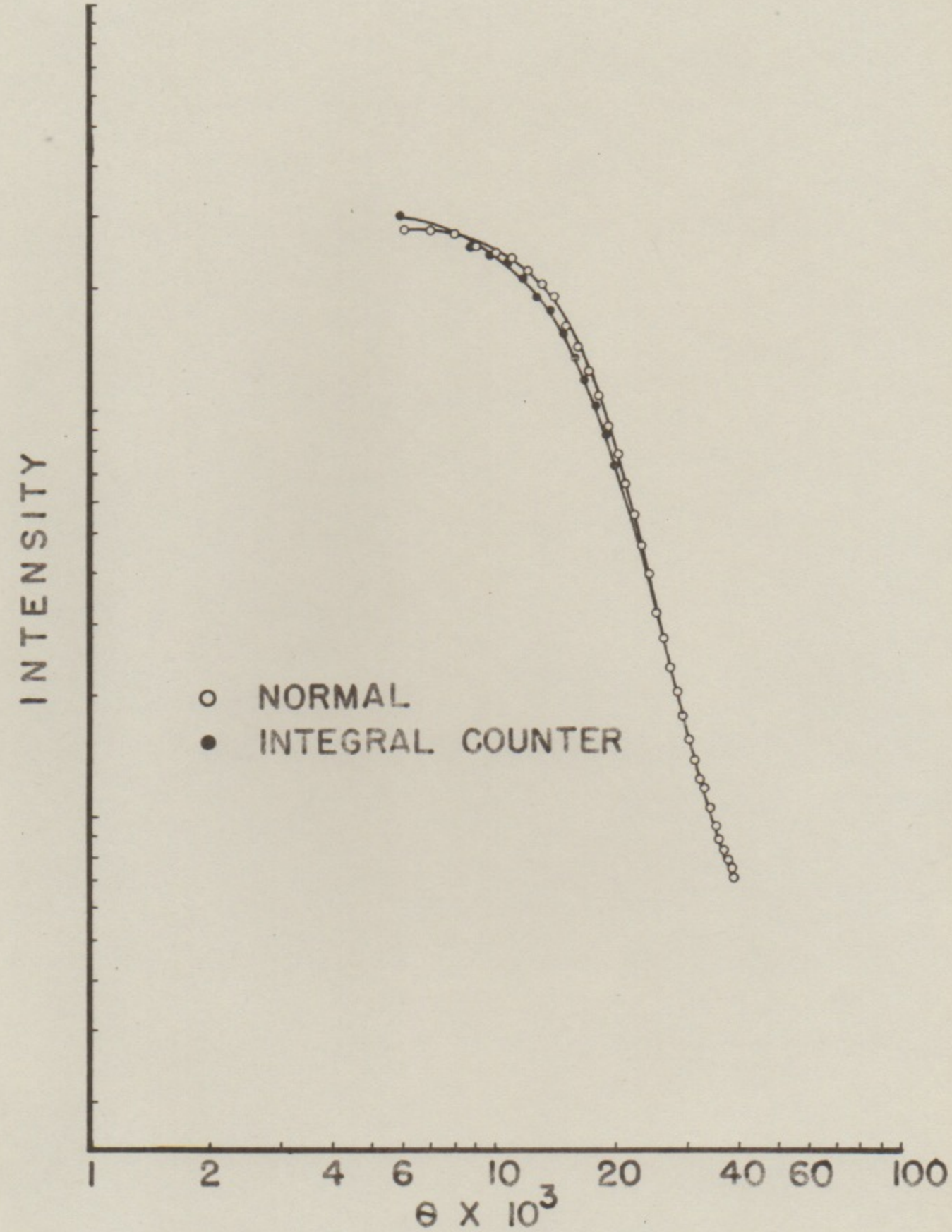
INTENSITY
NORMAL
INTEGRAL COUNTER
1
2
4
6
10
20
40
60
100
θ X 10³

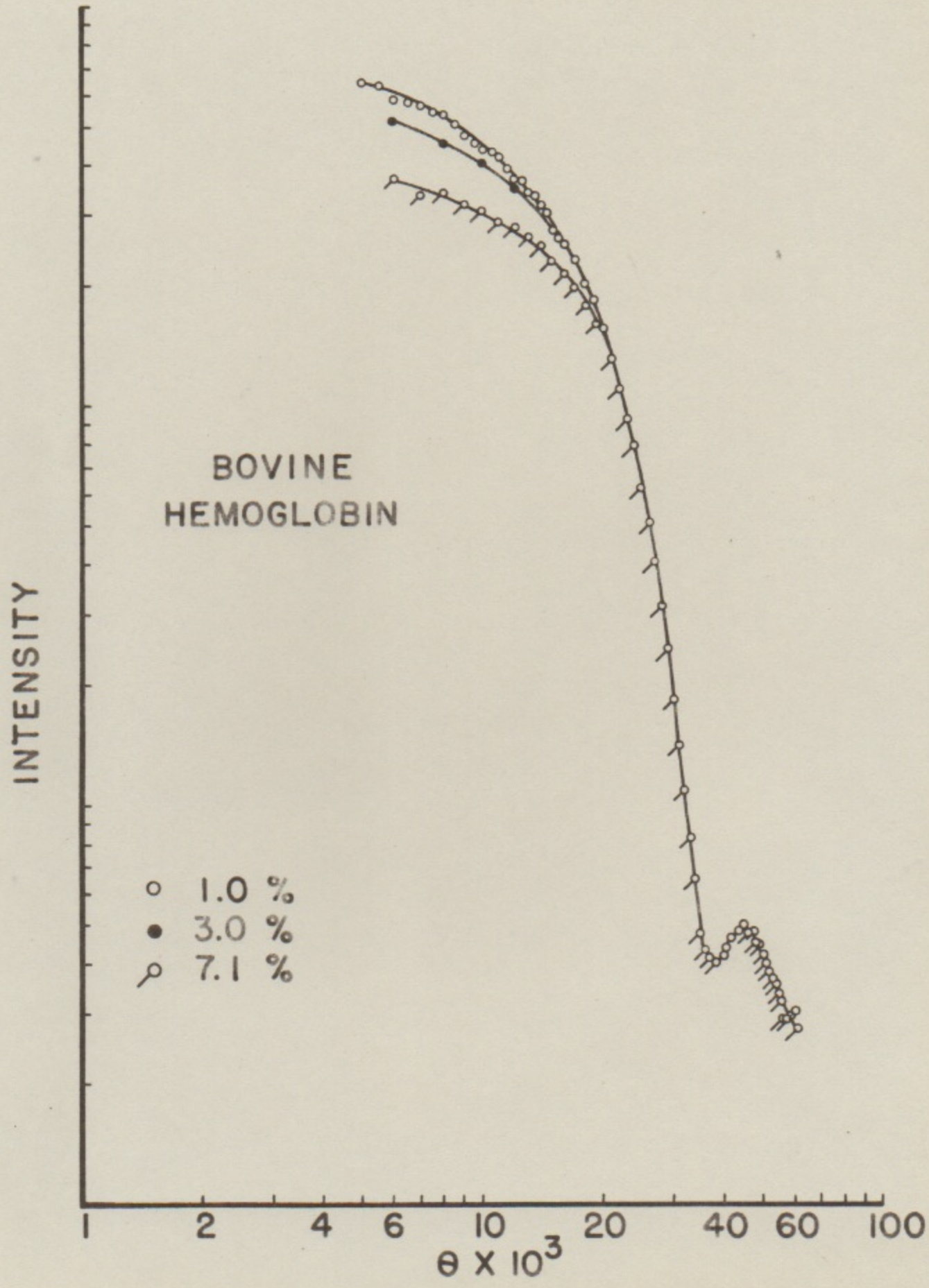
BOVINE
HEMOGLOBIN
INTENSITY
1.0 %
3.0 %
7.1 %
1
2
4
6
10
20
40
60
100
θ X 10³

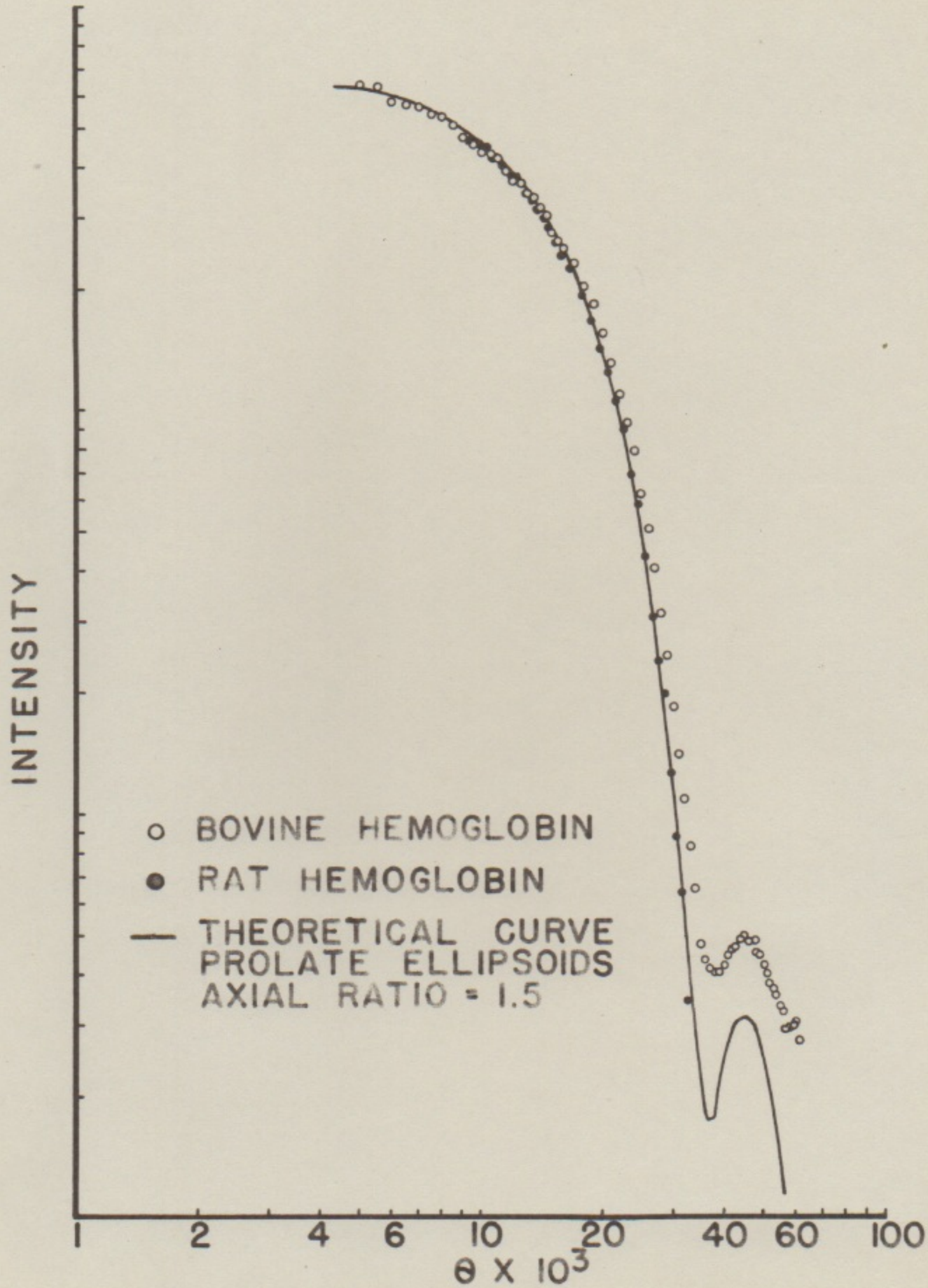
INTENSITY
BOVINE HEMOGLOBIN
RAT HEMOGLOBIN
THEORETICAL CURVE
PROLATE ELLIPSOIDS
AXIAL RATIO = 1.5
1
2
4
6
10
20
40
60
100
θ X 10³

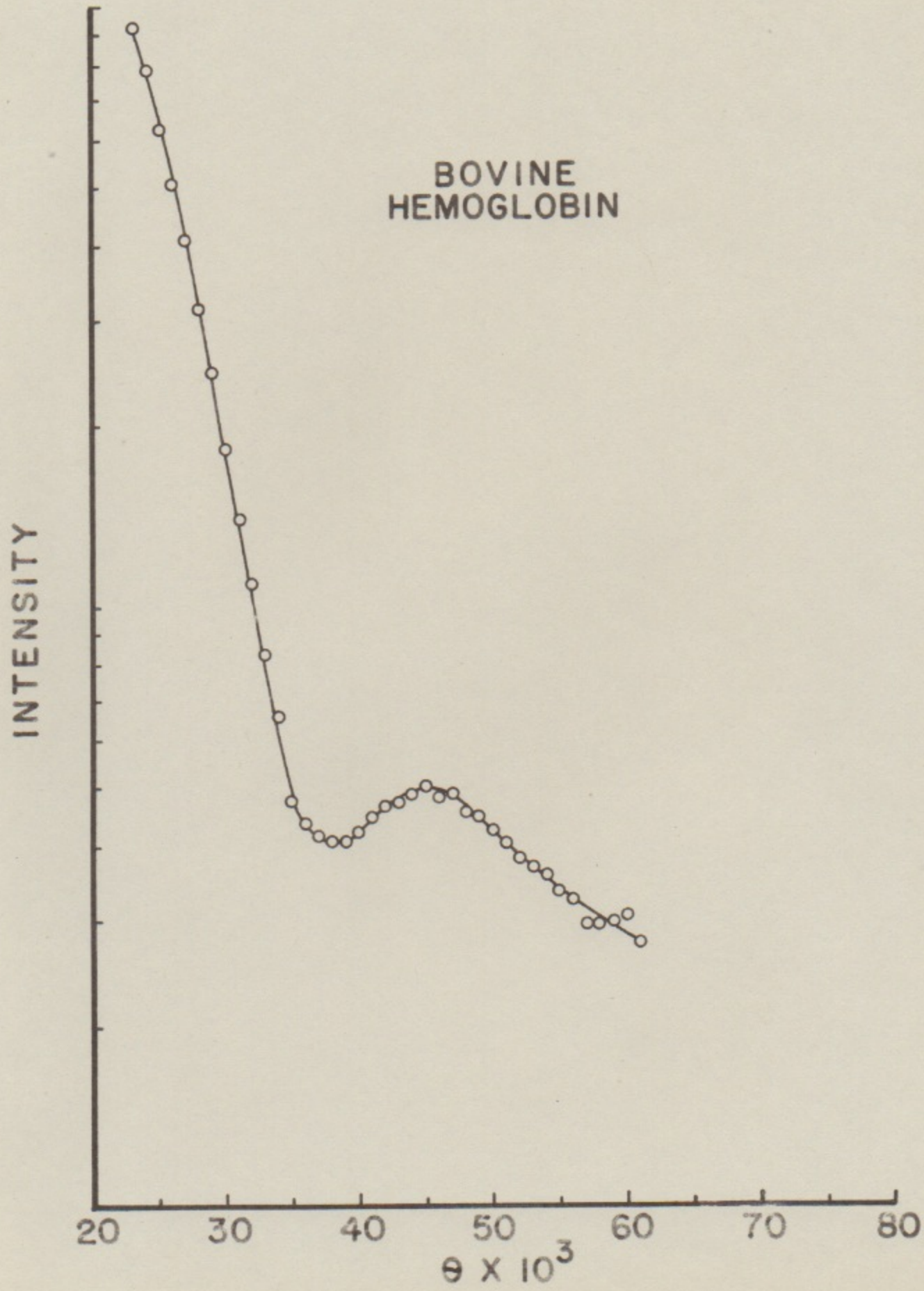
BOVINE
HEMOGLOBIN
INTENSITY
20
30
40
50
60
70
80
θ X 10³

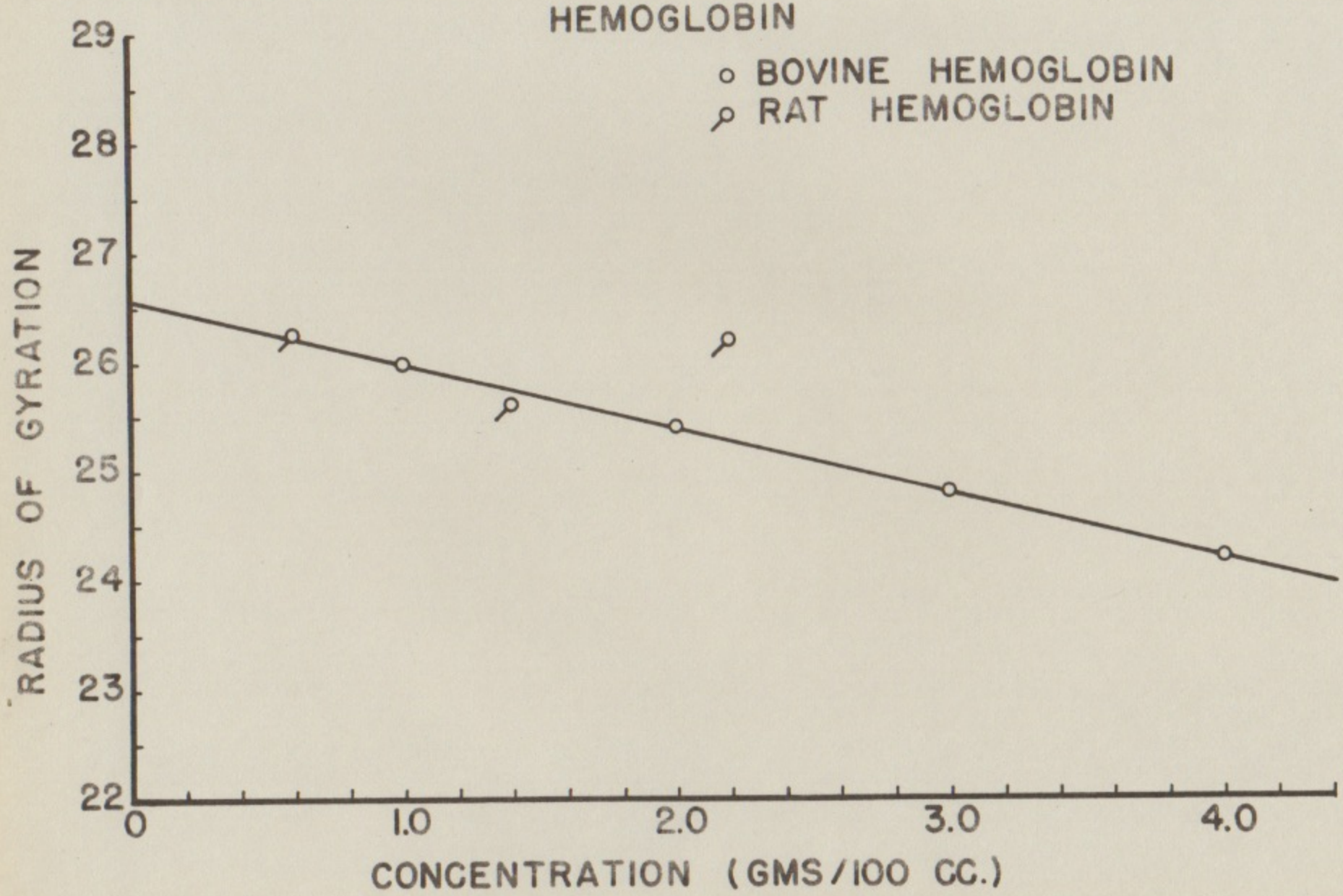
HEMOGLOBIN
BOVINE HEMOGLOBIN
RAT HEMOGLOBIN
RADIUS OF GYRATION
29
28
27
26
25
24
23
22
0
1.0
2.0
3.0
4.0
CONCENTRATION (GMS/100 CC.)

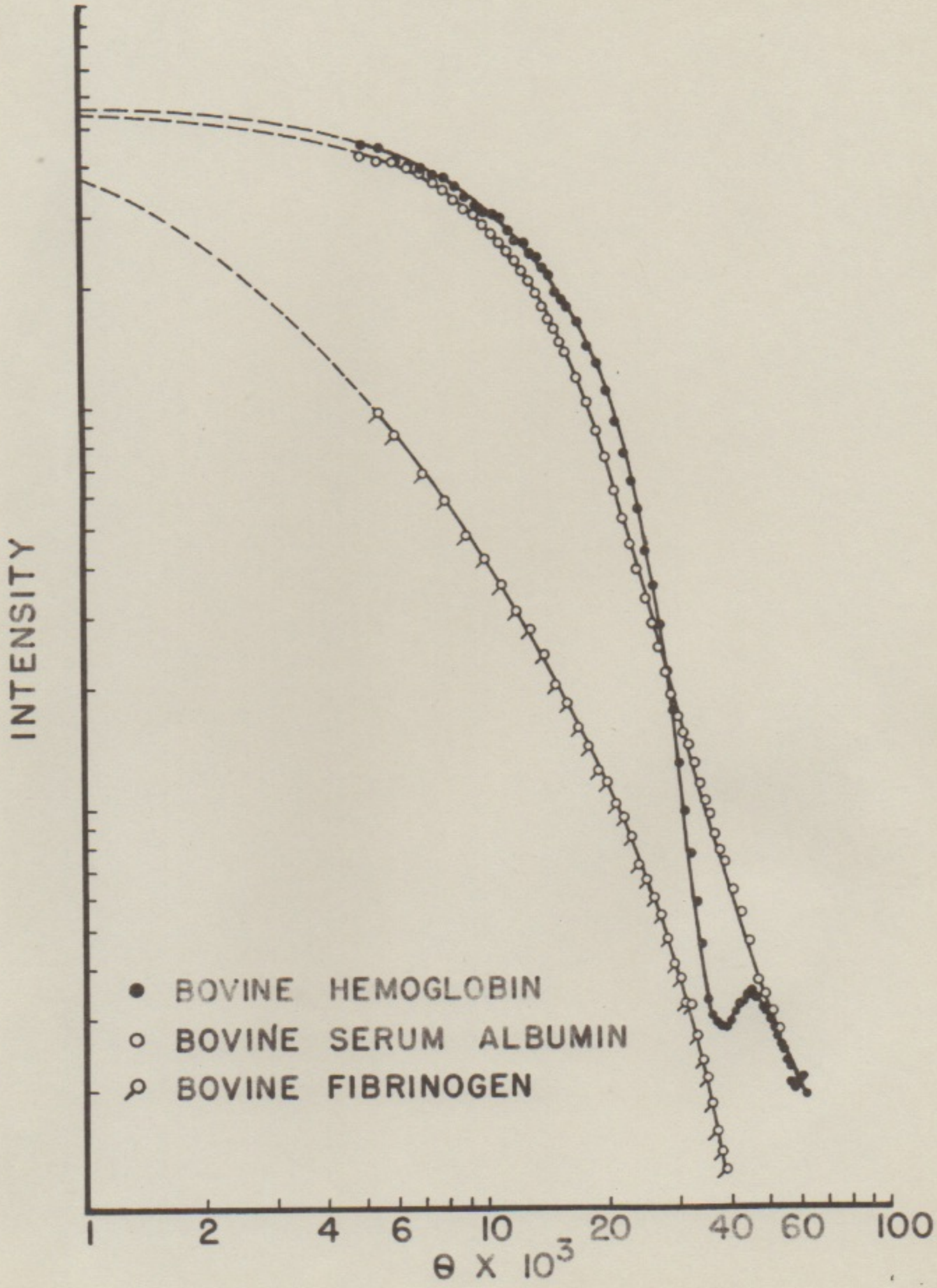
INTENSITY
BOVINE HEMOGLOBIN
BOVINE SERUM ALBUMIN
BOVINE FIBRINOGEN
1
2
4
6
10
20
40
60
100
θ X 10³